

# **Examination of Fire Dynamics Analysis Techniques: Assessment of Predictive Fire Algorithms and Models**

Mark McKinnon  
Joseph Willi  
Daniel Madrzykowski

UL Firefighter Safety Research Institute  
Columbia, MD 20145

**UNDERWRITERS  
LABORATORIES™**





# Examination of Fire Dynamics Analysis Techniques: Assessment of Predictive Fire Algorithms and Models

Mark McKinnon  
Joseph Willi  
Daniel Madrzykowski

UL Firefighter Safety Research Institute  
Columbia, MD 21045

March 31, 2021

UNDERWRITERS  
LABORATORIES™



Underwriters Laboratories Inc.  
*Terrence Brady, President*

UL Firefighter Safety Research Institute  
*Stephen Kerber, Director*

In no event shall UL be responsible to anyone for whatever use or non-use is made of the information contained in this Report and in no event shall UL, its employees, or its agents incur any obligation or liability for damages including, but not limited to, consequential damage arising out of or in connection with the use or inability to use the information contained in this Report. Information conveyed by this Report applies only to the specimens actually involved in these tests. UL has not established a factory Follow-Up Service Program to determine the conformance of subsequently produced material, nor has any provision been made to apply any registered mark of UL to such material. The issuance of this Report in no way implies Listing, Classification or Recognition by UL and does not authorize the use of UL Listing, Classification or Recognition Marks or other reference to UL on or in connection with the product or system.

# Contents

<b>List of Figures</b>	<b>iii</b>
<b>List of Tables</b>	<b>iv</b>
<b>List of Abbreviations</b>	<b>v</b>
<b>1 Introduction</b>	<b>1</b>
1.1 Motivation . . . . .	1
<b>2 Literature Review</b>	<b>3</b>
<b>3 Description of Experiments</b>	<b>5</b>
3.1 Fuel Loads . . . . .	5
3.2 Instrumentation . . . . .	7
3.3 Compartment Experiments . . . . .	8
3.3.1 Structure . . . . .	9
3.3.2 Instrumentation . . . . .	11
<b>4 Predictive Fire Algorithms &amp; Models</b>	<b>15</b>
4.1 Model Background . . . . .	15
4.1.1 NRC Fire Dynamics Tools . . . . .	15
4.1.2 Zone Models . . . . .	20
4.1.3 Field Models . . . . .	21
4.2 Model Construction for Compartment Experiments . . . . .	22
4.2.1 FDTs . . . . .	23
4.2.2 CFAST . . . . .	24
4.2.3 FDS . . . . .	24
4.3 Model Sensitivity . . . . .	26
<b>5 Model Assessment</b>	<b>27</b>
5.1 Temperatures . . . . .	28
5.1.1 Layer Temperatures . . . . .	33
5.1.2 Layer Heights . . . . .	36
5.2 Flame Heights . . . . .	41
5.3 Heat Flux . . . . .	44
5.4 Velocity . . . . .	49
5.5 Oxygen Concentration . . . . .	51

<b>6</b>	<b>Discussion</b>	<b>56</b>
<b>7</b>	<b>Recommendations</b>	<b>58</b>
<b>8</b>	<b>Research Needs</b>	<b>59</b>
<b>9</b>	<b>Summary</b>	<b>60</b>
	<b>References</b>	<b>61</b>
<b>A</b>	<b>Detailed Results</b>	<b>66</b>
A.1	Compartment Experiments . . . . .	66
A.1.1	Gas Temperature . . . . .	66
A.1.2	Plume Temperature and Velocity . . . . .	87
A.1.3	Flame Height . . . . .	107
A.1.4	Heat Flux . . . . .	115

# List of Figures

3.1	Natural Gas Burners Used in Experiments . . . . .	6
3.2	Sofa Designs Used as Experimental Fuel Loads . . . . .	7
3.3	Fuel Load Positions . . . . .	9
3.4	Dimensioned Floor Plan & Image of the Compartment . . . . .	10
3.5	Fixed Instrumentation Layout for the Compartment Experiments . . . . .	11
3.6	Locations of Ceiling Jet BDPs . . . . .	12
4.1	Furniture Designs Used as Experimental Fuel Loads . . . . .	25
5.1	Comparison of Temperature Predictions to Experimental Data Collected in Compartment Experiments with Burners . . . . .	29
5.2	Comparison of Temperature Predictions to Experimental Data Collected in Compartment Experiments with Furniture . . . . .	31
5.3	Comparison of Layer Temperature Predictions to Experimental Data Collected in Compartment Experiments with Burners . . . . .	33
5.4	Comparison of Layer Temperature Predictions to Experimental Data Collected in Compartment Experiments with Furniture . . . . .	35
5.5	Comparison of Layer Interface Elevation Predictions to Experimental Data Collected in Compartment Experiments with Burners . . . . .	37
5.6	Comparison of Layer Interface Elevation Predictions to Experimental Data Collected in Compartment Experiments with Furniture . . . . .	39
5.7	Comparison of Flame Height Predictions to Experimental Data Collected in Compartment Experiments with Burners . . . . .	41
5.8	Comparison of Flame Height Predictions to Experimental Data Collected in Compartment Experiments with Furniture . . . . .	43
5.9	Comparison of Heat Flux Predictions to Experimental Data Collected in Compartment Experiments with Burners . . . . .	45
5.10	Comparison of Heat Flux Predictions to Experimental Data Collected in Compartment Experiments with Furniture . . . . .	46
5.11	Comparison of Velocity Predictions to Experimental Data Collected in Compartment Experiments with Burners . . . . .	49
5.12	Comparison of Velocity Predictions to Experimental Data Collected in Compartment Experiments with Furniture . . . . .	51
5.13	Comparison of Oxygen Concentration Predictions to Experimental Data Collected in Compartment Experiments with Burners . . . . .	52
5.14	Comparison of Oxygen Concentration Predictions to Experimental Data Collected in Compartment Experiments with Furniture . . . . .	54

# List of Tables

3.1	Summary of Compartment Experiments . . . . .	9
4.1	Material Properties Used in Models . . . . .	22
4.2	Radiative Fraction Calculated for Each Fuel Package . . . . .	23
4.3	Grid Resolution Metrics . . . . .	26
5.1	Color Code for Bias and Uncertainty Tables . . . . .	28
5.2	Model Fitness Metrics for Temperature in Compartment Burner Experiments . . .	30
5.3	Model Fitness Metrics for Temperature in Compartment Furniture Experiments . .	32
5.4	Model Fitness Metrics for Layer Temperature in Compartment Burner Experiments	34
5.5	Model Fitness Metrics for Layer Temperature in Compartment Furniture Experi- ments . . . . .	36
5.6	Model Fitness Metrics for Layer Interface Elevation in Compartment Burner Ex- periments . . . . .	38
5.7	Model Fitness Metrics for Layer Interface Elevation in Compartment Furniture Experiments . . . . .	40
5.8	Model Fitness Metrics for Flame Height in Compartment Burner Experiments . .	42
5.9	Model Fitness Metrics for Flame Height in Compartment Furniture Experiments .	44
5.10	Model Fitness Metrics for Heat Flux in Compartment Burner Experiments . . . .	47
5.11	Model Fitness Metrics for Heat Flux in Compartment Furniture Experiments . . .	48
5.12	Model Fitness Metrics for Velocity in Compartment Burner Experiments . . . . .	50
5.13	Model Fitness Metrics for Velocity in Compartment Furniture Experiments . . . .	50
5.14	Model Fitness Metrics for Oxygen Concentration in Compartment Burner Experi- ments . . . . .	53
5.15	Model Fitness Metrics for Oxygen Concentration in Compartment Furniture Ex- periments . . . . .	55

# List of Abbreviations

AF	Above floor
ATF	Bureau of Alcohol, Tobacco and Firearms
BC	Below ceiling
BDP	Bi-directional probe
CFAST	Consolidated Model of Fire and Smoke Transport
CFD	Computational Fluid Dynamics
EPRI	Electric Power Research Institute
FIVE	Fire Induced Vulnerability Evaluation
FDS	Fire Dynamics Simulator
FDTs	Fire Dynamics Tools
HGL	Hot Gas Layer
HRR	Heat Release Rate
HRRPUA	Heat Release Rate per Unit Area
HRRPUL	Heat Release Rate per Unit Length
NBS	National Bureau of Standards
NFPA	National Fire Protection Association
NIJ	National Institute of Justice
NIST	National Institute of Standards and Technology
NRC	Nuclear Regulatory Commission
PUF	Polyurethane Foam
RI	Resolution Index
SI	International System of Units
TC	Thermocouple
UL	Underwriters Laboratories
UL FSRI	UL Firefighter Safety Research Institute
V&V	Verification and Validation
VTT	Technical Research Centre of Finland

# Acknowledgments

This project was supported by Award No. 2017-DN-BX-O163, provided by the National Institute of Justice, Office of Justice Programs, U.S. Department of Justice. The opinions, findings, and conclusions or recommendations expressed in this publication are those of the author(s) and do not necessarily reflect those of the Department of Justice.

The authors would also like to acknowledge Kelly Opert and the technical staff of the UL Large Fire Lab for their assistance in preparing and conducting the full-scale experiments. Staff that provided particularly valuable assistance include Andres Sarmineto, Jeff Mlyniec, Eric Anderson, and Derek Dziekonski. These experiments would not have been possible without the support of the UL FSRI team. The UL FSRI team instrumented, conducted, and collected data from these experiments. Special thanks go to Craig Weinschenk and Jack Regan of UL FSRI, and Roy McLane of Thermal Fabrications.

# Abstract

Fire investigations are an integral piece of a holistic fire protection strategy that has been developed to improve the safety of the built environment for occupants. The use of fire dynamics analyses that utilize specialized fire dynamics routines, zone fire models, and field fire models is encouraged in the course of an investigation. In these analyses, there is a need to understand the accuracy of the models, the inherent uncertainties in each model, and the limitations of application of the fire models to ensure a given model is appropriate and physical phenomena are accurately represented. This work is focused on conducting an engineering assessment of three types of models that are commonly used in fire investigations on the ability of each to predict characteristics of the fire environment generated from gas burners and modern upholstered furniture composed of synthetic materials in a compartment with a single entrance. A quantitative analysis of the accuracy of predicting plume and compartment temperatures, flow velocities, flame heights, heat fluxes, the elevation of the interface between the upper and lower layers in the compartment, and oxygen concentrations is provided for each model.

The specialized fire dynamics routines were capable of accurately characterizing the flame height, but did not accurately predict the other quantities for the furniture-fueled fire experiments conducted in the compartment. The zone fire model accurately predicted the layer interface heights, layer temperatures, flame heights, and oxygen concentrations in the compartment fire scenarios. The field model predicted accurate temperatures throughout the compartment, layer interface heights, velocities through the open door of the compartment, flame heights, and oxygen concentrations. In general, the predictive ability of all the models was better in the gas burner experiments than in the furniture experiments. More research is needed to develop recommendations on geometry and burning definitions for upholstered furniture in field models as well as improved methods for model practitioners to predict heat flux.

# 1 Introduction

Fire investigations are an integral piece of a holistic fire protection strategy that has been developed to improve the safety of the built environment for occupants. Investigations provide a means to identify the cause of a fire as well as collect data that may provide insight about the development and spread of the fire. By determining the cause of a fire and identifying products and phenomena that contributed to fire spread, investigators may be able to prove guilt or innocence in criminal proceedings, assign blame in civil proceedings, or contribute to the knowledge base that may inform the fire protection and safety community in future designs, effectively reducing the losses from fires. Data such as the area of fire origin, the time until target materials or products ignite, the time to flashover of a compartment, the influence of ventilation on the dynamics of the developing fire, and the ultimate cause of the fire are critical to understanding and reducing the number and severity of fires.

Fire models are increasingly relied upon in fire investigations, the design process, and scientific studies to test hypotheses and improve the understanding of fire dynamics and fire-induced fluid flows. Models that are currently available range in complexity from simple algebraic heuristics that are derived from fundamental physical concepts and empirical data to generalized, physics-based computational fluid dynamics (CFD) codes that require a wide range of property values as inputs and may require significant computational resources. Due to the complexity of fire phenomena, empirical correlations are often adopted in various sub-models within CFD codes to reduce the computational expense of fire dynamics analyses.

NFPA 921 *Guide for Fire and Explosion Investigations* encourages the use of fire dynamics analyses that utilize specialized fire dynamics routines (simple heuristics), zone fire models, and CFD (field) fire models to answer specific questions that arise in the course of an investigation. NFPA 921 emphasizes the need to understand the uncertainties inherent in each potential model as well as the limitations of fire models to ensure a given model is appropriate and physical phenomena are accurately represented [1]. This work is focused on evaluating three types of models that are commonly used in fire investigations on the ability of each to predict characteristics of the fire environment generated from gas burners as well as burning modern upholstered furniture composed of synthetic materials.

## 1.1 Motivation

Many of the heuristics and correlations that are used in fire dynamics analyses rely on experimental data collected in tests conducted with a gas burner or a liquid pool fire source and have had minimal, if any, validation against data collected in experiments with solid fuel packages. Additionally, studies conducted to validate field models and zone models generally use laboratory fuels as fire sources to minimize the contribution of uncertainty in the heat release rate, combustion by-product

yields, and fuel configuration effects to the total uncertainty of all measurands over the course of the experiments. Because of the relative lack of data collected in experiments conducted with upholstered furniture fuel packages, the efficacy of these models to describe the fire environment generated by furniture-fueled fires is uncertain.

The materials used in the manufacturing of typical upholstered furniture have changed over the past few decades as synthetic polymers have proliferated all industries due to the low cost of these materials relative to the natural materials used in legacy designs. This change has largely resulted in petroleum-based materials with relatively high heating values displacing natural materials throughout the built environment. This shift in the upholstered furniture industry has contributed to a phenomenon in which modern residential occupancies facilitate more rapid fire growth than residential occupancies did in the mid-to-late 1900s [2].

Every household in the U.S. contains an average of approximately four pieces of upholstered furniture [3, 4]. The ubiquity of upholstered furniture throughout the built environment makes it a primary fuel source in residential fires. From 2010 to 2014, there was an average of 5,360 structure fires per year in the U.S. in which upholstered furniture was the first item ignited. These fires accounted for an average of 440 civilian deaths, 700 civilian injuries, and an estimated \$269 million in direct damage annually [5]. It was also estimated that between 2006 and 2010, residential fires in the U.S. in which an item of upholstered furniture was not the first item ignited, but was the primary fuel source accounted for an additional 2,200 residential fires and 130 civilian deaths annually [6]. Similar trends are evident in Europe, where furniture fires account for an estimated 6% of all residential fires and 15% of fatalities from fires [7]. Particularly important to the fire investigation community were the approximately 890 residential fires that originated from intentionally ignited furniture in the U.S. annually from 2010 to 2014 [8].

An objective assessment of the ability of the analytical and computational tools to perform fire dynamics analyses is required to develop an understanding of the uncertainties and limitations associated with the tools. This exercise also helps to evaluate the level of confidence in applying the tools in situations that may be outside of the conditions at which the tools were developed and have been validated. The assessment of these tools and development of recommendations for fire investigators to use in analyses involving residential structure fires will support the appropriate use of mathematical models in fire investigations. In this work, experiments compartment fires fueled by natural gas burners and upholstered furnishings were conducted to assess the accuracy of a range of predictive fire algorithms and models.

## 2 Literature Review

Several research efforts have been undertaken to evaluate the predictive capabilities of the models available for characterizing the dynamics of fire scenarios. In 2002, Floyd conducted a study in which hand calculations and computational zone and field models were validated against data collected in propane burner and oil pool fire experiments conducted in compartments within a decommissioned nuclear reactor building [9]. It was concluded that hand calculations yielded relatively imprecise, yet useful information when they were applied within the limits of their underlying assumptions. The zone model generally predicted near-field phenomena more accurately than far-field phenomena, but also yielded some problematic predictions in the near-field as well. The field model showed promise for predicting detailed information that zone models and hand calculations were and still are incapable of predicting.

In 2006, Rein et al. conducted a study in which real fire scenarios were modeled using a simplified analytical model, a zone model, and a field model [10]. Each model was parameterized with data collected during a forensic investigation of each scenario, and it was noted that the input parameters were independent of each other, in part to show the sensitivity of the model predictions to variation in inputs. It was concluded that each model was capable of accurately predicting simple aspects of the fires in the early stages of fire growth, but the models diverged at later stages of the fire. The analytical model provided reasonable results, but it was noted that only the field model had the capability of representing flame spread.

The U.S. Nuclear Regulatory Commission (NRC) funded model validation research conducted by the NRC, National Institute of Standards and Technology (NIST), and the Electric Power Research Institute (EPRI) that culminated in 2007. The aim of the research was to validate the predictive capabilities of field, zone, and simple fire dynamics analysis models that are all currently used in nuclear power plants [11]. Empirical correlations in the form of closed-form algebraic expressions collected in a group called the Fire Dynamics Tools (FDTs) [12] as well as a collection of algebraic engineering calculations referred to as Fire Induced Vulnerability Evaluation (FIVE) [13] were validated against experimental data. Additionally, the zone fire models Consolidated Model of Fire Growth and Smoke Transport (CFAST) developed by NIST and MAGIC developed by Electricite de France, and the field model Fire Dynamics Simulator (FDS) developed by NIST were validated against the same corpus of data. The validation data were collected from several experimental series in which almost all used liquid or gaseous fuel as the fire source. A single experimental series used mattresses and chairs, but the maximum heat release rate (HRR) in these experiments was approximately 350 kW.

It was concluded that measured room pressures, oxygen concentrations, flame heights, plume temperatures, ceiling jet temperatures, hot gas layer heights, and hot gas layer temperatures were predicted approximately within experimental uncertainty by the zone and field models. Flame height was also accurately predicted by the empirical correlations investigated in the study. Smoke concentrations, target temperatures, radiant heat fluxes, total heat fluxes, and wall temperatures were physically represented by the zone and field models, but the error in the predictions was outside

the experimental uncertainty.

Overholt conducted a study in 2014 that involved validation of the set of empirical correlations collected in the FDTs [14]. The data used in the validations were collected in experiments conducted in compartments that had been compiled for validation of FDS. The fuels for the fires in the experiments were primarily hydrocarbon, with few experiments collected in experiments that involved upholstered furniture. The results of the study indicated generally good agreement between the correlation predictions and the peaks of the experimental data, although many of the comparisons of the quantities exhibited significant scatter.

A supplement to the NRC study was published in 2016 that expanded the scope of the verification and validation (V&V) and utilized more developed versions of the computational models [15]. It was cautioned in the conclusions of the supplemental study that empirical correlations should only be used within their stated limitations and range of applicability. It was also concluded that the newer versions of the zone and field models and the validation data added to the corpus in the interim increased the range of applicability for both types of models.

Janssens et al. conducted a study in 2012 aimed at evaluating and reducing uncertainty in characterizing upholstered furniture fires [16]. The authors conducted experiments on chair and chair mock-ups constructed of permutations of two fabrics and six padding materials. Bench-scale experiments were also conducted on the component materials. The data collected in full-scale furniture mock-up experiments and bench-scale tests were used to assess the predictive capability of several empirical upholstered furniture burning rate models and to make modifications as necessary. The authors also used FDS and CFAST to determine modifications required for the empirical models to describe the HRR of the furniture to yield the most accurate results. Additional experiments were conducted on used upholstered furniture to validate the produced models. The authors concluded with recommendations of methods for fire investigators to predict upholstered furniture HRRs. It was determined that ignition source and ignition location have a significant effect on the burning rate and HRR histories and that FDS and CFAST accurately predict the hot upper gas layer temperature when the HRR of the furniture item is accurately represented.

# 3 Description of Experiments

A series of experiments were conducted with gas burners and upholstered furniture inside a compartment. Temperatures and velocities of the ceiling jet, plume, and the flow through the door opening, and oxygen concentrations in the compartment experiments were also collected. Experiments were conducted at the UL Large Fire Lab in Northbrook, IL. The experiments and fuel loads are described in more detail in the following sections.

## 3.1 Fuel Loads

Experiments were performed with two sizes of gas burners, one upholstered chair design, and one upholstered sofa design. Figure 3.1 displays photographs of the gas burners that were used in the gas burner experiments. Both gas burners had a square cross-section with the surface of the large burner elevated 0.5 m above the floor and the surface of the small burner elevated 0.65 m above the floor. The cross-section side length of the smaller burner was 0.3 m and the cross-section side length of the larger burner was 0.6 m. The burners were fueled by natural gas supplied to the laboratory from the local gas utility company. For experiments conducted at the NIST facility, the chemical composition of the gas was provided as 95% methane, 3.4% ethane, 0.3% propene, with the balance trace gases and no nitrogen or carbon dioxide. The heat of combustion of the natural gas supplied to the NIST experimental facility was approximately 46,900 kJ/kg. The composition at the UL facility was approximately 92.2% methane, 5.8% ethane, 1.3% nitrogen, and 0.7% carbon dioxide with a heat of combustion of approximately 53,100 kJ/kg. The composition of the natural gas supplied to the ATF facility was unknown, but the heat of combustion was measured as approximately 53,400 kJ/kg. For experiments in which a gas burner was used, ignition was achieved via a pilot light and the opening of a valve to allow natural gas to flow to the burner. In the experiments with furniture, ignition of the furniture item was performed via an electric match.



(a) 0.3 m Natural Gas Burner



(b) 0.6 m Natural Gas Burner

Figure 3.1: Image of the natural gas burners used during experiments.

Figure 3.2 displays the chair designs that served as the fuel sources for the compartment experiments. The “Red Accent Chair” was approximately 0.71 m wide, 0.76 m deep, and approximately 0.88 m high with a seat height of 0.45 m. The outer covering of the Red Accent Chair was polyester, and the frame of the chair was constructed from wood. The cushions of the chair were comprised of polyurethane foam covered by polyester batting on its top and bottom. The mean mass of the Red Accent Chair was  $20.4 \text{ kg} \pm 0.3 \text{ kg}$ . The Red Accent Chair was also a fuel source in the compartment experiments.

The “Overstuffed Sofa” was approximately 2.26 m wide, 0.97 m deep, and approximately 0.96 m high with a seat height of 0.55 m. The construction of the Overstuffed Sofa was identical to the Overstuffed Chair in that the outer covering was polyester, the frame was oriented strand board, and the cushions consisted of polyurethane foam covered by polyester batting on both sides. The average mass of the sofa across experiments was  $49.1 \text{ kg} \pm 0.8 \text{ kg}$ . The Overstuffed Sofa was also a fuel source in the compartment experiments.



(a) Red Accent Chair



(b) Overstuffed Sofa

Figure 3.2: Images of the upholstered sofas utilized during experiments.

## 3.2 Instrumentation

HRR data were measured during all experiments conducted with the compartment door open. The UL oxygen consumption calorimetry hood had a diameter of 7.6 m and was positioned approximately 7.6 m above the floor. In a previous study, Bryant and Mullholland estimated the total expanded uncertainty of oxygen consumption calorimeters during full-scale fire experiments to be  $\pm 11\%$  [17]. The authors identified several sources of error within the calorimeter, with one of the primary sources being the uncertainty of the gas concentration measurements.

Nominal 25 mm diameter, water-cooled Schmidt-Boelter gauges were utilized to measure the total heat flux at several locations in the experiments. Zirconium plates were installed over the faces of select gauges to prevent heat flux contributions from convection to exclusively measure radiant heat flux incident to the gauge. These gauges are referred to as radiometers throughout the remainder of this report. Results from an international study on total heat flux gauge calibration and response demonstrated that the total expanded uncertainty of a Schmidt-Boelter gauge is typically  $\pm 8\%$  [18].

Bi-directional probes (BDPs) paired with type K, inconel-sheathed thermocouples with nominal diameters of 1.6 mm were utilized to measure gas flow velocity. The stainless steel probes were connected to Setra Model 264 differential pressure transducers ( $\pm 125$  Pa measurement range). A previous gas velocity measurement study focused on flow through doorways during pre-flashover compartment fires yielded total expanded uncertainties ranging from  $\pm 14\%$  to  $\pm 22\%$  for measurements from BDPs similar to those described here [19]. Therefore, the total expanded uncertainty for gas velocity measured during these experiments is estimated to be  $\pm 18\%$ .

Arrays of bare-bead thermocouples were positioned throughout the compartment. Thermocouple measurements may be affected by imperfect weldments between the dissimilar metals, radiative

heat transfer from the fire source or the hot gas layer, and small variations in orientation along the thermocouple array. Theoretical error as high as approximately 11% (measured in Celsius) for upper layer temperatures and significantly higher for lower layer temperatures measured using bare-bead type-K thermocouples with bead diameters ranging from 1 mm to 1.5 mm have been reported by researchers at NIST [20, 21]. The total expanded relative uncertainty associated with the temperature measurements from these experiments is estimated to be  $\pm 15\%$ .

Gas samples were collected through stainless steel tubes to measure oxygen ( $O_2$ ) concentration. After they were collected from the interior of the compartment, the gas samples were drawn through a coarse, 2 micron paper filter followed by a condensing trap to remove moisture. Then, they passed through a high-efficiency particulate air filter before oxygen concentrations of the samples were measured by Servomex  $O_2$  Analyzers. Based on a study by Lock et al. [22], the estimated total expanded uncertainty of the  $O_2$  concentration data is considered to be  $\pm 12\%$ .

In addition to the instrumentation discussed in this section, videos of the experiments were recorded and a machine learning algorithm was deployed to determine the mean flame heights (50% visual intermittency). Additional information about the algorithm and flame height determination is available in a related report [23]. The machine learning algorithm employed an object detection model that returned the known heights of a calibration standard within  $\pm 0.08$  m. Due to the accuracy of this model, the total expanded uncertainty of the flame heights presented in this work is estimated to be  $\pm 6\%$ .

### 3.3 Compartment Experiments

A total of 117 experiments were conducted with gas burners and furniture items inside a simple compartment constructed under a large hood equipped with oxygen consumption calorimetry. The compartment was instrumented throughout to characterize the fire environment during the experiments. The effect of the location of the fuel package on the fire environment as well as the ventilation conditions were investigated in this set of experiments. The door to the compartment was either open or closed through the entirety of each experiment.

Experiments were conducted with the fuel item in four distinct locations within the compartment. The locations are referenced as the center, side, corner, and back of the compartment and are presented in Figure 3.3. A summary of the set of configurations for the compartment experiments are organized by fuel type in Table 3.1. Almost every combination of fuel, location, and state of the door was tested in triplicate. Additional information about the experiments and the results are presented in a related report [23].

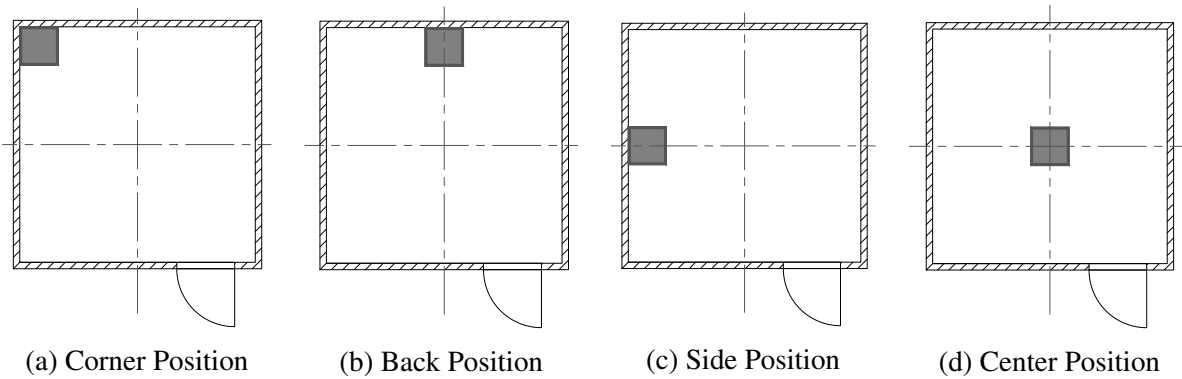


Figure 3.3: Schematics showing the four positions of the fuel (represented by the gray square).

Table 3.1: Summary of Compartment Experiments

Fuel	Door Status	Fuel Position(s)	Experiments per Configuration
0.3 m Burner at 100 kW	Open, Closed	Corner, Back, Side, Center	3
0.6 m Burner at 100 kW	Open, Closed	Corner, Back, Side, Center	3
0.6 m Burner at 250 kW	Open, Closed	Corner, Back, Side, Center	3
0.6 m Burner at 500 kW	Open, Closed	Back, Side, Center	3
0.6 m Burner at 500 kW	Open, Closed	Corner	1
Red Accent Chair	Open, Closed	Corner, Center	3
Red Accent Chair	Open, Closed	Back	1
Overstuffed Sofa	Open, Closed	Corner	3
Overstuffed Sofa	Open	Back	3
Overstuffed Sofa	Closed	Back	1

### 3.3.1 Structure

Experiments were conducted inside a compartment with interior dimensions of 3.66 m by 3.66 m and a ceiling height of 2.44 m. The wall frames of the compartment were constructed with 18 gauge steel studs with an 89 mm web depth and were spaced 0.4 m on center. The ceiling frame was constructed from 18 gauge joists with an approximate 0.15 m web depth and were spaced 0.4 m on center. A layer of approximately 16 mm thick Type X gypsum board was attached to the steel frame. The ceiling and walls were lined on the interior with approximately 13 mm thick Type I marinite board. The floor of the compartment was covered with approximately 13 mm thick cement board. There was a ventilation opening at the front of the compartment in the form of a doorway measuring 2.0 m high by 0.9 m wide. The door and frame were composed of steel and had a 45 minute fire rating. The interior side of the door and frame were covered with a layer of Kaowool approximately 25 mm thick. A dimensioned floor plan view of the compartment and an image of the exterior of the compartment are presented in Figure 3.4.

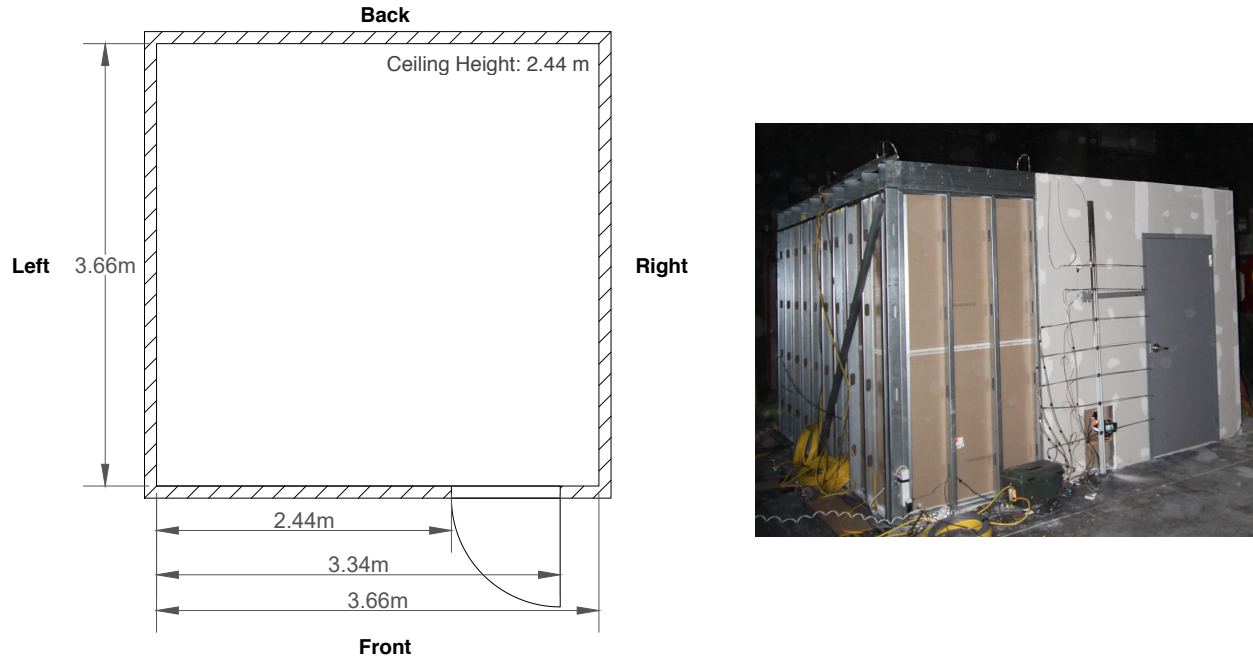


Figure 3.4: Dimensioned floor plan and image of the compartment utilized during the experiments. The image is a view of the front left corner from the compartment exterior.

## Leakage

To characterize ventilation within the experimental compartment, a leakage test was conducted with all exterior vents closed. The standard test method described in ASTM E 779 *Standard Test Method for Determining Air Leakage Rate by Fan Pressurization* was followed to determine the air changes per hour and the equivalent leakage area [24]. The leakage from the compartment was 2.75 air changes per hour (ACPH) at 50 Pa with an effective leakage area of approximately 0.0019 m<sup>2</sup> at 4 Pa. This effective leakage area was calculated with Equation 3.1 and Equation 3.2, assuming a pressure exponent,  $n$ , of 0.65, which is the approximate mean pressure exponent for single-family homes in the United States [25].

$$A_L = \dot{V}_L \sqrt{\frac{\rho}{2|p_{test}|}} \quad (3.1)$$

$$A_{L,eff} = A_L \left( \frac{p_{ref}}{p_{test}} \right)^{n-0.5} \quad (3.2)$$

Appendix A of NFPA 92 *Standard for Smoke Control Systems* provides a table of typical leakage ratios collected from experimental research conducted on commercial and multi-family structures. According to NFPA 92, the effective leakage area for the compartment used in these experiments would be 0.0016 m<sup>2</sup> for tight construction, 0.0056 m<sup>2</sup> for average construction, 0.012 m<sup>2</sup> for loose construction, and 0.041 m<sup>2</sup> for very loose construction. The leakage rate calculated for the

compartment in these experiments is between tight and average construction.

### 3.3.2 Instrumentation

Figure 3.5 displays a dimensioned plan view of the experimental compartment with the locations of the fixed instrumentation denoted by symbols. Total and radiative heat flux to the right side wall were measured by gauges centered along the wall and positioned 0.65 m and 1.3 m below the ceiling. These total heat flux gauges and radiometers, represented by the blue diamond and red pentagon in Figure 3.5, were installed such that their faces were flush with the interior side of the wall. Additionally, a pair of gauges at identical heights were used to measure the total heat flux from the fire plume to the nearest wall during experiments in which the fuel load was against a wall (i.e., at the corner, back, or side location). These two gauges were also flush with the interior surface of the wall and were aligned with the center of the fuel load. These gauges are not displayed in the figure because their locations moved when the fuel location changed.

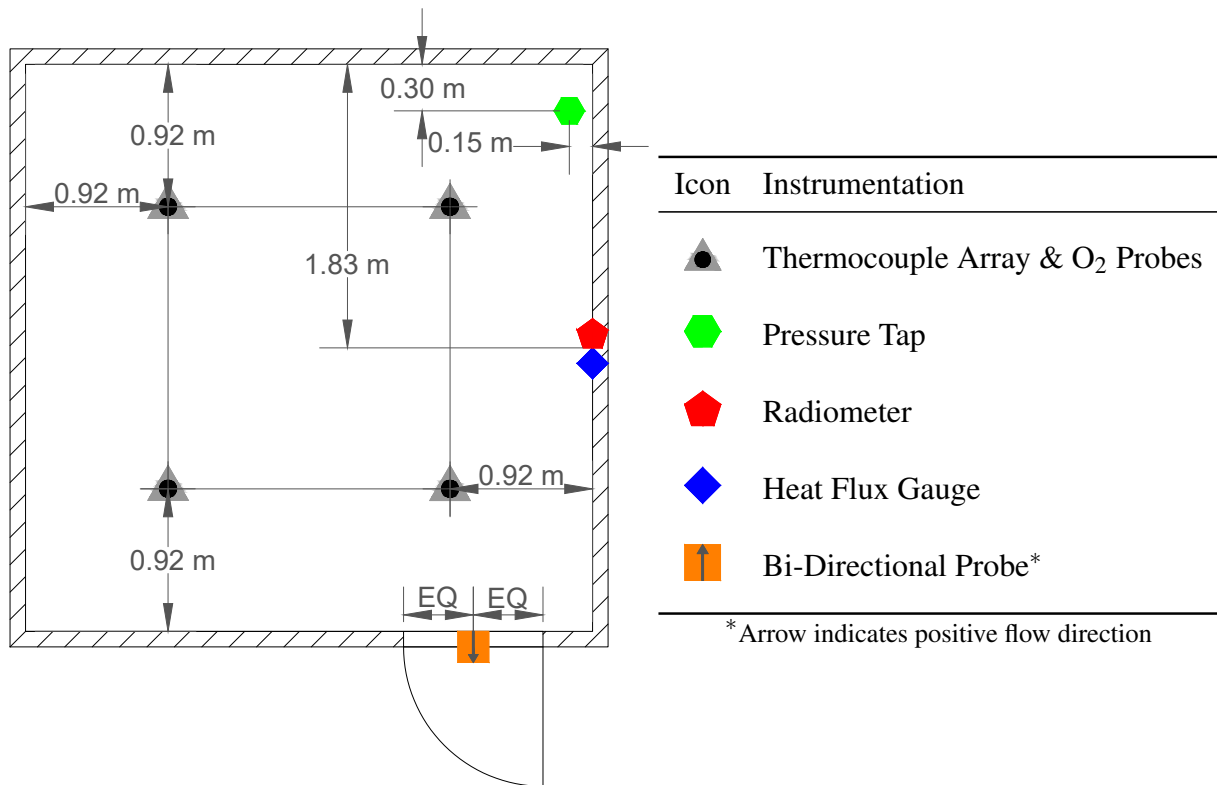


Figure 3.5: Floor plan showing location of fixed instrumentation for the compartment experiments.

BDPs paired with thermocouples were installed at the door opening to measure the flow velocity through the compartment doorway during open door experiments. These BDPs, represented by the orange square in Figure 3.5, were installed along the exterior side of the compartment and positioned so that they were horizontally-centered in the doorway. The seven BDPs were spaced 0.25 m apart between the top of the doorway and the floor. Additionally, during experiments in

which the fuel load was against a wall (i.e., at the corner, back, or side location), two BDPs paired with thermocouples located 0.65 m and 1.3 m below the ceiling were positioned over each fuel load to measure the gas velocity and temperature within the fire plume.

BDPs and paired thermocouples were also installed 0.3 m below the ceiling. These BDPs were positioned such that they were directed radially away from the burner or furniture item and were intended to characterize the ceiling jet within the compartment. Figure 3.6 displays the locations of the ceiling jet BDPs for each fuel position within the compartment. In the figure, the orange squares indicate the BDPs and the arrow in the square denotes the direction of positive flow.

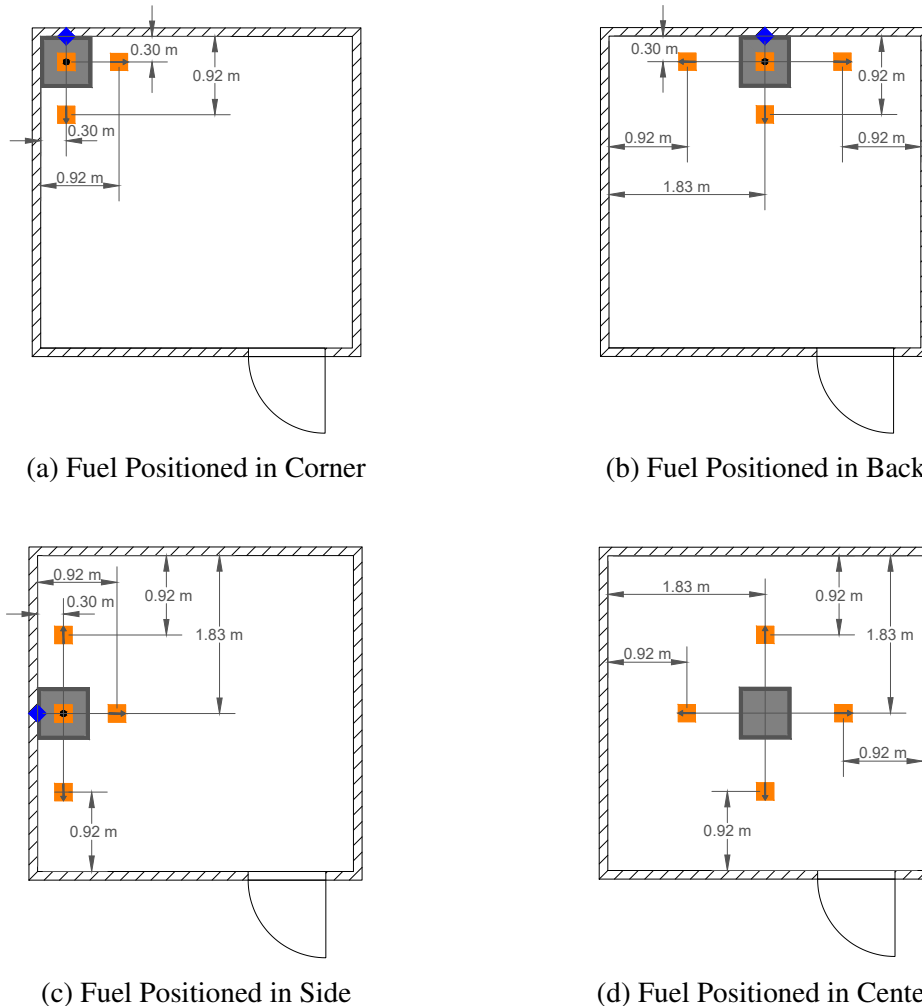


Figure 3.6: Locations of paired BDPs and thermocouples intended to characterize the ceiling jet in compartment experiments

Copper sampling tubes that acted as pressure taps were positioned 0.3 m, 1.2 m, and 2.1 m below the ceiling at the location marked by the green hexagon in Figure 3.5. The probes were horizontally-aligned approximately 0.3 m from the back wall and 0.15 m from the right side wall.

Four vertical arrays of type K, bare-bead thermocouples with nominal diameters of 0.5 mm were

installed in the compartment. Each array contained eight thermocouples positioned at 25 mm, 0.3 m, 0.6 m, 0.9 m, 1.2 m, 1.5 m, 1.8 m, and 2.1 m below the compartment ceiling. These arrays were centered in each quadrant of the compartment, as shown in Figure 3.5. Gas samples were collected through stainless steel tubes located 0.6 m and 1.8 m below the ceiling at the center of each quadrant as shown in Figure 3.5.

HRR and flow velocities through the door opening were not measured for experiments conducted with the door to the compartment closed. Video analysis of the flame height was not possible when the fuel was positioned in the center location because the field of the video frame was limited at the available distance and there was no reference against which flame heights could be compared, so mean flame height data was unavailable for these experiments. The smoke layer development in the closed door experiments obstructed the view of the fire plume, which limited the amount of time for which flame height data could be collected.

### Determination of Layer Temperatures and Interface Elevation

A method developed by Janssens and Tran [26] to estimate the upper gas layer and lower gas layer temperatures as well as the elevation of the interface between the two layers from a continuous, vertical profile of temperature was used to estimate these quantities from data collected in experiments conducted in the compartment described in this report. This method has also been adopted by the developers of FDS for fire model validation.

Data from the quadrant thermocouple arrays were used to define  $T(z)$ , a continuous function that designates temperature ( $T$ ) as a function of height above the compartment floor ( $z$ ) where  $z = 0$  at the floor and  $z = H$  at the ceiling. Then, the upper layer temperature ( $T_u$ ), the lower layer temperature ( $T_l$ ), and the height of the interface between the two layers ( $z_{int}$ ) were estimated at each time step by computing  $I_1$  and  $I_2$  as in Equation 3.3 and Equation 3.4.

$$I_1 = \int_0^H T(z) dz = (H - z_{int})T_u + z_{int}T_l \quad (3.3)$$

$$I_2 = \int_0^H \frac{1}{T(z)} dz = (H - z_{int})\frac{1}{T_u} + z_{int}\frac{1}{T_l} \quad (3.4)$$

The definitions of  $I_1$  and  $I_2$  were combined into the form of Equation 3.5, which was solved to determine the interface elevation ( $z_{int}$ ). In these equations,  $T_l$  is the temperature measured by the thermocouple nearest to the floor and  $T_u$  is defined according to Equation 3.6. The total expanded uncertainty of the layer interface height was estimated as  $\pm 14\%$  [27].

$$z_{int} = \frac{T_l(I_1 I_2 - H^2)}{I_1 + I_2 T_l^2 - 2T_l H} \quad (3.5)$$

$$(H - z_{int})T_u = \int_{z_{int}}^H T(z)dz \quad (3.6)$$

# 4 Predictive Fire Algorithms & Models

When choosing a model, it is useful to understand the input data needed for the model and the sensitivity of the model to uncertainties in the input parameters. In this section, model inputs are discussed and the results of sensitivity analyses for the models are reviewed.

Three types of models were used in this study to predict the fire environment generated by the experiments described in Section 3. These models included simple fire dynamics analyses in the form of algebraic expressions coded into spreadsheets, a zone fire model, and a field fire model. Data collected at steady state for each set point HRR were compared across each modeling method for the gas burner experiments. Because most of the algebraic expressions provided a single predicted value based on a single HRR, it was necessary for the experiments conducted with furniture that a representative HRR be defined. In these cases, the maximum HRR, the mean HRR, and the steady HRR in the decay phase were used to predict the desired measurands, which were compared to corresponding maximum, mean, and steady values of the measured quantities as well as the quantities predicted by the field and zone models.

## 4.1 Model Background

The models used in this study represent the three categories of models identified in NFPA 921. These models can be used to conduct fire dynamic analyses to test hypotheses regarding fire origin and development. The three categories of models are: specialized fire dynamics routines, zone models, and field, or CFD, models [1]. Further, each of the models chosen for this assessment are currently maintained and undergo verification and validation checks as part of the NRC and NIST program.

### 4.1.1 NRC Fire Dynamics Tools

The Fire Dynamics Tools (FDTs) is a set of quantitative methods that were originally compiled by the NRC to allow fire protection inspectors to quickly and easily conduct fire hazard analyses [12]. A collection of spreadsheets were developed to facilitate fire dynamics analyses using the FDTs. The convenience of these spreadsheets has led to adoption of the FDTs as a tool that is commonly used by investigators conducting fire dynamics analyses. The equations presented in this section require standard units as defined by the International System of Units (SI).

## Hot Gas Layer Temperature & Height

The collection of FDTs includes correlations for hot gas layer temperatures and interface height. A method for predicting hot gas layer temperature in a compartment with a single vertical wall opening with natural ventilation known as the Method of McCaffrey, Quintiere, and Harkleroad (MQH) is included in the collection of FDTs. The MQH method was derived based on an energy balance for a simplistic compartment fire scenario. Empirical constants in the functional form of the MQH correlation were determined based on analysis of 112 experiments with cellulosic and synthetic polymer sheets and cribs as well as gaseous hydrocarbon fuels in compartments with heights that ranged from 0.3 m to 2.7 m. The authors of the study indicated that the plume theory correlation used to derive the temperature rise correlation does not hold in scenarios in which the temperature rise in the upper gas layer exceeds 600°C [28]. In deriving the correlation for upper layer temperature, the study authors did not consider fire locations that deviated significantly from the center of the compartment, which introduces uncertainty about the ability of the correlation, as published in the FDTs, to predict the hot gas layer temperature when the fire source is located against a wall or in a corner.

The MQH correlation as it appears in the FDTs is displayed as Equation 4.1. In the equation,  $\Delta T_g$  is the temperature rise in the upper gas layer,  $\dot{Q}$  is the HRR,  $A_v$  is the total ventilation area,  $h_v$  is the height of the ventilation opening,  $A_T$  is the total surface area of the interior of the compartment less the ventilation area, and  $h_k$  is the total heat transfer coefficient. The quantity  $A_v\sqrt{h_v}$  is sometimes referred to as the ventilation factor, which will be adopted for the remainder of this report.

$$\Delta T_g = 6.85 \left[ \frac{\dot{Q}^2}{(A_v\sqrt{h_v})(A_T h_k)} \right]^{\frac{1}{3}} \quad (4.1)$$

For long periods of time in which conditions within the compartment achieve steady state,  $h_k$  is a constant defined as  $h_k = \frac{k}{\delta}$ , where  $k$  denotes the thermal conductivity of the wall lining material and  $\delta$  denotes the thickness of the wall. For times in which heat does not completely penetrate the material lining the compartment, the heat transfer coefficient may be defined as  $h_k = \sqrt{\frac{k\rho c}{t}}$ , where  $k$ ,  $\rho$ , and  $c$  are the thermal conductivity, density, and specific heat capacity of the wall lining, and  $t$  is the time after ignition.

The correlation for the hot gas layer temperature in a closed compartment was presented by Beyler in 1991 [29]. The experiments Beyler analyzed to develop the correlation were conducted in a test compartment with a 4 m x 6 m footprint and a ceiling height of 4.5 m. The fire source was a methane gas burner in the center of the room with a height ranging from 0.23 m to 2.06 m above the ground which supplied constant heat release rates (HRRs) in the range of 50 kW to 400 kW. The correlation was derived by solving a non-steady energy balance for the closed compartment that accounted for heat loss through the wall material assuming a constant HRR and ignoring energy lost through leakage. This correlation is presented as Equation 4.2. In the correlation,  $K_1$  is a constant described by Equation 4.3 where  $k$ ,  $\rho$ , and  $c$  are the thermal conductivity, density, and specific heat capacity of the wall lining material,  $m$  is the mass of gas in the compartment,  $c_p$  is the

specific heat capacity of the gas in the compartment.  $K_2$  is a constant described by Equation 4.4, where  $\dot{Q}$  is the HRR. The symbol  $t$  in Equation 4.2 is the time after ignition.

$$\Delta T_g = \frac{2K_2}{K_1^2} (K_1 \sqrt{t} - 1 + e^{-k\sqrt{t}}) \quad (4.2)$$

$$K_1 = \frac{0.8\sqrt{k\rho c}}{mc_p} \quad (4.3)$$

$$K_2 = \frac{\dot{Q}}{mc_p} \quad (4.4)$$

The Method of Yamana and Tanaka is a non-steady method to predict the height of the interface between the smoke layer and smoke-free air in a compartment with no smoke venting. The equation for the smoke layer interface was derived using a plume flow correlation and assuming the smoke layer density is constant [30]. The form of the correlation adopted for the FDTs was also derived under the assumption of a constant HRR. The correlation was validated against experiments conducted in an experimental facility with a footprint of 24 m x 30 m and a ceiling height of 26.3 m. The fire source for the experiments was an approximately 1.8 m x 1.8 m square methanol pool fire source located in the center of the facility on the floor [31]. The smoke layer height correlation is presented as Equation 4.5. In the correlation,  $k$  is a constant described by Equation 4.6 in which  $\rho_g$  is the hot gas density,  $\rho_a$  is the ambient density,  $g$  is the gravitational constant,  $c_p$  is the specific heat capacity of the air, and  $T_a$  is the ambient temperature. In Equation 4.5,  $\dot{Q}$  denotes the HRR,  $t$  is the time after ignition,  $A_c$  is the compartment floor area, and  $h_c$  is the compartment height.

$$z = \left( \frac{2k\dot{Q}^{\frac{1}{3}}t}{3A_c} + \frac{1}{h_c^{\frac{2}{3}}} \right)^{-\frac{3}{2}} \quad (4.5)$$

$$k = \frac{0.21}{\rho_g} \left( \frac{\rho_a^2 g}{c_p T_a} \right)^{\frac{1}{3}} \quad (4.6)$$

## Flame Height

The FDTs include two correlations for flame height developed by Heskestad and Thomas that represent fire plumes that are not influenced by walls, ceilings, other obstructions. The FDTs also include two correlations for fire plumes located adjacent to a wall, or in a corner of a compartment. Thomas derived the expression for flame height through a dimensional analysis accounting for temperatures and velocities in the plume as well as the entrainment rate of air into the plume. Empirical coefficients in the Thomas correlation were determined through analysis of photographic

evidence of flame heights from wood crib fire experiments conducted in an open laboratory environment [32]. The correlation derived by Thomas is displayed as Equation 4.7, where  $\dot{m}''$  is the burning rate of the fuel per unit area,  $\rho_a$  is the ambient density,  $g$  is the gravitational constant, and  $D$  is the equivalent diameter of the fire.

$$H_f = 42D \left( \frac{\dot{m}''}{\rho_a \sqrt{gD}} \right)^{0.61} \quad (4.7)$$

Heskestad derived a functional relationship between the flame height of a circular turbulent diffusion flame and several parameters associated with the geometry and chemistry of the fire source, primarily the HRR and fire source diameter. Correlation constants were determined through regression analysis of experimental data, which were mostly comprised of liquid and gaseous fuels burning in open laboratory conditions [33]. The correlation was later applied to palletized rack storage using an effective fire area and was found to reasonably represent flame heights measured from the base of the storage [34]. The correlation derived by Heskestad is displayed as Equation 4.8, where  $\dot{Q}$  is the HRR and  $D$  is the equivalent diameter of the fire.

$$H_f = 0.235\dot{Q}^{\frac{2}{5}} - 1.02D \quad (4.8)$$

Delichatsios developed the functional form of a correlation to describe the flame height from a line fire source and a two-dimensional fire source against a wall [35]. The proposed correlation was dependent primarily on the heat release rate, radiative fraction, combustion efficiency, and thermal properties of air. The correlation was simplified to the form published in the FDTs by fitting experimental data on small scale alcohol-fueled fires [36]. That form of the correlation is displayed here as Equation 4.9, where  $\dot{Q}'$  is the HRR per unit length along the wall.

$$H_f = 0.034\dot{Q}'^{\frac{2}{3}} \quad (4.9)$$

Hasemi and Tokunaga developed a correlation for the flame height in a corner using a non-dimensional HRR parameter known as the Froude number under the assumption that air may only be entrained from one side of the fire source [37]. The coefficient for the correlation developed by the study authors was determined by fitting data collected on buoyant plumes in an unconfined laboratory setting. Experiments involved square gas burners with side lengths ranging from 0.2 m to 0.5 m in a non-combustible corner. The correlation developed by Hasemi and Tokunaga is displayed here as Equation 4.10, where  $\dot{Q}$  is the HRR.

$$H_f = 0.075\dot{Q}^{\frac{3}{5}} \quad (4.10)$$

## Radiant Heat Flux to a Target

Three correlations are provided in the FDTs to determine the radiant heat flux from the fire to surrounding targets. These methods include:

1. point source fuel to target at ground level
2. solid flame radiation model to target at ground level
3. solid flame radiation model to target above ground level

The method for calculating the radiant heat flux to a target from a point source provided in the FDTs was derived as a straightforward, simplistic radiation heat transfer equation. The point source model is generally applicable for fire sources that are circular or that have a low aspect ratio radiating to far-field targets. The equation to describe the radiative heat flux from a point source is displayed here as Equation 4.11, where  $\chi_r$  is the radiative fraction,  $\dot{Q}$  is the HRR, and  $R$  is the radial distance from the center of the flame to the edge of the target. It has been suggested that the upper limit for heat fluxes that may be accurately described by the point source model is 5 kW/m<sup>2</sup> [38].

$$\dot{q}'' = \frac{\chi_r \dot{Q}}{4\pi R^2} \quad (4.11)$$

The solid flame method to calculate radiant heat flux at targets was presented by Shokri and Beyler and relies on configuration factors between the flame plume, which is assumed to be cylindrical, and the target [39]. The correlation for the solid flame model is presented as Equation 4.12, where  $F_{1 \rightarrow 2}$  is the total configuration factor. The flame height used to compute the total configuration factor is described by the Heskestad correlation, and the emissive power of the flame is estimated using a correlation derived from experimentally measured heat fluxes from liquid pool fires to external targets, presented here as Equation 4.13, where  $D$  is the effective diameter of the pool fire. A different set of configuration factors is utilized when the target is at ground level compared with an elevated target. Details of the configuration factors may be found in the original presentation of the correlation [39] or in standard references [12, 38].

$$\dot{q}'' = EF_{1 \rightarrow 2} \quad (4.12)$$

$$E = 58(10^{-0.00823D}) \quad (4.13)$$

## Centerline Temperature of a Buoyant Fire Plume

Heskestad presented a correlation for plume centerline temperature as a function of elevation from the fuel surface. The correlation was derived according to buoyant plume theory assuming all heat energy is released from a point source. Empirical coefficients in the correlations were determined through analysis of experimental data [40]. One set of experiments involved a heated air jet, and a second set of experiments involved hydrocarbon, methanol, and silicone pool fires of diameters ranging from 1.219 m to 2.438 m. The pool fire tests were conducted in a laboratory with a ceiling height of approximately 18.3 m where the pool was located a minimum of 17.7 m from the wall.

The correlation developed by Heskestad is provided as Equation 4.14. In the correlation equation,  $\dot{Q}_c$  is the convective HRR,  $T_a$  is the ambient temperature,  $g$  is the gravitational constant,  $c_p$  and  $\rho_a$  are the specific heat capacity and density of air,  $z$  is the elevation above the fire source, and  $z_0$  is the virtual origin. The virtual origin is defined in Equation 4.15, where  $D$  is the effective diameter of the fire source and  $\dot{Q}$  is the HRR.

$$T_{p(\text{centerline})} - T_a = \frac{9.1 \left( \frac{T_a}{g c_p \rho_a} \right)^{\frac{1}{3}} \dot{Q}_c^{\frac{2}{3}}}{(z - z_0)^{\frac{5}{3}}} \quad (4.14)$$

$$z_0 = -1.02D + 0.083\dot{Q}^{\frac{2}{5}} \quad (4.15)$$

### 4.1.2 Zone Models

Zone modeling was first introduced to the fire research community in the 1970s and is still widely in use today. Zone models are constructed with the assumption that the atmosphere within a computational domain may be divided into two control volumes that are well-mixed and that generally may be described by a single temperature and composition. The two control volumes are defined as an upper volume zone and a lower volume zone that are formed through buoyant stratification driven by the fire source [41]. The conservation equations for energy and mass are solved for each zone. Although pressure is not explicitly accounted for in zone models, it is accounted for implicitly in the energy conservation equations. Because of the formulation of many zone fire models and the disparity between time scales at which pressure equilibrates relative to other variables, compartment overpressures due to fire are generally not resolved. Due to the simplifying assumptions inherent in zone models, they are less computationally expensive than field models, but also suffer from a lack of accuracy when the real conditions deviate from the idealized modeled scenario.

A commonly used zone model is the NIST Consolidated Model of Fire Growth and Smoke Transport (CFAST) [42]. CFAST simulates fire growth through a time-dependent HRR definition. The mass loss rate of the fuel is calculated according to the defined HRR and heat of combustion. Rates of production of gaseous species are calculated from defined yields, an generalized assumed single-step reaction formula and the simulated mass loss rate. The heat release rate and the rate of

production of gaseous products decreases to zero when the oxygen concentration decreases below the lower oxygen limit. CFAST has the ability to model leakage to or from compartments to the surrounding atmosphere based on the pressure differential across the compartment wall. Leakage for a compartment is defined with a leakage ratio that relates the total area of leaks through the walls of a compartment to the total surface area of the walls and ceiling of the compartment.

Flame height, centerline temperature, and mass entrainment of the fire plume in CFAST are represented by the correlations developed by Heskestad [42]. Wall and corner plumes in CFAST are calculated using modified versions of the Heskestad correlations that utilize the virtual heat source concept in which the fire source is mirrored across the boundary to calculate a new virtual origin and augmented plume entrainment rate. Radiant heat transfer to defined targets is calculated through a heat transfer analysis and energy balance between the target, the six bounding surfaces in the compartment, the upper gas layer, and the lower gas layer. A companion program, Smokeview [43], is used for visualizing the results of the FDS computations

### 4.1.3 Field Models

Field models divide the computational domain into finite volumes with the assumption that the temperature, pressure, and mass fractions are uniform in each volume and that the velocity and fluxes are uniform over each surface of the volumes. Field models are capable of resolving more physical phenomena than zone models as well as transient effects in the development of fire-induced flow, but do so at a significantly higher computational cost than zone models.

The NIST Fire Dynamics Simulator (FDS) is the most commonly used field fire model in fire investigations and research. FDS is a CFD model used to simulate fire-driven fluid flow that has been developed by a multi-national team led by NIST and the Technical Research Centre of Finland (VTT) [44, 45]. FDS Version 1 was released in 2000 and has constantly been undergoing development, improvements, and validation since. FDS has undergone extensive and ongoing V&V [11, 27, 46]. The model numerically solves a form of the Navier-Stokes equations appropriate for low-speed, thermally-driven flow. The partial derivatives of the conservation equations of mass, momentum, and energy are approximated as finite differences, and the solution is updated in time on a three-dimensional, rectilinear grid. The model is open source and generalized for the widest possible set of applications. To make FDS as generalized as possible, it includes an array of submodels that represent phenomena characterized by length scales that are typically smaller or much larger than the computational grid or that cannot be explicitly described by the governing equations [44]. FDS typically uses the Large Eddy Simulation (LES) approach, which presumes that the grid resolution is sufficient to resolve the dominant eddy structures and the Deardorff submodel is used for unresolved turbulence.

FDS applies a lumped species approach to model combustion where three lumped species which represent fuel, air, and combustion products are tracked. Reaction rates are mixing-controlled [47] with a simple extinction model based on a critical flame temperature [48] by default. Thermal radiation is computed through solution of the radiation transport equation for a gray gas using the Finite Volume Method on the same grid as the flow solver. A companion program, Smokeview [43], is

used for visualizing the results of the FDS computations.

The resolution index (RI), which is the ratio of the characteristic fire diameter ( $D^*$ ) to the grid resolution ( $dx$ ), provides a metric by which model practitioners may evaluate the relative resolution of a model. The characteristic fire diameter is defined in Equation 4.16, where  $\dot{Q}$  is the HRR,  $\rho_\infty$  is the ambient air density,  $c_p$  is the specific heat capacity of air, and  $T_\infty$  is the ambient air temperature, and  $g$  is the gravitational constant. An RI between 4 and 10 is generally considered coarse resolution, 10 to 16 is considered moderate resolution, and above 16 is considered fine resolution.

The developers of FDS conducted a study to determine the optimal method to characterize the mean flame height in FDS simulations [27]. The authors developed a method whereby the HRR per unit length of elevation in the computational domain were integrated along the elevation above the fire source. The authors concluded that all available empirical flame height correlations are bounded by the elevations at which between 95% and 99% of the total HRR was realized. This method of defining the mean flame height has been adopted in this work.

$$D^* = \left( \frac{\dot{Q}}{\rho_\infty c_p T_\infty \sqrt{g}} \right)^{\frac{2}{5}} \quad (4.16)$$

## 4.2 Model Construction for Compartment Experiments

The following sections describe the model development for the compartment experiments. The input parameters that were defined for each of the modeling techniques are presented in the following sections. To develop a direct comparison for each type of model and yield the most accurate results, it was important for the material properties defined as inputs to be accurate and identical across each model. The material properties defined in Table 4.1 were used in all models for the compartment experiments.

Table 4.1: Material Properties Used in Models

Material	$k$ (W/m-K)	$c_p$ (kJ/kg-K)	$\rho$ (kg/m <sup>3</sup> )
Marinite [49]	0.12	1.17	737
Fiber Cement [50]	0.25	0.84	1380
Gypsum [51]	0.28	1.0	810
Steel [52]	54	0.47	7833
Concrete [53]	1.8	1.04	2280

## Radiative Fraction

The UL testing facility where the experiments were conducted is equipped to conduct calorimetry using the oxygen-depletion method (ASTM E2067) as well as the thermopile method (ASTM E906). These methods provide the chemical and convective HRR, respectively. With both of these quantities measured, the radiative fraction,  $\chi_r$ , of the fire that results from burning each fuel was determined. The  $\chi_r$  values presented in the following tables were determined through direct measurement of the HRR components.

Table 4.2 displays the radiative fraction that was directly determined for each fuel in preliminary experiments conducted outside the compartment. The uncertainty in the radiative fraction,  $\sigma_{\chi_r}$ , is expressed as plus or minus two standard deviations of the radiative fraction for each fuel. There were typically three replicates of each experiment conducted at the UL laboratory. The small sample size resulted in large standard deviations relative to the mean values.

Table 4.2: Radiative Fraction Calculated for Each Fuel Package

Fuel Package	$\chi_r$	$\sigma_{\chi_r}$
Red Accent Chair	0.35	$\pm 0.11$
Overstuffed Sofa	0.32	$\pm 0.10$

### 4.2.1 FDTs

The FDT methods typically required a single representative value for the HRR of the fire. Because the HRR of the furniture items evolved over a significant range over the course of the experiments, three representative values of the HRR were used in FDT predictions for the furniture experiments. The maximum, mean, and steady HRRs were calculated from the mean data of all replicates conducted over the three experimental facilities. The mean HRR was calculated over the entire duration of the mean experimental data. The steady HRR was also a mean of the data with the lower limit of the time range over which the mean was calculated defined as the time at which the mean burning rate decreased to below 36.8% ( $1/e$ ) of the peak HRR value and the rate of change of the burning rate was below 3% of the maximum rate of change of the burning rate for 30 s continuously. These criteria accounted for noise and other spurious data in the mean data. The steady HRR was always taken during the portion of the experiments in which the HRR was in decay.

The inputs required for the methods to predict heat flux, plume temperature, and flame height that are collected in the FDTs require knowledge of the geometry of the experimental setup and the HRR of the fire. The gas burners had a square cross-section, so an effective diameter was calculated that was defined as the diameter of a circular cross-section burner with an equivalent surface area. The radiative fraction of the gas burner flame was determined to be 0.23 through direct measurement.

The MQH correlation for the hot gas layer temperature requires the total surface area of the interior

of the compartment, the area and height of the doorway, and the total heat transfer coefficient. The total surface area of the compartment was 60.7 m<sup>2</sup> and the doorway had an area of 1.8 m<sup>2</sup> and a height of 2.0 m. The walls and ceiling of the compartment were lined with a 16 mm thick layer of gypsum wallboard on top of a 13 mm thick layer of marinite. The effective  $k\rho c$  for the wall lining materials was approximately 0.145 (kW/m<sup>2</sup>K)<sup>2</sup>s.

#### 4.2.2 CFAST

CFAST (Version 7.5.0) was used to construct models to simulate the gas burner and furniture experiments conducted in the compartment. The duration of the simulations was defined as 600 s and data were output at 15 s intervals. The initial and ambient temperature was defined as 15°C and the lower oxygen index was defined as 0.15. The thermal properties of marinite were defined and assigned to the walls and ceiling of the compartment. The thermal properties of the fiber cement board were assigned to the floor of the compartment. The emissivity of the marinite board and the fiber cement board was assumed to be 0.95 and defined as such.

A single vent in the front of the compartment was defined with the dimensions of the door opening for the simulations of open door experiments. A leakage ratio of 0.526 cm<sup>2</sup>/m<sup>2</sup> was defined over the walls of the compartment to simulate leakage in the closed door experiments. Targets were defined at the locations of the heat flux gauges and radiometers in the compartment experiments.

The fire source was located consistent with the experiment to be simulated at an elevation of 0.5 m. The area of the fire source was defined as 0.09 m<sup>2</sup> for the 0.3 m burner and 0.36 m<sup>2</sup> for the 0.6 m burner. The fuel chemistry was defined as methane (CH<sub>4</sub>) with a heat of combustion of 53100 kJ/kg for the simulations of the gas burner experiments. The radiative fraction for the fire was defined as 0.23. The HRR for the fire source was defined to achieve the set point HRR in 10 s and no decay period was included at the end of the simulation.

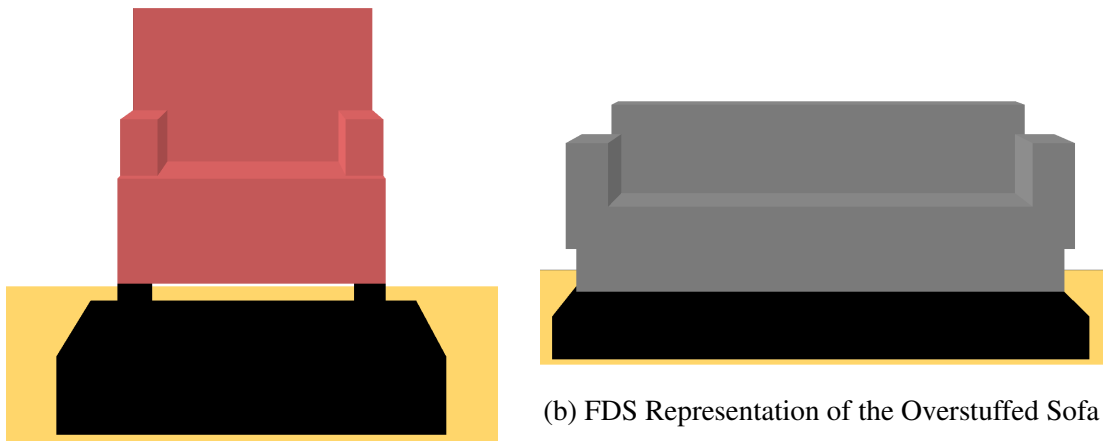
The fire sources for the furniture experiments were defined with areas that approximated the projection of the specific furniture item to the floor (i.e., 0.54 m<sup>2</sup> for the Red Accent Chair and 2.18 m<sup>2</sup> for the Overstuffed Sofa) and the elevation of the fire source was defined as the seat height. The fuel chemistry was defined with a chemical formula that approximated polyurethane (C<sub>6.3</sub>H<sub>7.1</sub>O<sub>2.1</sub>N). The heat of combustion was defined as the mean measured heat of combustion from the experiments and the soot yield was defined as 0.18. The HRR defined for each CFAST simulation mimicked the mean measured HRR for each furniture item with a resolution of 15 s.

#### 4.2.3 FDS

FDS (Version 6.7.5) was used to simulate the experiments in which the burners and furniture items were ignited in the compartment to match conditions in the laboratory as closely as possible. The fuel sources and instrumentation were positioned as geometrically similar to the experiments as possible. The ambient temperature was assumed to be 15°C in all simulations.

The gas burner was represented in each model as a supply vent attached to a solid obstruction with a predefined total mass flux that yielded the set point HRR from the experiments. The fuel for the gas burners was defined according to the chemical composition provided by the gas utility company for the experiments conducted at the UL facility (92.2% methane, 5.8% ethane, 1.3% nitrogen, and 0.7% carbon dioxide) with a heat of combustion of 53,100 kJ/kg. The sides of the burner were assigned the thermal properties of steel (see Table 4.1) with a thickness of 0.003 m.

The furniture items were represented as closely as possible to their physical dimensions while adhering to the underlying rectilinear grid. This allowed conclusions to be drawn about the importance of representing an approximation of the actual geometry for accurately predicting quantities including heat fluxes and flame height. Images of the geometric representations of the furniture items are displayed in Figure 4.1. These may be directly compared to the images presented in Figure 3.2. A single simple reaction was defined to describe combustion of the pyrolyzate released from the condensed phase sofa materials during burning. The only pyrolyzate species released was defined as polyurethane with a heat of combustion defined as approximately 16,180 kJ/kg and a soot yield of 0.18, which was the approximate mean of values that have been reported for flexible polyurethane foams [54]. For each furniture item, the heat release rate per unit area (HRRPUA) for all surfaces was defined such that the total HRR matched the mean time-dependent HRR measured in the experiments. By doing so, the model did not accurately represent the real spatial flame spread or the material burn away process, however the overall energetics of the burning process were represented.



(a) FDS Representation of the Red Accent Chair

Figure 4.1: Renderings of the upholstered chair and sofa geometries utilized in FDS simulations.

The computational domain was defined with dimensions of 3.9 m by 5.4 m by 4.8 m. This allowed the computational domain to coincide with the boundaries of the compartment and extend 1.6 m from the front of the compartment to resolve flow through the door and 2.4 m above the compartment to resolve the thermal plume that flowed out the door. All boundaries, with the exception of the ground were defined with the ‘OPEN’ surface definition. The fire source was defined consistent with the location of the fire source in the experiment to be simulated with the surface of the burner elevated either 0.5 m above the floor of the compartment (0.3 m burner) or 0.65 m above

the floor of the compartment (0.6 m burner) and the furniture items represented with geometry as similar to the actual geometries as possible. The time-dependent HRR of the furniture items for the simulations of the experiments conducted with the door open and closed was defined to follow the instantaneous mean of the measured HRR across all replicate experiments with the door open for the furniture item in the location to be simulated.

The compartment was defined as a pressure zone for the simulations of the experiments conducted with the door closed. The pressure zone leakage method was applied to assign a leakage area of 0.0019 m<sup>2</sup> to the closed door of the compartment. Two levels of resolution were investigated. Two levels of resolution were investigated. The grid was defined to be uniform throughout the computational domain with all cubic elements and cell sizes of 0.1 m and 0.05 m. These resolutions corresponded to the characteristic fire diameters and RIs provided in Table 4.3. The table indicates that simulations with a grid size of 0.1 m had coarse resolution for the burner experiments and ranged from coarse to moderate for the furniture items. The simulations with a grid size of 0.05 m ranged from coarse to fine resolution with greater HRR yielding better resolution. The grid was defined to be uniform throughout the computational domain with all cubic elements and cell sizes of 0.1 m and 0.05 m.

Table 4.3: Characteristic fire diameter and resolution index for compartment experiment simulations

Fire Size	$D^*$	$D^*/0.1$	$D^*/0.05$
50 kW	0.29	2.9	5.8
100 kW	0.38	3.8	7.7
500 kW	0.73	7.3	14.7
Red Accent Chair (mean)	0.53	5.3	10.6
Overstuffed Sofa (mean)	0.76	7.6	15.2

### 4.3 Model Sensitivity

The proper use of predictive fire models requires a complete understanding of the sensitivity of the model results to the input parameters. By understanding the sensitivity of the model to the inputs to the model, uncertainty in the inputs may be propagated through to the final results to assign a level of confidence to the conclusions drawn from the use of the model. Determining the sensitivity of the model to specific model inputs is straightforward for the algebraic models collected as the FDTs, but it is more difficult for the computational models utilized in this work. Several researchers have conducted sensitivity analyses on these computational models and detailed descriptions of the findings of these sensitivity analyses are left to the original authors [55–58]. It is essential that model practitioners have a comprehensive and complete understanding of the affect of changes in each parameter on the results of the model.

# 5 Model Assessment

The following sections present a quantitative assessment of the ability of the models to predict each measurand. All comparisons of FDS predictions that are presented in this section used the results from the higher resolution (cell size of 0.05 m) simulations. Also presented are metrics calculated to describe the ability of each model to predict the fire environment. In the following figures, the solid black line that runs from the bottom left to the upper right corner of the plot indicates the expected perfect agreement between the experimentally measured data and the model prediction. The dashed black lines offset from the solid black line represent the total estimated expanded experimental uncertainty for each measurement as presented in Section 3.2.

It is assumed that deviations from perfect agreement between the predictions and the experimental data are the result of simplifying assumptions, model implementation, and uncertainty in defined parameters which manifests as a systematic bias in the predictions. In the analysis presented in this section, the bias is assumed to scale the expectation line by a bias factor. The biased expectation line runs through the center of the distribution of points which indicate the comparison for the indicated collection of data with the specific model. The bias-adjusted model uncertainty presented in the tables in this section represents the scatter in the distribution of points which represent the agreement between the model predictions and the corresponding experimental data about the biased expectation line.

The bias factors presented in the following tables can be considered a measure of the typical accuracy of the model for the collection of data points considered, where a bias factor of 1 indicates perfect agreement and larger deviations above and below 1 indicate less accurate predictions. The uncertainty presented in the following tables is the observed total expanded uncertainty of the bias factor, which is analogous to the dashed lines presented in the figures. This can be taken as a measure of how closely grouped the points are which represent the comparison of measured to predicted quantities. Bias factors and uncertainty in the bias factors have been calculated according to the equations described in the FDS Validation Guide [27].

Model developers strive for predictions to be consistently within the experimental uncertainty of measured quantities. Deviation of the bias factor beyond the total expanded uncertainty of a measured quantity indicates the model does not accurately represent the physics of the scenario, with larger deviations from perfect agreement indicating less accuracy in the predictive capabilities of the model. For example, if the bias factor for a collection of predictions of a particular measurement is 1.1, the model overpredicts the measurement by 10% on average, and if the bias factor for a set of measurement-prediction pairs is 0.91 (1/1.1), the model underpredicts the measurement by 10% on average.

Large uncertainty in the bias factor indicates significant scatter in the agreement between the measurements and the predictions. This uncertainty represents the level of confidence a practitioner may have in the bias factor, with low uncertainty correlated to more confident determinations of the bias factor for a given scenario. As an example, the bias factor may be 1 but the uncertainty may

be  $\pm 50\%$ , which indicates that 95% of the measurement-prediction pairs lies in the range of bias factors from 0.667 (1/1.5) to 1.5. Although the average bias factor indicates perfect agreement, the uncertainty indicates that the model does not consistently yield perfect agreement. For the purposes of this work, uncertainty of the bias factor that is within the total expanded experimental uncertainty of the measurement indicates the predictions are consistent and evokes the highest confidence in the bias factor. Deviations of the uncertainty in the bias factor above the total expanded experimental uncertainty indicate decreased confidence in the presented bias factor.

The values in the tables have been shaded to simplify the visual representation of the predictive assessment for each dataset. Table 5.1 provides a definition for each color presented in the tables in this section. The symbol  $\sigma$  in the table corresponds to the total expanded uncertainty of the measurand. As an example, a green shaded cell in the ‘Bias’ column indicates that, on average, the quantity was predicted to within the total expanded uncertainty. A green shaded cell in the ‘Uncertainty’ column indicates that the scatter in the agreement between the prediction and the measured quantity, as quantified by the standard deviation of the bias, exceeds the total expanded uncertainty of the measured quantity.

Table 5.1: Color Code for Bias and Uncertainty Tables

Shading	Range
	$\leq \pm \sigma$
	$\pm \sigma$ to $\pm 2\sigma$
	$\pm 2\sigma$ to $\pm 3\sigma$
	$> \pm 3\sigma$

Because the furniture experiments involved a growth phase and a long duration decay phase, three metrics were used to provide a comprehensive assessment of the agreement between the model predictions and the experimental data. The method used to determine the mean and steady HRR used in FDT calculations was described in Section 4.2. The same method was adopted to determine the mean and steady values for each measurand from the experimental data, the CFAST predictions, and the FDS predictions. An inner shading color of black inside the symbols in all figures that display the agreement between model predictions and experimental data for furniture items denotes the maximum value, an inner shading of silver denotes the mean value, and an inner shading of white denotes the steady value attained in the decay phase of the experiment.

Individual comparisons for each experiment with commentary on the agreement between each model and the experimental data are provided in Appendix A.

## 5.1 Temperatures

The agreement between the steady temperatures and the model predictions for the compartment experiments with the gas burners is presented in Figure 5.1. The figure includes data from thermocouples located to measure the fire plume, the ceiling jet, and the flow through the door. An FDT

method was only available for the plume temperatures.

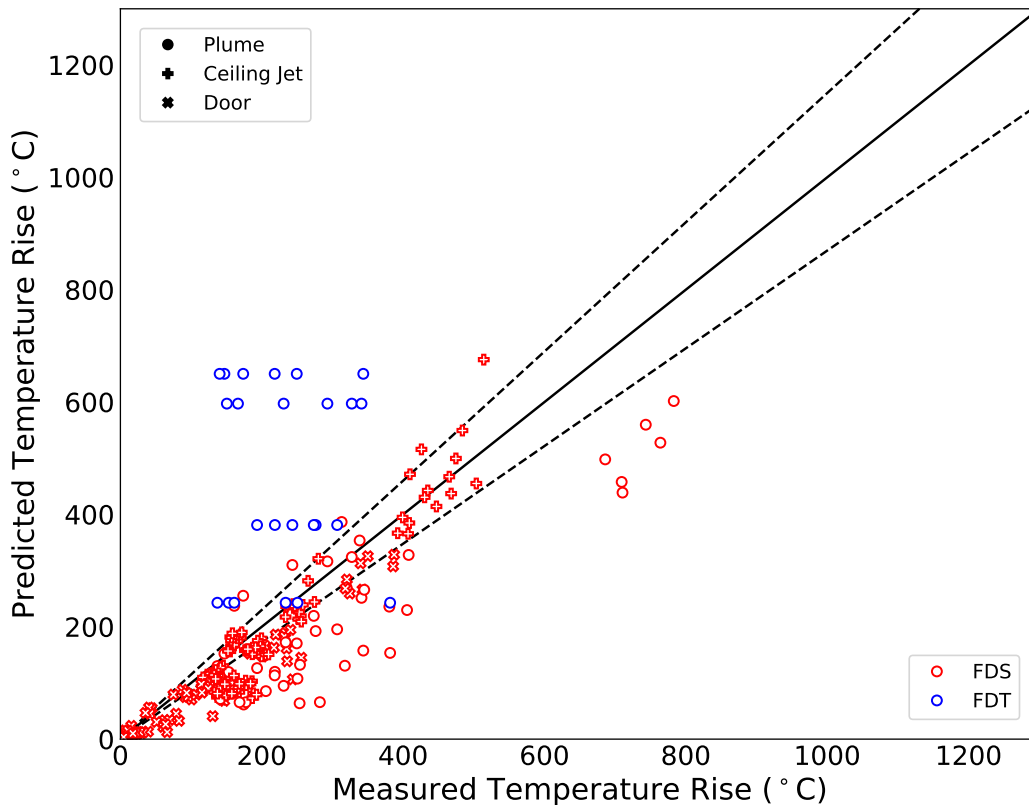


Figure 5.1: Comparison of Steady Temperature Predictions to Experimental Data Collected in Compartment Experiments with Burners

Prediction biases and uncertainties calculated for the gas burner compartment experiments are presented in Table 5.2 in which the 0.3 m burner experiments are denoted with labels that include ‘SB’ and 0.6 m burner experiments are denoted with the set point HRR.. The FDT method over-predicted the plume temperatures. The magnitude of overprediction increased with increasing HRR, was higher when the door was closed than when it was open, and was not dependent on the location of the burner in the compartment. The majority of the steady temperatures predicted by FDS were less than 200°C and many of these predictions were within the experimental uncertainty of the measurement. Overall, FDS provided reasonable agreement with the temperature measured in the compartment gas burner experiments, with a slight underprediction of the temperatures and high scatter in the agreement. The accuracy of the FDS predictions was highest for the 100 kW experiments with the 0.3 m burner, in the experiments with the open door, and the experiments with the burner in the back position.

Table 5.2: Model Fitness Metrics for Temperature in Compartment Burner Experiments

Model	Collection	N	Bias	Uncertainty
FDS	Overall	280	0.83	±41%
	Ceiling Jet	120	0.85	±25%
	Plume	48	0.7	±41%
	Door	112	0.92	±56%
	100kWSB	70	0.99	±42%
	100kW	70	0.92	±46%
	250kW	70	0.79	±35%
	500kW	70	0.7	±42%
	Open	196	0.88	±42%
	Closed	84	0.72	±35%
	Center	60	0.86	±34%
	Back	76	0.95	±44%
	Corner	76	0.81	±43%
	Side	68	0.7	±35%
FDT	Overall	48	6.17	±98%
	100kWSB	12	3.37	±63%
	100kW	12	2.38	±63%
	250kW	12	6.04	±74%
	500kW	12	18.31	±120%
	Open	24	4.14	±73%
	Closed	24	9.07	±117%
	Back	16	7.08	±97%
	Corner	16	6.69	±103%
	Side	16	5.54	±102%

The comparison between the model predictions and the experimental data from the upholstered furniture experiments conducted in the compartment is presented in Figure 5.2. Prediction biases and uncertainties calculated for the furniture compartment experiments are presented in Table 5.3. The FDT method significantly overpredicted the maximum, mean, and steady plume temperatures in the furniture compartment experiments. The magnitude of the overprediction decreased from the maximum value to the mean value and further to the steady value. The magnitude of the overprediction was higher when the compartment door was closed than when it was open.

FDS overpredicted the ceiling jet temperatures and underpredicted the plume temperatures and the temperature of flow through the door. The overprediction in the maximum temperatures for the Overstuffed Sofa was of a greater magnitude and the comparisons had higher scatter than the predictions for the Red Accent Chair. The FDT method overpredicted the maximum plume temperatures as well as most of the mean and steady temperatures.

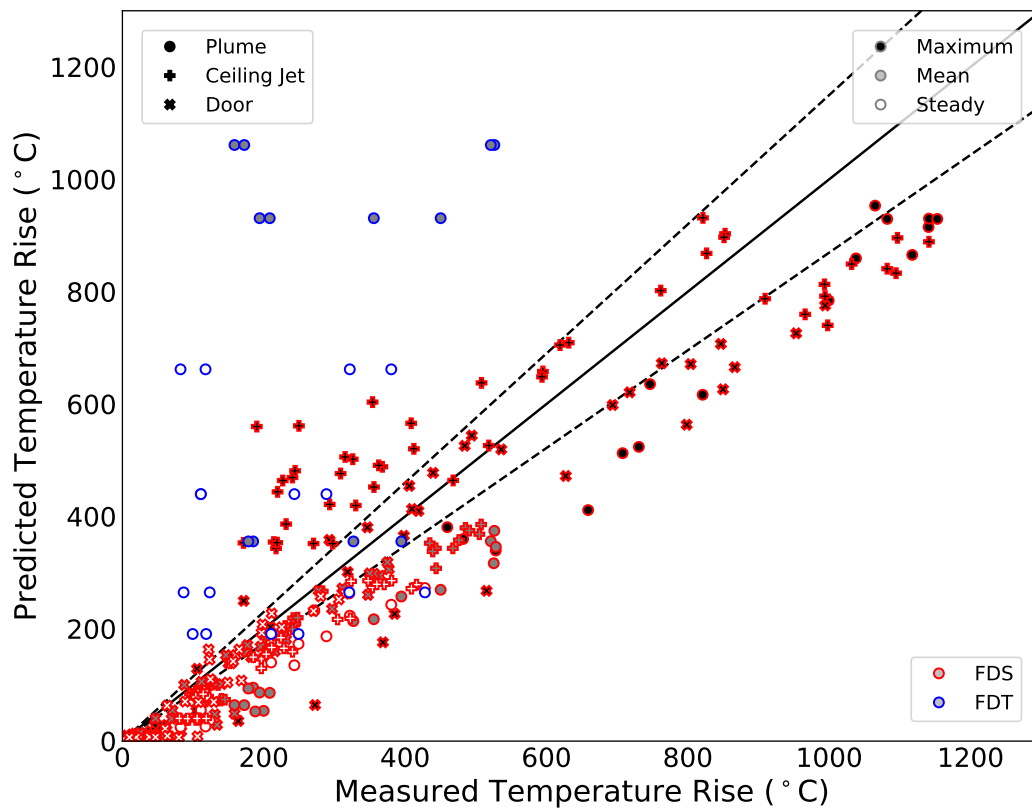


Figure 5.2: Comparison of Temperature Predictions to Experimental Data Collected in Compartment Experiments with Furniture

Table 5.3: Model Fitness Metrics for Temperature in Compartment Furniture Experiments

Model	Metric	Maximum			Mean			Steady		
	Collection	N	Bias	Uncertainty	N	Bias	Uncertainty	N	Bias	Uncertainty
FDS	Overall	104	1.01	±42%	104	0.69	±35%	104	0.68	±58%
	Ceiling Jet	48	2.41	±97%	48	1.56	±102%	48	1.15	±88%
	Plume	16	0.78	±10%	16	0.53	±31%	16	0.57	±38%
	Door	42	0.81	±44%	42	0.72	±51%	42	0.75	±86%
	Overstuffed Sofa	51	0.93	±48%	51	0.62	±38%	51	0.59	±63%
	Red Accent Chair	53	1.09	±31%	53	0.76	±29%	53	0.75	±49%
	Open	74	1.33	±87%	74	1.18	±91%	74	1.04	±95%
	Closed	32	1.4	±38%	32	0.62	±27%	32	0.56	±36%
	Center	30	3.21	±130%	30	2.41	±135%	30	1.7	±128%
	Back	38	0.97	±34%	38	0.69	±35%	38	0.67	±52%
Corner	38	0.96	±39%	38	0.69	±42%	38	0.7	±61%	
FDT	Overall	12	50.22	±140%	16	6.14	±96%	16	2.51	±71%
	Overstuffed Sofa	4	70.67	±47%	8	10.71	±92%	8	3.14	±86%
	Red Accent Chair	8	24.45	±131%	8	2.49	±57%	8	2.06	±58%
	Open	6	36.5	±136%	8	3.48	±82%	8	1.27	±44%
	Closed	6	77.15	±151%	8	9.3	±94%	8	3.77	±53%
	Back	6	56.16	±147%	8	6.49	±98%	8	2.82	±82%
	Corner	6	57.24	±148%	8	6.49	±104%	8	2.43	±69%

### 5.1.1 Layer Temperatures

The agreement between the steady layer temperatures and the model predictions for the compartment experiments with the gas burners is presented in Figure 5.3. Table 5.4 displays the calculated bias and uncertainty in agreement between the models and the experimental data. FDS provided the most accurate predictions of the gas layer temperatures, although the agreement exhibited high scatter about the bias value. with moderate scatter. CFAST yielded reasonable predictions of the gas layer temperatures Gas layer temperatures were generally overpredicted with the FDT method, although the estimates for the upper gas layer temperature with the door open were remarkably accurate and were closely clustered together. The most significant variable for the magnitude and direction of the bias for FDS was the state of the door, with FDS underpredicting the layer temperatures when the door was open and accurately predicting the temperatures when the door was closed.

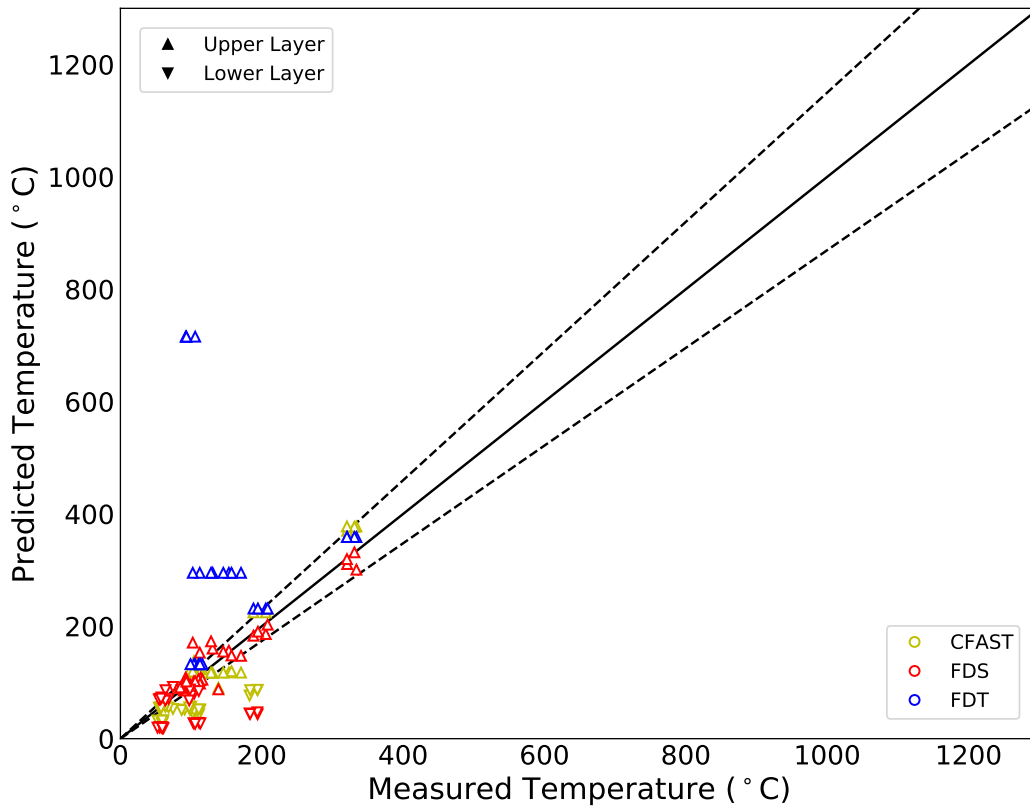


Figure 5.3: Comparison of Steady Layer Temperature Predictions to Experimental Data Collected in Compartment Experiments with Burners

Table 5.4: Model Fitness Metrics for Layer Temperature in Compartment Burner Experiments

Model	Collection	N	Bias	Uncertainty
FDS	Overall	64	0.86	±56%
	100kWSB	16	0.86	±49%
	100kW	16	0.9	±53%
	250kW	16	0.93	±66%
	500kW	16	0.84	±65%
	Open	32	0.62	±60%
	Closed	32	1.05	±16%
	Center	16	0.9	±58%
	Back	16	0.99	±62%
	Corner	16	0.86	±59%
	Side	16	0.79	±55%
FDT	Overall	32	3.55	±92%
	100kWSB	8	1.67	±31%
	100kW	8	1.76	±36%
	250kW	8	4.82	±99%
	500kW	8	10.41	±139%
	Open	16	1.17	±4%
	Closed	16	6.86	±86%
	Center	8	3.91	±98%
	Back	8	4.18	±99%
	Corner	8	3.9	±103%
	Side	8	3.24	±89%
CFAST	Overall	64	0.82	±35%
	100kWSB	16	0.78	±40%
	100kW	16	0.82	±34%
	250kW	16	0.91	±40%
	500kW	16	0.86	±40%
	Open	32	0.81	±44%
	Closed	32	0.83	±23%
	Center	16	0.84	±39%
	Back	16	0.92	±39%
	Corner	16	0.83	±38%
	Side	16	0.78	±38%

The comparison between the model predictions and the experimental data from the upholstered furniture experiments in the compartment is presented in Figure 5.4. Table 5.5 displays the calculated bias and uncertainty in agreement between the models and the experimental data from the compartment furniture experiments. FDS and CFAST generally provided more accurate predictions than the FDT methods. The maximum layer temperatures were accurately represented by FDS, although the scatter in the agreement was large. The mean and steady temperatures were less accurately predicted by FDS, although the scatter in the agreement was lower than for the

maximum layer temperature. FDS overpredicted the maximum layer temperatures when the door was closed and underpredicted the temperatures when the door was open.

CFAST underpredicted the maximum measured layer temperatures and more accurately predicted the mean and steady layer temperatures. As with the gas burner experiments, the FDT method provided a remarkably accurate prediction of the upper layer temperature when the door was open.

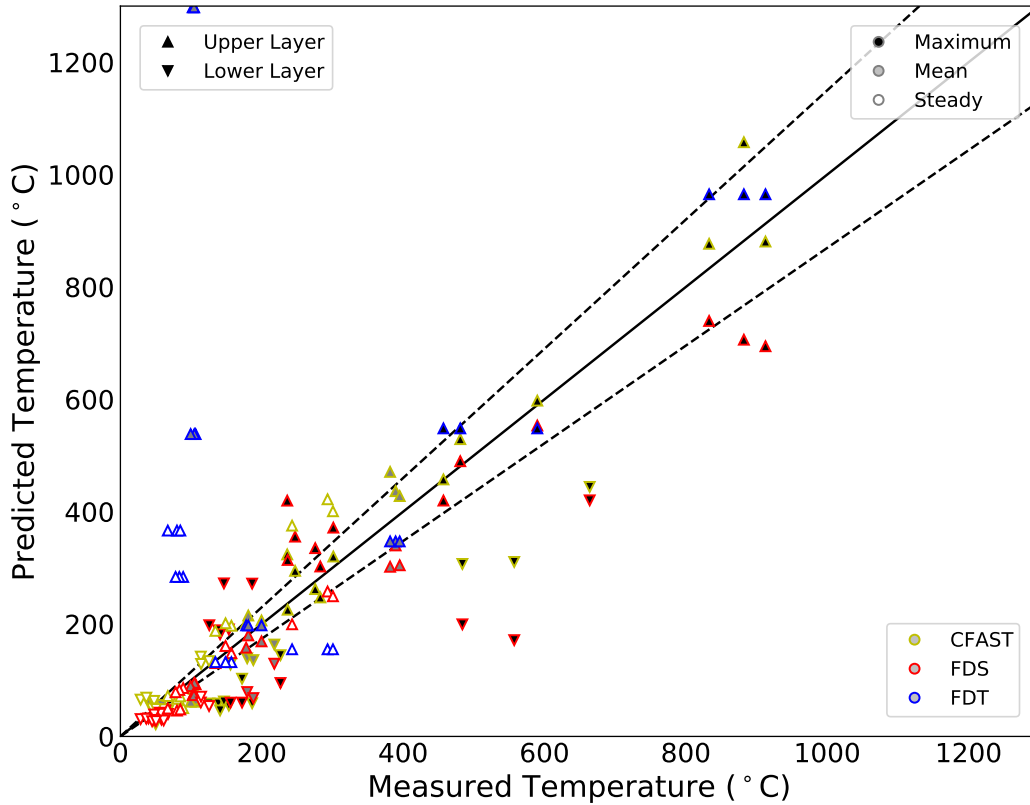


Figure 5.4: Comparison of Layer Temperature Predictions to Experimental Data Collected in Compartment Experiments with Furniture

Table 5.5: Model Fitness Metrics for Layer Temperature in Compartment Furniture Experiments

Metric		Maximum			Mean			Steady		
Model	Collection	N	Bias	Uncertainty	N	Bias	Uncertainty	N	Bias	Uncertainty
FDS	Overall	24	1.03	±52%	24	0.72	±19%	24	0.75	±23%
	Overstuffed Sofa	12	1.11	±56%	12	0.65	±22%	12	0.63	±20%
	Red Accent Chair	12	0.97	±49%	12	0.8	±12%	12	0.89	±13%
	Open	12	0.65	±43%	12	0.72	±31%	12	0.81	±28%
	Closed	12	1.39	±11%	12	0.75	±13%	12	0.73	±25%
	Center	8	1.17	±56%	8	0.71	±19%	8	0.72	±25%
	Back	8	1.0	±49%	8	0.75	±23%	8	0.82	±24%
	Corner	8	1.03	±60%	8	0.74	±30%	8	0.77	±32%
FDT	Overall	12	11.04	±141%	12	5.34	±114%	12	2.56	±92%
	Overstuffed Sofa	6	20.87	±168%	6	9.39	±144%	6	3.22	±117%
	Red Accent Chair	6	6.74	±121%	6	3.39	±86%	6	2.26	±72%
	Open	6	1.09	±6%	6	0.98	±8%	6	0.73	±27%
	Closed	6	17.33	±49%	6	9.04	±48%	6	4.1	±19%
	Center	4	15.87	±160%	4	6.35	±129%	4	2.76	±98%
	Back	4	12.41	±154%	4	6.17	±126%	4	3.06	±107%
	Corner	4	14.09	±157%	4	6.39	±128%	4	2.82	±104%
CFAST	Overall	24	0.78	±42%	24	0.86	±27%	22	1.14	±32%
	Overstuffed Sofa	12	0.82	±45%	12	0.84	±14%	12	1.1	±18%
	Red Accent Chair	12	0.75	±40%	12	0.88	±37%	10	1.21	±47%
	Open	12	0.84	±24%	12	1.07	±23%	12	1.43	±20%
	Closed	12	0.73	±54%	12	0.68	±18%	10	0.82	±21%
	Center	8	0.84	±45%	8	0.84	±25%	8	1.03	±32%
	Back	8	0.77	±48%	8	0.91	±33%	8	1.24	±43%
	Corner	8	0.8	±45%	8	0.88	±37%	6	1.24	±28%

## 5.1.2 Layer Heights

The agreement between the steady depth of descent of the layer interface and the model predictions for the compartment experiments with the gas burners is presented in Figure 5.5. Table 5.6 displays the calculated bias and uncertainty in agreement between the models and the experimental data from the compartment burner experiments. The FDT method consistently overpredicted the depth of descent of the layer interface when the door was closed and underpredicted the depth of descent when the door was open. When the door was closed, the model predicted that the layer descended to the floor, and when the door was opened, the method was limited by the height of the door, which was 2 m.

Because the calculation of bias and uncertainty involves logarithms, and all of the FDT closed door predictions reached approximately 0, the closed door predictions were excluded from the table. Model practitioners should understand that the FDT method provides a prediction of the layer interface height that is not necessarily accurate and is directly correlated with the status of the door for a fire in the size of compartment that was investigated in this work.

FDS provided a reasonable prediction of the layer interface when the door was open but overpre-

dicted its depth of descent in all the other situations. CFAST provided accurate overall predictions but underpredicted the descent when the door was open and overpredicted its descent when the door was closed.

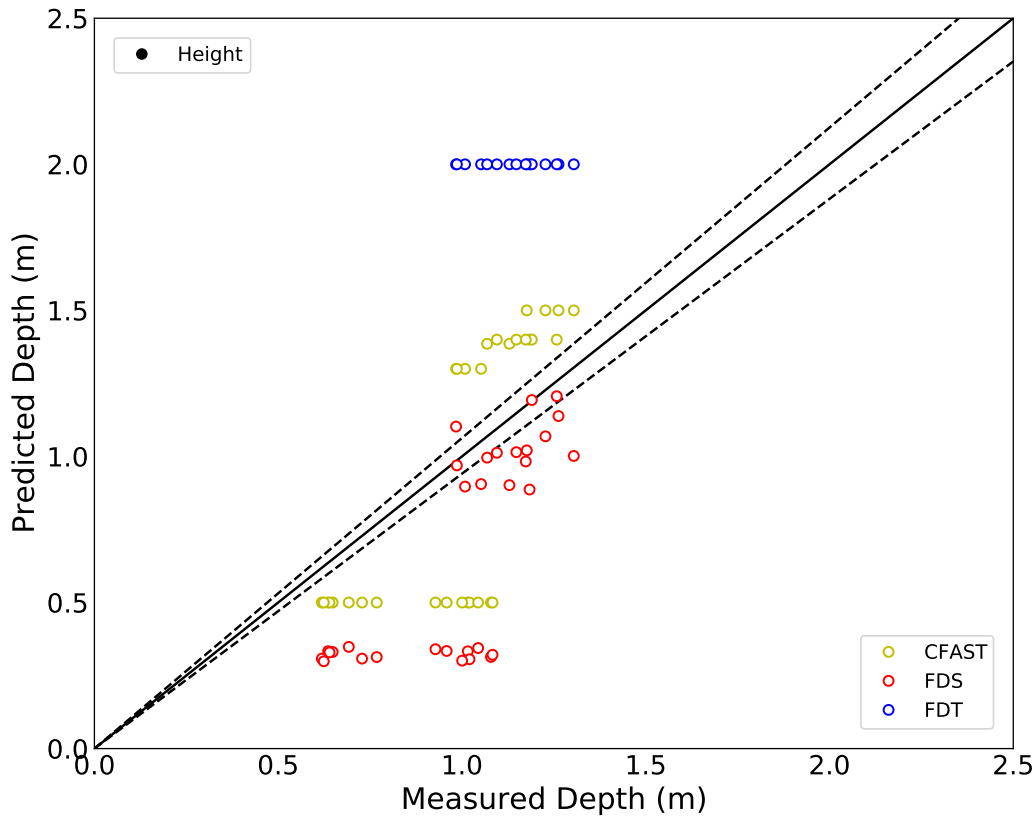


Figure 5.5: Comparison of Steady Layer Interface Elevation Predictions to Experimental Data Collected in Compartment Experiments with Burners

The comparison between the model predictions and the experimental data from the upholstered furniture is presented in Figure 5.6. Table 5.7 displays the calculated bias and uncertainty in agreement between the models and the experimental data from the compartment furniture experiments. The same trend for the FDT method that was observed in the gas burner experiments was also observed in the furniture experiments. FDS provided an accurate prediction of the mean and steady layer interface elevation for all experiments but overpredicted the maximum depth of descent of the layer in all cases. CFAST provided reasonable overall predictions, but generally underpredicted the layer descent when the door was open and overpredicted its descent when the door was closed.

Table 5.6: Model Fitness Metrics for Layer Interface Elevation in Compartment Burner Experiments

Model	Collection	N	Bias	Uncertainty
FDS	Overall	32	0.64	±43%
	100kWSB	8	0.68	±28%
	100kW	8	0.66	±39%
	250kW	8	0.64	±56%
	500kW	8	0.67	±58%
	Open	16	0.9	±10%
	Closed	16	0.4	±23%
	Center	8	0.61	±42%
	Back	8	0.65	±51%
	Corner	8	0.72	±52%
	Side	8	0.68	±44%
FDT	Overall	16	1.76	±6%
	100kWSB	4	1.61	±4%
	100kW	4	1.68	±4%
	250kW	4	1.79	±5%
	500kW	4	1.99	±3%
	Open	16	1.76	±8%
	Center	4	1.73	±9%
	Back	4	1.83	±7%
	Corner	4	1.72	±12%
	Side	4	1.8	±10%
	CFAST	Overall	32	0.92
100kWSB		8	0.99	±24%
100kW		8	0.94	±32%
250kW		8	0.89	±48%
500kW		8	0.93	±51%
Open		16	1.23	±4%
Closed		16	0.62	±22%
Center		8	0.92	±40%
Back		8	0.93	±47%
Corner		8	0.93	±40%
Side		8	0.99	±35%

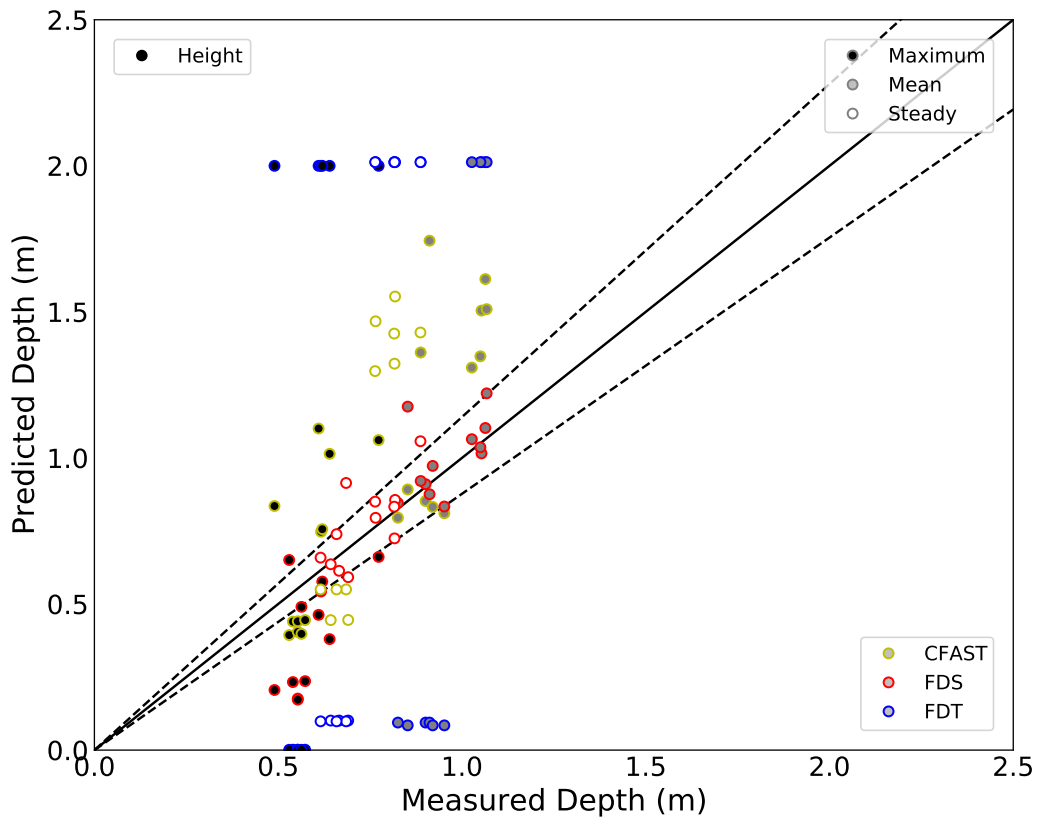


Figure 5.6: Comparison of Layer Interface Elevation Predictions to Experimental Data Collected in Compartment Experiments with Furniture

Table 5.7: Model Fitness Metrics for Layer Interface Elevation in Compartment Furniture Experiments

Metric		Maximum			Mean			Steady		
Model	Collection	N	Bias	Uncertainty	N	Bias	Uncertainty	N	Bias	Uncertainty
FDS	Overall	11	0.7	±41%	12	1.03	±0%	12	1.03	±0%
	Overstuffed Sofa	6	0.79	±51%	6	1.06	±14%	6	1.09	±12%
	Red Accent Chair	6	0.56	±36%	6	1.02	±5%	6	1.0	±10%
	Open	6	0.75	±30%	6	1.03	±4%	6	1.05	±9%
	Closed	5	0.67	±57%	6	1.05	±15%	6	1.05	±15%
	Center	3	0.51	±44%	4	0.98	±7%	4	1.03	±2%
	Back	4	0.8	±46%	4	1.11	±15%	4	1.04	±20%
	Corner	4	0.79	±38%	4	1.05	±7%	4	1.09	±11%
FDT	Overall	11	156.97	±379%	12	1.46	±155%	12	1.75	±146%
	Overstuffed Sofa	6	366.48	±410%	6	1.82	±169%	6	2.08	±155%
	Red Accent Chair	6	159.88	±388%	6	1.55	±157%	6	1.89	±151%
	Open	6	3.26	±14%	6	1.97	±6%	6	2.48	±4%
	Closed	5	0.0	±13%	6	0.1	±8%	6	0.15	±3%
	Center	3	2287.86	±421%	4	2.13	±175%	4	2.3	±160%
	Back	4	538.04	±418%	4	1.84	±169%	4	2.27	±163%
	Corner	4	456.8	±416%	4	1.91	±172%	4	2.22	±161%
CFAST	Overall	11	1.14	±33%	12	1.24	±21%	11	1.3	±42%
	Overstuffed Sofa	6	1.04	±34%	6	1.13	±18%	6	1.31	±40%
	Red Accent Chair	6	1.18	±36%	6	1.35	±24%	5	1.37	±53%
	Open	6	1.48	±17%	6	1.41	±7%	6	1.75	±6%
	Closed	5	0.77	±4%	6	1.1	±30%	5	0.77	±13%
	Center	3	1.5	±46%	4	1.21	±29%	4	1.36	±50%
	Back	4	1.1	±35%	4	1.2	±21%	4	1.29	±52%
	Corner	4	1.03	±33%	4	1.39	±31%	3	1.42	±39%

## 5.2 Flame Heights

The agreement between the observed steady flame heights and the model predictions for the compartment experiments with the gas burners is presented in Figure 5.7. Table 5.8 displays the bias and uncertainty in the agreement between the model predictions and the experimental flame heights from the burner experiments conducted in the compartment. FDS typically overpredicted the flame heights, which were limited by the ceiling height in the compartment. The FDT method for the flame height when the fuel source was adjacent to a wall or corner tended to overpredict the measured flame height. CFAST slightly overpredicted the flame height on average, but provided the most accurate representation of the flame height for the burner experiments conducted in the compartment.

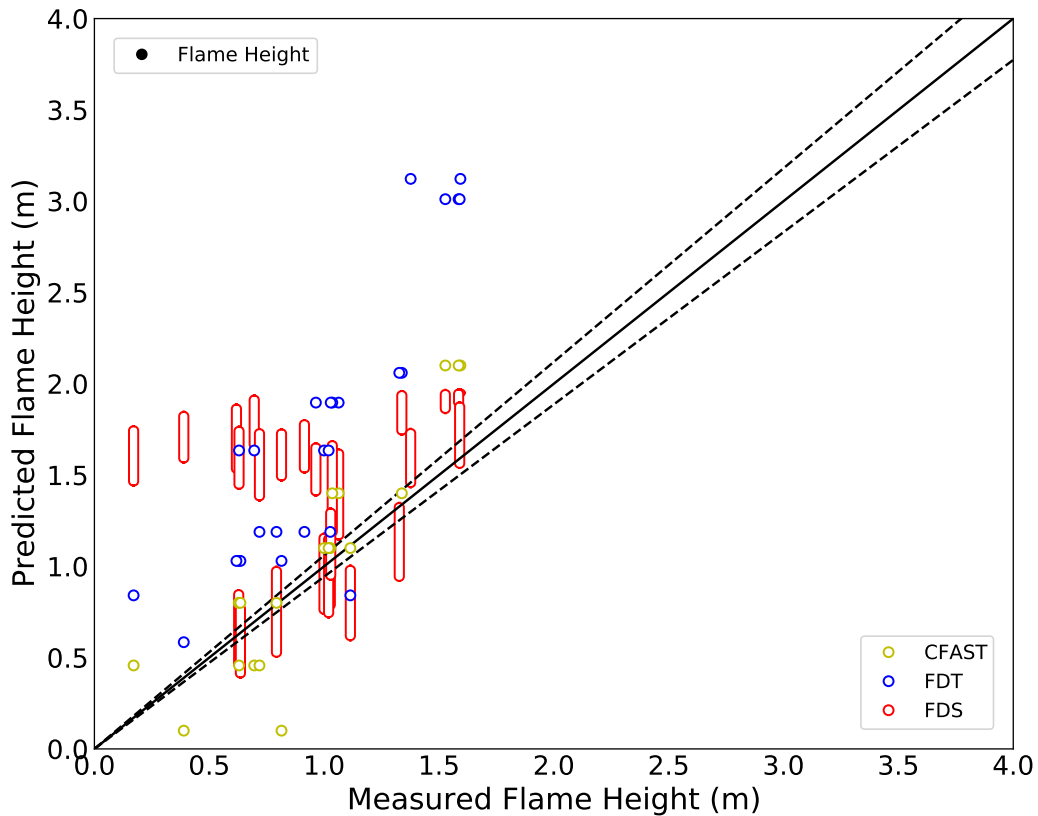


Figure 5.7: Comparison of Steady Mean Flame Height Predictions to Experimental Data Collected in Compartment Experiments with Burners

Table 5.8: Model Fitness Metrics for Flame Height in Compartment Burner Experiments

Model	Collection	N	Bias	Uncertainty
FDS (Upper Limit)	Overall	26	1.93	±54%
	100kWSB	8	2.75	±80%
	100kW	7	2.25	±51%
	250kW	6	1.43	±20%
	500kW	5	1.23	±2%
	Open	13	1.26	±14%
	Closed	13	2.73	±63%
	Center	3	7.61	±125%
	Back	7	1.83	±37%
	Corner	8	1.46	±29%
	Side	8	1.56	±32%
FDS (Lower Limit)	Overall	26	1.55	±63%
	100kWSB	8	2.23	±92%
	100kW	7	1.8	±72%
	250kW	6	1.11	±26%
	500kW	5	1.14	±10%
	Open	13	0.93	±29%
	Closed	13	2.29	±67%
	Center	3	7.31	±142%
	Back	7	1.47	±49%
	Corner	8	1.17	±39%
	Side	8	1.22	±43%
FDT	Overall	26	1.82	±32%
	100kWSB	8	2.11	±56%
	100kW	7	1.5	±11%
	250kW	6	1.75	±10%
	500kW	5	2.0	±7%
	Open	13	1.61	±25%
	Closed	13	2.04	±35%
	Center	3	2.77	±95%
	Back	7	1.85	±12%
	Corner	8	1.61	±20%
	Side	8	1.82	±19%
CFAST	Overall	19	1.16	±67%
	100kWSB	8	1.11	±45%
	100kW	5	0.98	±107%
	250kW	3	1.24	±13%
	500kW	3	1.34	±2%
	Open	13	1.19	±11%
	Closed	6	0.93	±104%
	Center	3	1.75	±117%
	Back	5	1.16	±30%
	Corner	5	1.02	±26%
	Side	6	1.19	±93%

The comparison between the model predictions and the experimental data from the upholstered furniture is presented in Figure 5.8. Table 5.9 displays the bias and uncertainty in the agreement between the model predictions and the experimental flame heights from the compartment furniture experiments. FDS overpredicted the the maximum flame height and underpredicted the mean and steady flame heights. The FDT methods overpredicted the maximum, mean, and steady flame heights. CFAST overpredicted the maximum and mean flame heights and underpredicted the steady flame heights.

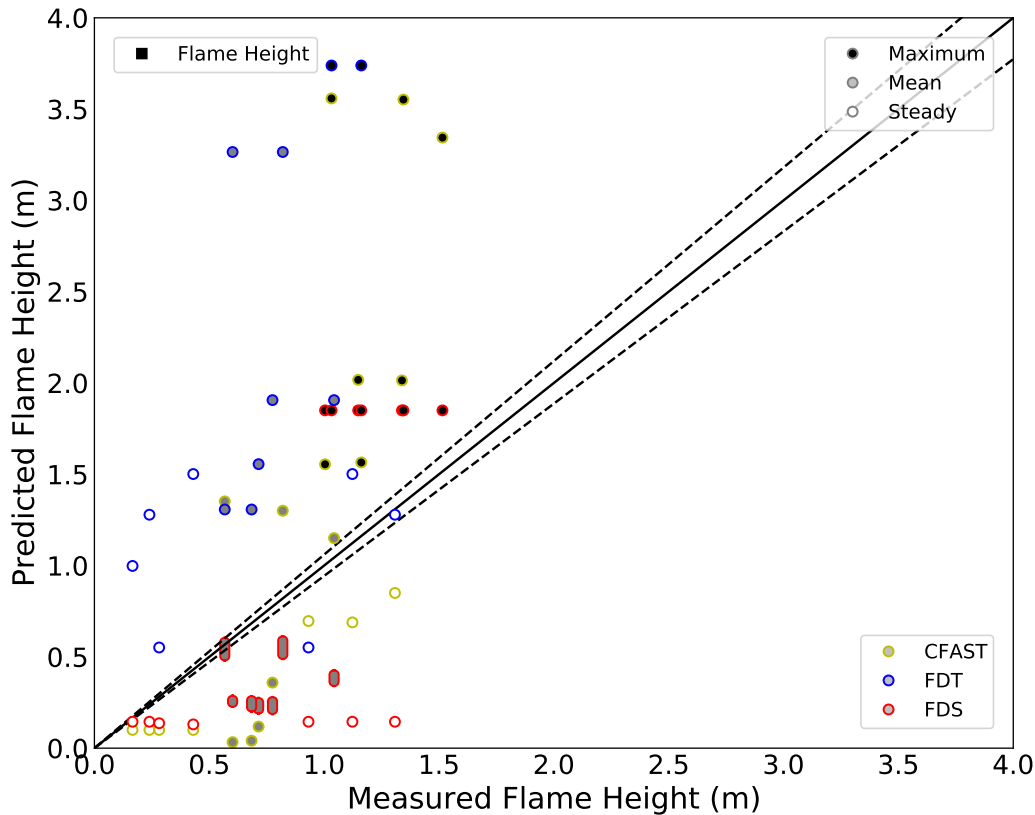


Figure 5.8: Comparison of Flame Height Predictions to Experimental Data Collected in Compartment Experiments with Furniture

For the burner experiments, the base of the flame was easily determined, but in the furniture experiments, the elevation of the base of the flame changed as the chair or sofa material burned away. This contributed to uncertainty in the comparisons because the model did not represent the decreasing elevation of the base of the flame. Given that the compartment ceiling was 2.44 m above the floor, predicted maximum vertical flame heights above 2.44 m are not physically possible. However, flames in excess of the wall height would continue to spread across the ceiling. The FDT methods and CFAST predicted flame heights above 2.4 m in some compartment experiments. These predictions of the flame height may have affected prediction of other quantities including the upper layer temperature and the heat fluxes.

Table 5.9: Model Fitness Metrics for Flame Height in Compartment Furniture Experiments

Metric		Maximum			Mean			Steady		
Model	Collection	N	Bias	Uncertainty	N	Bias	Uncertainty	N	Bias	Uncertainty
FDS (Upper Limit)	Overall	7	1.54	±14%	7	0.52	±42%	7	0.4	±81%
	Overstuffed Sofa	4	1.65	±12%	4	0.66	±45%	4	0.28	±61%
	Red Accent Chair	3	1.4	±13%	3	0.36	±5%	3	0.71	±110%
	Open	3	1.47	±19%	3	0.75	±49%	3	0.13	±16%
	Closed	4	1.61	±11%	4	0.38	±11%	4	0.58	±44%
	Back	3	1.67	±7%	3	0.62	±59%	3	0.59	±88%
	Corner	4	1.46	±17%	4	0.48	±33%	4	0.31	±79%
FDS (Lower Limit)	Overall	7	1.54	±14%	7	0.45	±43%	7	0.4	±81%
	Overstuffed Sofa	4	1.65	±12%	4	0.57	±44%	4	0.28	±61%
	Red Accent Chair	3	1.4	±13%	3	0.3	±12%	3	0.71	±110%
	Open	3	1.47	±19%	3	0.64	±47%	3	0.13	±16%
	Closed	4	1.61	±11%	4	0.32	±18%	4	0.58	±44%
	Back	3	1.67	±7%	3	0.53	±61%	3	0.59	±88%
	Corner	4	1.46	±17%	4	0.42	±36%	4	0.31	±79%
FDT	Overall	7	4.64	±36%	7	2.87	±40%	7	3.05	±88%
	Overstuffed Sofa	4	5.49	±45%	4	3.5	±48%	4	2.0	±74%
	Red Accent Chair	3	3.66	±7%	3	2.15	±14%	3	5.27	±101%
	Open	3	4.46	±34%	3	2.76	±40%	3	1.0	±41%
	Closed	4	4.88	±42%	4	3.04	±47%	4	4.36	±51%
	Back	3	3.61	±10%	3	2.13	±10%	3	3.74	±116%
	Corner	4	5.54	±44%	4	3.53	±49%	4	3.05	±80%
CFAST	Overall	7	2.07	±34%	7	1.25	±155%	7	0.53	±41%
	Overstuffed Sofa	4	2.29	±44%	4	2.68	±204%	4	0.51	±53%
	Red Accent Chair	3	1.83	±18%	3	0.69	±95%	3	0.56	±23%
	Open	3	2.78	±22%	3	1.73	±38%	3	0.67	±9%
	Closed	4	1.54	±10%	4	0.21	±100%	4	0.41	±39%
	Back	3	2.26	±48%	3	1.75	±190%	3	0.58	±38%
	Corner	4	1.99	±27%	4	1.43	±151%	4	0.5	±47%

### 5.3 Heat Flux

The agreement between the measured heat fluxes and the model predictions for the compartment experiments with the gas burners is presented in Figure 5.9. Table 5.10 displays the calculated bias and uncertainty in agreement between the models and the experimental data. FDS overpredicted all the measured heat fluxes. CFAST significantly underpredicted all the measured heat fluxes. The solid flame model and the point source model overpredicted all the measured heat fluxes. Notable exceptions for the point source model were the experiments in which the burners were located in the center of the compartment. Every model predicted heat fluxes that were closer to the measurements when the door was open compared to when it was closed.

The comparison between the model predictions and the experimental data from the upholstered furniture experiments is presented in Figure 5.10. Table 5.11 displays the calculated bias and uncertainty in agreement between the models and the experimental heat flux data for the compartment furniture experiments. FDS overpredicted all the low magnitude heat fluxes and tended to underpredict maximum, mean, and steady heat fluxes over approximately 50 kW/m<sup>2</sup>. CFAST typically

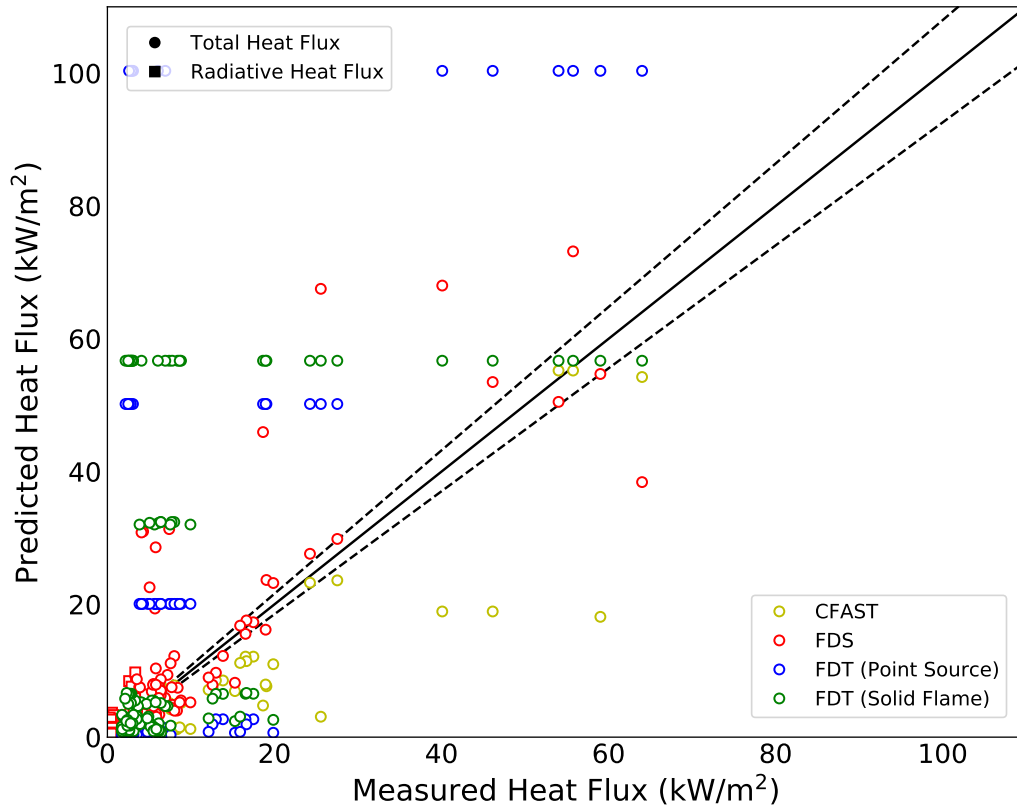


Figure 5.9: Comparison of Steady Heat Flux Predictions to Experimental Data Collected in Compartment Experiments with Burners

overpredicted the heat fluxes and the magnitude of the overprediction was larger at low measured heat fluxes.

The solid flame model underpredicted the maximum heat fluxes and overpredicted the mean and steady heat fluxes. The solid flame model yielded higher heat flux predictions when the door was closed compared to when the door was open. This may be due to the Heskestad correlation estimate of the flame height being independent of the status of the door. The point source model underpredicted the maximum, mean, and steady heat fluxes in most cases. The point source model slightly overpredicted the heat fluxes measured when the door was closed and underpredicted the heat fluxes when the door was open.

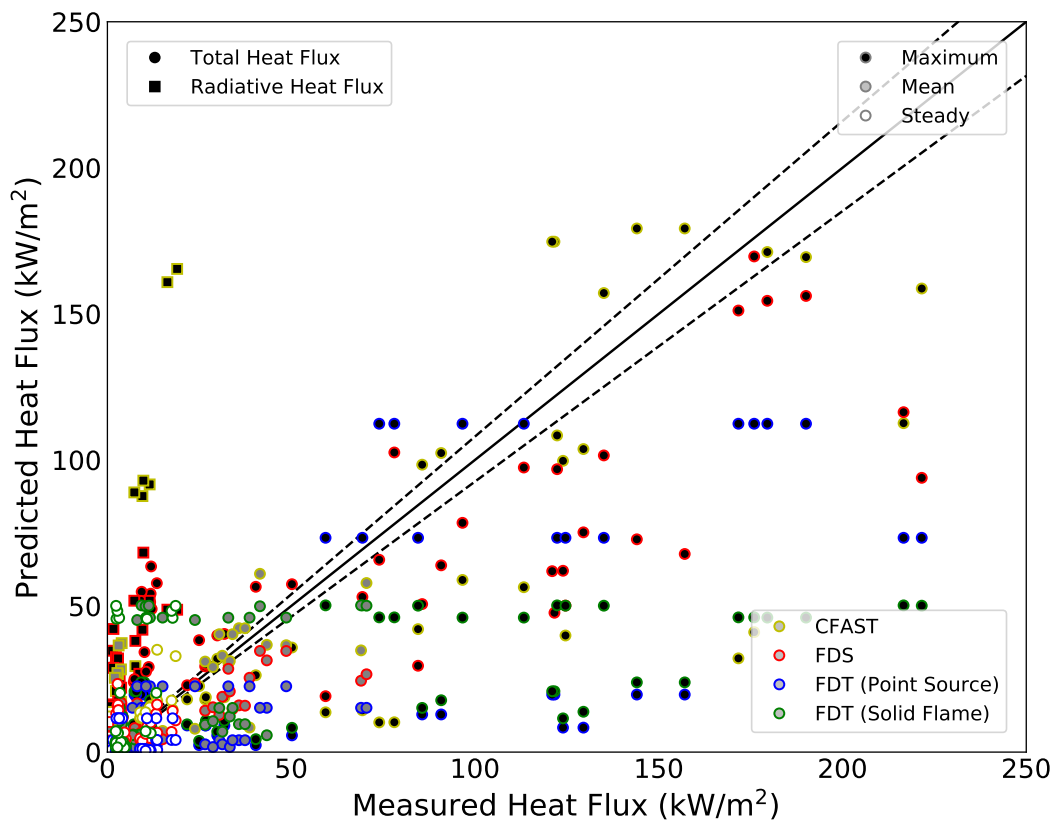


Figure 5.10: Comparison of Heat Flux Predictions to Experimental Data Collected in Compartment Experiments with Furniture

Table 5.10: Model Fitness Metrics for Heat Flux in Compartment Burner Experiments

Model	Collection	N	Bias	Uncertainty
FDS	Overall	187	1.75	±90%
	100kWSB	48	1.99	±82%
	100kW	47	2.44	±94%
	250kW	46	1.43	±73%
	500kW	46	1.17	±94%
	Open	96	1.4	±53%
	Closed	91	2.23	±117%
	Center	48	1.9	±92%
	Back	47	2.17	±81%
	Corner	44	1.49	±88%
	Side	48	1.45	±92%
FDT (Solid Flame)	Overall	122	3.22	±138%
	100kWSB	32	2.07	±133%
	100kW	26	2.49	±131%
	250kW	32	4.76	±136%
	500kW	32	3.82	±145%
	Open	61	1.55	±103%
	Closed	61	6.19	±162%
	Center	32	1.01	±64%
	Back	30	4.64	±129%
	Corner	30	5.29	±174%
	Side	30	4.15	±155%
FDT (Point Source)	Overall	128	3.53	±197%
	100kWSB	32	2.01	±191%
	100kW	32	1.86	±183%
	250kW	32	4.85	±197%
	500kW	32	7.29	±209%
	Open	64	1.36	±160%
	Closed	64	8.74	±227%
	Center	32	0.3	±67%
	Back	32	5.93	±188%
	Corner	32	9.31	±242%
	Side	32	6.64	±224%
CFAST	Overall	128	0.44	±50%
	100kWSB	32	0.44	±62%
	100kW	32	0.37	±43%
	250kW	32	0.48	±39%
	500kW	32	0.47	±52%
	Open	64	0.59	±39%
	Closed	64	0.29	±33%
	Center	32	0.46	±40%
	Back	32	0.46	±48%
	Corner	32	0.41	±51%
	Side	32	0.43	±61%

Table 5.11: Model Fitness Metrics for Heat Flux in Compartment Furniture Experiments

Metric		Maximum			Mean			Steady		
Model	Collection	N	Bias	Uncertainty	N	Bias	Uncertainty	N	Bias	Uncertainty
FDS	Overall	72	4.64	±118%	72	2.53	±110%	72	3.03	±140%
	Overstuffed Sofa	36	4.79	±134%	36	1.84	±109%	36	1.22	±122%
	Red Accent Chair	36	4.46	±99%	36	3.2	±103%	36	4.85	±125%
	Open	36	2.31	±98%	36	1.74	±89%	36	1.84	±91%
	Closed	36	7.51	±118%	36	3.64	±126%	36	5.1	±178%
	Center	24	4.97	±112%	24	2.22	±99%	24	2.92	±140%
	Back	24	3.14	±96%	24	2.01	±80%	24	2.27	±112%
	Corner	24	6.64	±144%	24	3.81	±144%	24	4.53	±169%
FDT (Solid Flame)	Overall	48	0.68	±91%	48	1.86	±100%	32	3.17	±126%
	Overstuffed Sofa	24	0.91	±111%	24	2.28	±120%	8	7.23	±132%
	Red Accent Chair	24	0.5	±66%	24	1.54	±78%	24	2.19	±116%
	Open	24	0.24	±43%	24	0.65	±65%	16	1.35	±89%
	Closed	24	1.13	±65%	24	2.99	±67%	16	6.27	±142%
	Center	16	1.18	±109%	16	1.53	±94%	8	0.84	±48%
	Back	16	0.54	±69%	16	2.27	±109%	8	3.73	±148%
	Corner	16	0.45	±82%	16	1.94	±101%	16	5.08	±132%
FDT (Point Source)	Overall	48	0.79	±102%	48	0.7	±110%	48	0.78	±127%
	Overstuffed Sofa	24	0.93	±115%	24	0.77	±119%	24	0.58	±122%
	Red Accent Chair	24	0.69	±90%	24	0.65	±101%	24	1.02	±131%
	Open	24	0.31	±78%	24	0.25	±78%	24	0.33	±105%
	Closed	24	1.2	±66%	24	1.14	±81%	24	1.31	±121%
	Center	16	1.06	±109%	16	0.51	±89%	16	0.27	±49%
	Back	16	0.7	±81%	16	0.99	±109%	16	1.64	±143%
	Corner	16	0.66	±113%	16	0.67	±125%	16	0.93	±152%
CFAST	Overall	72	2.13	±109%	72	1.65	±121%	66	2.32	±133%
	Overstuffed Sofa	36	2.77	±110%	36	2.24	±128%	36	2.92	±135%
	Red Accent Chair	36	1.56	±103%	36	1.19	±110%	30	1.71	±129%
	Open	36	3.04	±113%	36	2.87	±109%	36	3.98	±107%
	Closed	36	1.37	±96%	36	0.6	±89%	30	0.46	±77%
	Center	24	2.25	±94%	24	1.74	±119%	24	2.25	±142%
	Back	24	1.77	±105%	24	1.43	±115%	24	2.02	±125%
	Corner	24	2.46	±126%	24	1.93	±132%	18	3.06	±135%

## 5.4 Velocity

The agreement between the measured plume, ceiling jet, and door velocities and the model predictions for the compartment experiments with the gas burners is presented in Figure 5.11. Table 5.12 presents the calculated bias and uncertainty for the FDS predictions of the velocities measured in the burner experiments. The velocities below approximately 0.5 m/s were overpredicted and the plume velocities above 0.5 m/s were underpredicted. FDS predicted higher velocities at the door opening more accurately.

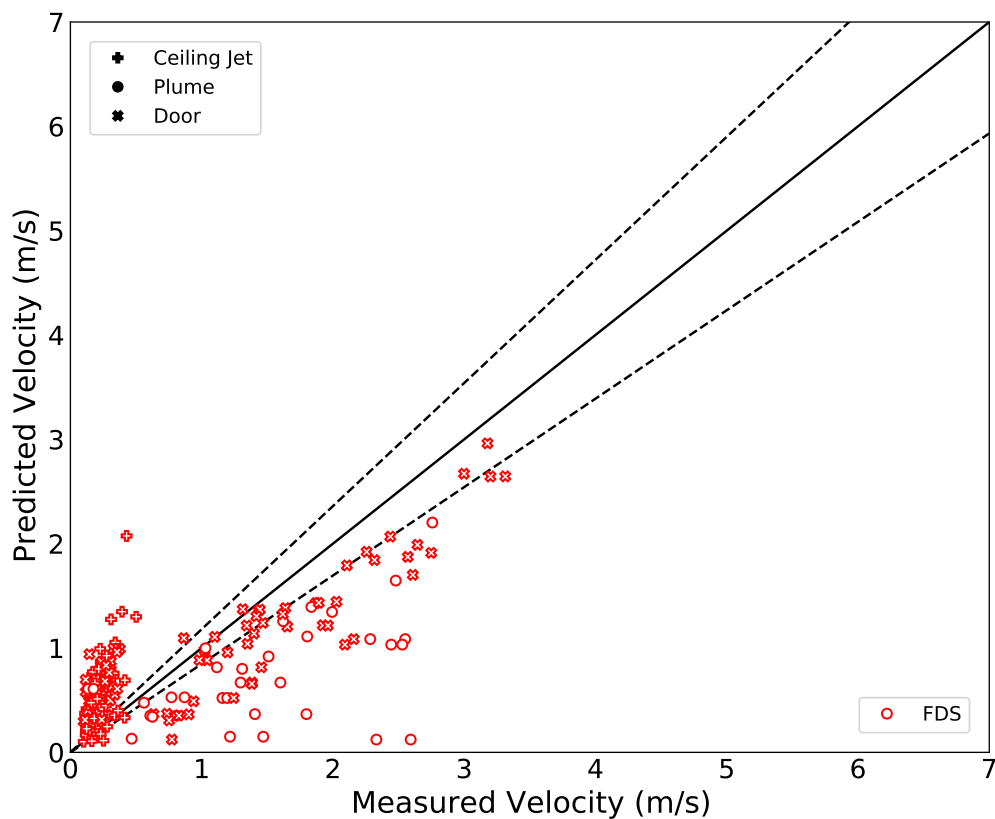


Figure 5.11: Comparison of Steady Velocity Predictions to Experimental Data Collected in Compartment Experiments with Burners

Table 5.12: Model Fitness Metrics for Velocity in Compartment Burner Experiments

Model	Collection	N	Bias	Uncertainty
FDS	Overall	177	1.83	±88%
	Ceiling Jet	52	2.36	±54%
	Plume	33	0.7	±90%
	Door	92	1.76	±75%
	100kWSB	42	1.83	±117%
	100kW	50	1.78	±66%
	250kW	45	1.76	±75%
	500kW	40	1.91	±86%
	Open	162	1.88	±85%
	Closed	15	1.19	±103%
	Center	36	1.61	±59%
	Back	52	1.83	±84%
	Corner	42	2.35	±124%
	Side	47	1.63	±73%

The comparison between the model predictions and the experimental data from the upholstered furniture experiments is presented in Figure 5.12. Table 5.12 presents the calculated bias and uncertainty for the FDS predictions of the measured velocities in the furniture experiments. FDS generally overpredicted the maximum velocities while overpredicting the mean velocities by a smaller margin.

Table 5.13: Model Fitness Metrics for Velocity in Compartment Furniture Experiments

Metric		Maximum			Mean			Steady		
Model	Collection	N	Bias	Uncertainty	N	Bias	Uncertainty	N	Bias	Uncertainty
FDS	Overall	106	1.8	±55%	106	1.14	±62%	106	1.27	±86%
	Ceiling Jet	48	2.68	±45%	48	1.22	±57%	48	1.25	±100%
	Plume	16	0.88	±42%	16	0.73	±96%	16	1.09	±114%
	Door	42	1.2	±14%	42	1.17	±23%	42	1.29	±30%
	Overstuffed Sofa	53	1.86	±61%	53	1.18	±62%	53	1.32	±97%
	Red Accent Chair	53	1.74	±49%	53	1.1	±62%	53	1.22	±73%
	Open	74	1.48	±37%	74	1.3	±38%	74	1.53	±55%
	Closed	32	2.71	±78%	32	0.68	±69%	32	0.44	±70%
	Center	30	2.21	±59%	30	1.22	±44%	30	1.28	±73%
	Back	38	1.58	±47%	38	1.07	±71%	38	1.23	±91%
	Corner	38	1.71	±57%	38	1.14	±63%	38	1.31	±91%

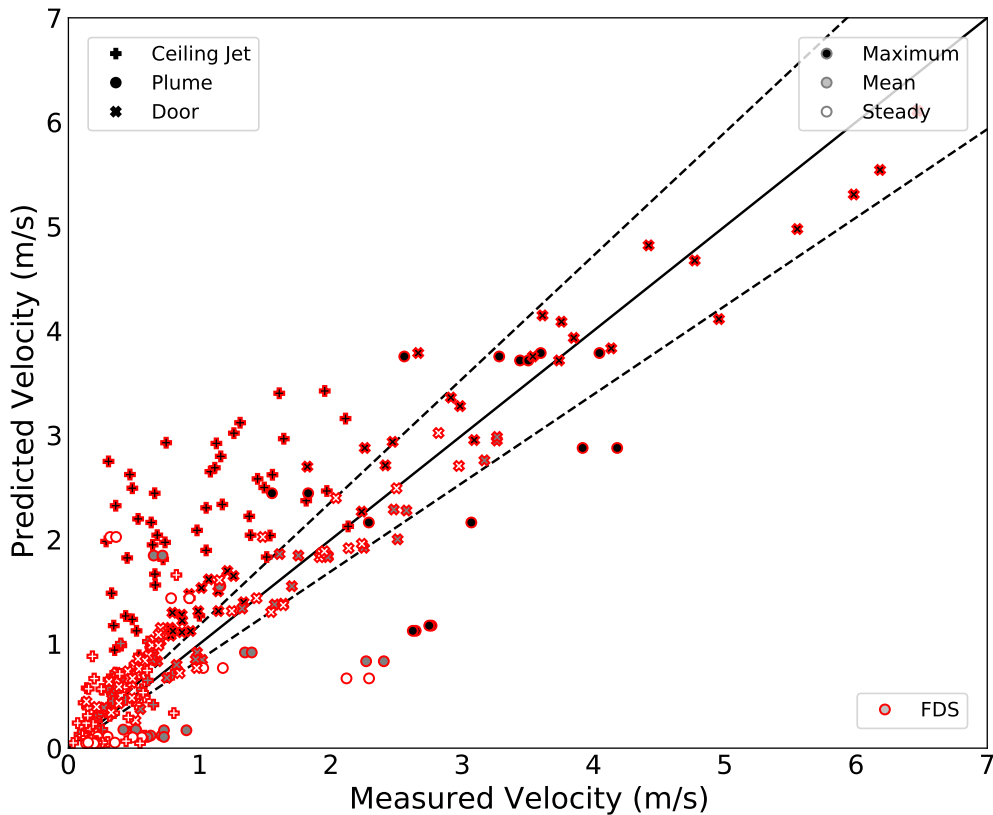


Figure 5.12: Comparison of Velocity Predictions to Experimental Data Collected in Compartment Experiments with Furniture

## 5.5 Oxygen Concentration

The agreement between the measured oxygen concentrations and the model predictions for the compartment experiments with the gas burners is presented in Figure 5.13. Table 5.14 presents the calculated bias and uncertainty for the FDS predictions of the minimum oxygen concentrations in the burner experiments. The CFAST and FDS predictions for the steady oxygen concentration in the compartment burner experiments were generally accurate, although FDS showed more consistently accurate predictions. The CFAST predictions were distributed according to the elevation of the measurement, with the higher elevation prediction of approximately 10% O<sub>2</sub> and the lower elevation minimum prediction of approximately 20% O<sub>2</sub>. The comparisons between the predictions and measurements for both models was more repeatable when the door was open compared to when the door was closed.

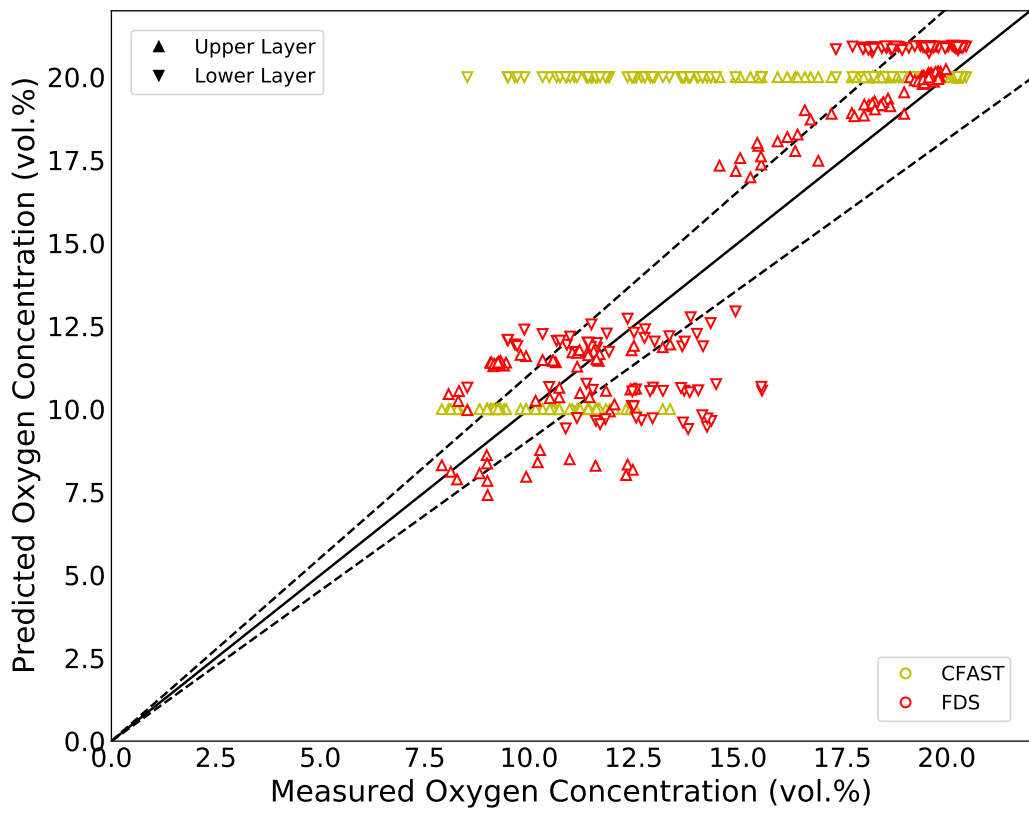


Figure 5.13: Comparison of Oxygen Concentration Predictions to Experimental Data Collected in Compartment Experiments with Burners

Table 5.14: Model Fitness Metrics for Oxygen Concentration in Compartment Burner Experiments

Model	Collection	N	Bias	Uncertainty
FDS	Overall	248	1.0	±10%
	100kWSB	64	1.09	±8%
	100kW	59	1.0	±6%
	250kW	61	0.98	±14%
	500kW	64	0.97	±20%
	Open	125	1.06	±3%
	Closed	123	0.96	±18%
	Center	61	1.02	±18%
	Back	64	0.98	±12%
	Corner	61	1.03	±15%
	Side	62	1.02	±11%
CFAST	Overall	248	1.17	±20%
	100kWSB	64	1.22	±26%
	100kW	59	1.12	±23%
	250kW	61	1.17	±22%
	500kW	64	1.24	±19%
	Open	125	1.06	±6%
	Closed	123	1.32	±29%
	Center	61	1.2	±24%
	Back	64	1.13	±22%
	Corner	61	1.21	±23%
	Side	62	1.21	±23%

The comparison between the model predictions and the experimental data from the upholstered furniture experiments is presented in Figure 5.14. Table 5.15 presents the calculated bias and uncertainty for the FDS predictions of the minimum oxygen concentrations in the compartment experiments. CFAST and FDS generally accurately predicted the mean and steady oxygen concentrations and overpredicted the minimum oxygen concentration.

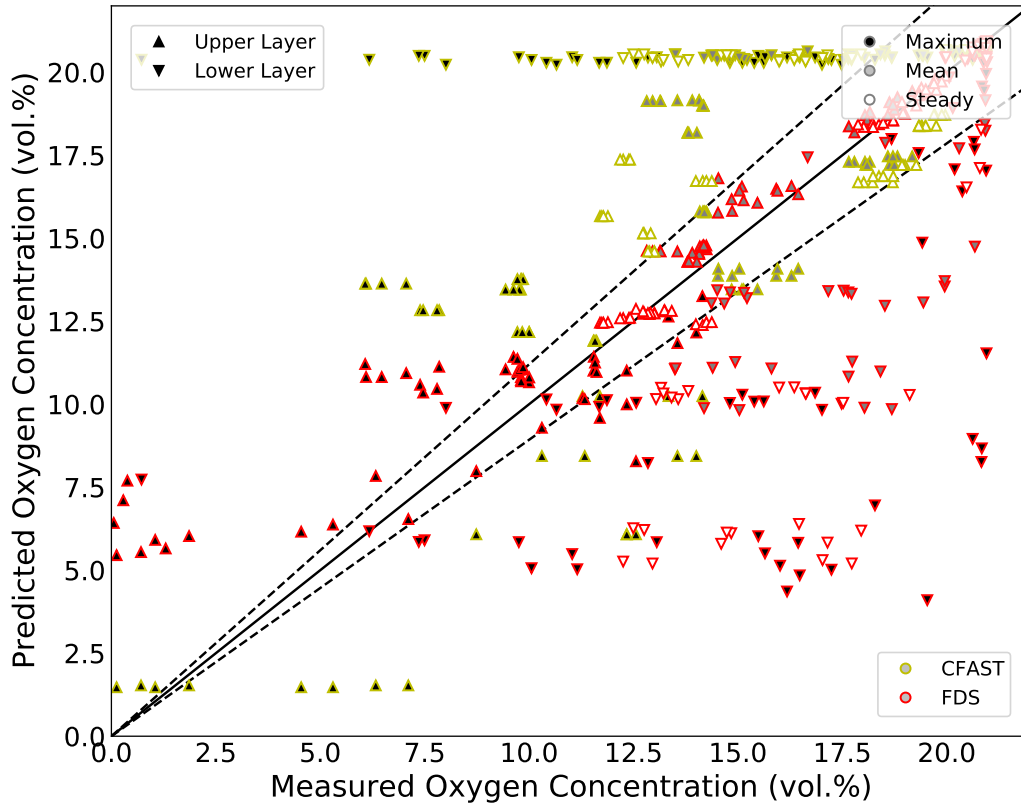


Figure 5.14: Comparison of Oxygen Concentration Predictions to Experimental Data Collected in Compartment Experiments with Furniture

Table 5.15: Model Fitness Metrics for Oxygen Concentration in Compartment Furniture Experiments

Metric		Minimum			Mean			Steady		
Model	Collection	N	Bias	Uncertainty	N	Bias	Uncertainty	N	Bias	Uncertainty
FDS	Overall	96	1.69	±99%	96	0.93	±13%	96	0.87	±30%
	Overstuffed Sofa	48	3.12	±138%	48	0.92	±20%	48	0.84	±41%
	Red Accent Chair	48	0.9	±18%	48	0.96	±8%	48	0.91	±16%
	Open	48	2.97	±130%	48	0.99	±10%	48	0.99	±4%
	Closed	48	0.94	±46%	48	0.9	±21%	48	0.77	±40%
	Center	32	2.99	±132%	32	0.94	±19%	32	0.9	±36%
	Back	32	1.03	±64%	32	0.93	±16%	32	0.87	±31%
	Corner	32	1.61	±90%	32	0.96	±18%	32	0.89	±31%
CFAST	Overall	92	1.49	±63%	96	1.11	±12%	88	1.11	±13%
	Overstuffed Sofa	44	1.98	±81%	48	1.14	±16%	48	1.14	±17%
	Red Accent Chair	48	1.14	±35%	48	1.09	±10%	40	1.08	±13%
	Open	44	1.37	±83%	48	0.97	±5%	48	0.96	±3%
	Closed	48	1.57	±24%	48	1.28	±10%	40	1.31	±11%
	Center	28	1.71	±67%	32	1.11	±14%	32	1.14	±18%
	Back	32	1.23	±55%	32	1.11	±15%	32	1.11	±15%
	Corner	32	1.67	±68%	32	1.16	±19%	24	1.11	±19%

## 6 Discussion

Each of the modeling methods has advantages and disadvantages relative to the other methods. The FDT methods are simplistic and have been compiled into convenient and freely available spreadsheets. These spreadsheets make interpretation of data and assessment of the sensitivity of input parameters straightforward and may help investigators attain a better understanding of the fire dynamics of given fire scenarios. CFAST is open source and provides more functionality than the FDT spreadsheets while also requiring relatively little computational expense. CFAST is limited to compartment scenarios and the assumptions that govern the two-zone model limit the breadth of quantities that may be predicted. FDS is open source and provides the most functionality and predicted quantities of the three modeling methods that have been investigated. Because of its complexity relative to the other methods, FDS simulations are the most computationally expensive and generally require more inputs to be defined. The larger set of required inputs for FDS also increases the degrees of freedom and the likelihood that the results will be overly sensitive to uncertainty in a specific input parameter.

The FDT correlation for plume temperatures yielded predictions that were significantly higher than the maximum plume temperatures for the furniture experiments. FDS overpredicted the maximum plume temperatures for the burner experiments. The plume temperatures in the compartment experiments were underpredicted, which indicates the influence of compartment effects which were not adequately represented with the physics invoked in the FDS models presented here. FDS provided reasonable predictions of the ceiling jet temperatures and temperatures of gas flow through the door for the compartment experiments.

The FDT method to predict the temperature of the upper layer yielded accurate predictions for the open door compartment experiments, but it significantly overpredicted the upper layer temperature when the door was closed. FDS and CFAST accurately predicted the upper and lower layer temperatures for the compartment experiments with the gas burners but predicted the gas layer temperatures less accurately for the furniture experiments. CFAST predicted the maximum and mean depth of descent of the layer interface while FDS accurately predicted the mean depth of descent of the gas layer and overpredicted the maximum depth of descent. The FDT method yielded a binary result with the layer interface located either at the floor of the compartment or at the top of the door, which corresponded to underpredictions with the compartment door open and overpredictions with the compartment door closed.

The Heskestad and Thomas flame height correlations generally overpredicted the flame height in the compartment experiments with the fuel source located at a wall or in a corner. The range of flame heights predicted by FDS encompassed the observed flame height for the compartment burner experiments conducted with the door open. The observed flame height for the compartment burner experiments when the door was closed and for the furniture experiments in the compartment were generally overpredicted. CFAST overpredicted most of the measured flame heights in the compartment experiments.

The point source heat flux model overpredicted the measured fluxes in the compartment experiments. The solid flame model overpredicted heat fluxes in all experiments. FDS tended to predict maximum and mean heat fluxes with large scatter in agreement for the compartment experiments. CFAST underpredicted the heat fluxes in the compartment experiments with the burners and generally overpredicted the heat fluxes in the experiments with the furniture items.

Plume velocities were reasonably predicted in the compartment experiments with furniture, but were underpredicted in the compartment burner experiments. Mean and steady ceiling jet velocities were accurately predicted but maximum ceiling jet velocities were overpredicted and velocities of flow through the open compartment door were typically accurately predicted by FDS.

CFAST and FDS both provided reasonable estimates for the minimum oxygen concentration, although both models appeared to have difficulty representing ventilation-limited conditions in which the oxygen concentration was measured as approximately 0%. The mean and steady oxygen concentrations were typically accurately predicted by both models. In general, CFAST tended to overpredict oxygen concentrations and FDS tended to underpredict oxygen concentrations.

# 7 Recommendations

Because fire investigators are expected to almost exclusively encounter compartment fires fueled by materials and products that are common to residential and commercial occupancies, the recommendations presented in this work focus on the furniture experiments conducted in the compartment. The FDT methods for predicting flame height are the only FDT methods investigated in this work that yielded accurate predictions. The FDT methods for flame height were generally accurate when the observed flame heights were below the ceiling height and also correctly indicated when the flame impinged on the ceiling. The FDT predictions of plume temperature and layer temperature were overly conservative and cannot be recommended to investigators.

CFAST is recommended for predicting the layer interface height with the understanding that the maximum depth of descent was typically underpredicted when the door was open and overpredicted when the door was closed. If CFAST is used for layer temperature prediction, practitioners should understand that all predicted temperatures were typically lower than the measurements. CFAST was able to accurately predict that flames impinged on the ceiling in the furniture compartment experiments and is expected to slightly overestimate flame heights below the ceiling when the door to the compartment is open. Temperature and flame height predictions in CFAST are most sensitive to the uncertainty in the HRR, so it is recommended that uncertainty in the defined HRR be reduced and that a sensitivity analysis be conducted to define the uncertainty in the predictions and declare a level of confidence for the conclusions drawn from the analysis.

FDS is capable of predicting realistic temperatures throughout the computational domain. It is the recommended method for predicting layer temperatures because it generally yielded accurate predictions for the maximum layer temperatures. If FDS is used to predict the depth of descent of the layer interface, the mean and steady layer interface heights are more reliable than the predicted maximum depth of descent of the interface. FDS is capable of conservative plume velocity and ceiling jet velocity predictions as well as accurate prediction of the flow velocity through the open compartment door. Model practitioners should understand the relatively high uncertainty when using FDS for velocity predictions. FDS was capable of predicting flame impingement on the ceiling for the furniture-fueled fires and is a recommended method to predict flame heights when the compartment door is open and flames are not expected to impinge on the ceiling.

Both FDS and CFAST are recommended for oxygen concentration predictions. In general, CFAST and FDS are capable of accurate predictions of the mean oxygen concentration but model practitioners should be cognizant of the uncertainties when using either model to predict the minimum oxygen concentration in a compartment. Both models have shown issues simulating underventilated fires and those concerns have been confirmed in this work.

The scatter exhibited in all the modeling methods for heat flux predictions make recommendation of a method for predicting heat flux from a furniture-fueled fire in a compartment impossible. Because of the uncertainty in the results in each case, none of the methods can reliably be considered to provide a conservative estimate. This is an area that requires further research and development.

## 8 Research Needs

Additional research is necessary to determine a heat flux correlation or modeling method that is more consistently accurate and representative of the dynamics of furniture-fueled enclosure fires. Because the flame, fire plume, hot gas layer, and walls participate in radiative heat flux incident to a target in a compartment, it is not surprising that the simplistic FDT methods did not accurately represent the experimental heat fluxes. The zone modeling approach improves on the simplistic algebraic equations for heat flux from the fire by including other participating surfaces, but the calculation is too heavily reliant on empirical correlations to represent the heat flux from a complex-shaped burning furniture item. FDS further improves on the representation of heat flux in CFAST by allowing geometric shapes to be represented in the model, but this work has shown that the representations of the furniture in the FDS models did not ultimately result in accurate heat flux predictions. Research on the effect of burning definitions, defined geometry, spatial resolution, and model-specific input parameters on the heat flux as well as all the predicted quantities will provide recommendations for fire investigators on the use of FDS.

The idealistic use of a computational fire model for fire scene reconstruction involves defining all the required material properties for component materials and the geometry of the scene and allowing for complete prediction of flame spread over furniture items and throughout the compartment to test hypotheses. This type of model is theoretically possible with the current version of FDS but the implementation of such a complicated representation of burning has yet to be standardized and validated. Additional research to understand the best methods to implement such a model for burning items will improve the state of fire modeling and the conclusions that may be drawn from models like FDS and CFAST. Additionally, the wide breadth of material properties and input parameters required for such an implementation are generally not available or, when they are available, are incomplete or do not represent the exact component materials in the fire scenario. The development of a comprehensive fire material properties database will expand the possibilities for fire investigators that use FDS and similar models and help to realize the full potential and predictive capabilities of field fire models.

## 9 Summary

UL Firefighter Safety Research Institute conducted a study to evaluate the ability of commonly-used fire dynamics analyses to predict the fire environment generated from gas burners and modern upholstered furniture in a simple compartment. Two sizes of burners were used in experiments with heat release rates ranging from 50 kW to 500 kW. Two furniture items including one upholstered chair and one upholstered sofas were tested. Variables investigated in the compartment experiments included location of the burner or fuel package and the status of the door.

Specialized fire dynamics routines, a zone fire model, and a field fire model were used to predict various quantities measured in the compartment experiments. The accuracy of each model was calculated based on a comparison of the maximum observed and predicted quantities in the burner experiments and the maximum, mean, and steady values in the decay period for the compartment experiments. The accuracy of each model was evaluated for collections of experimental parameters (fuel package, location of the fuel package, status of the door, etc.) to define the limitations of each model.

The specialized fire dynamics routines were capable of accurately characterizing the flame height, but did not accurately predict the other quantities for the furniture-fueled fire experiments conducted in the compartment. The zone fire model accurately predicted the layer interface heights, layer temperatures, flame heights, and oxygen concentrations in the compartment fire scenarios. The field model predicted accurate temperatures throughout the compartment, layer interface heights, velocities through the open door of the compartment, flame heights, and oxygen concentrations. In general, the predictive ability of all the models was better in the gas burner experiments than in the furniture experiments. More research is needed to develop recommendations on geometry and burning definitions for upholstered furniture in field models as well as improved methods for model practitioners to predict heat flux.

# References

- [1] National Fire Protection Association. *NFPA 921, Guide for Fire and Explosion Investigations*, 2021.
- [2] S. Kerber. Analysis of Changing Residential Fire Dynamics and Its Implications on Firefighter Operational Timeframes. Technical report, Underwriters Laboratories, Northbrook, Illinois, 2012.
- [3] C.L. Smith. Preliminary Regulatory Analysis of a Draft Proposed Rule to Address Cigarette and Small Open Flame Ignitions of Upholstered Furniture. Directorate for Economic Analysis, U.S. Consumer Product Safety Commission, Washington, D.C., November 2005.
- [4] U.S. Census Bureau. Quickfacts. <https://www.census.gov/quickfacts/fact/table/US/HSD410218>, 2020.
- [5] M. Ahrens. Home Fires That Began with Upholstered Furniture. Report, National Fire Protection Agency (NFPA), February 2017.
- [6] National Fire Protection Agency (NFPA). White Paper on Upholstered Furniture Flammability. Report, September 2013.
- [7] Eric Guillaume, Rene de Feijter, and Laurens van Gelderen. An overview and experimental analysis of furniture fire safety regulations in Europe. *Fire and Materials*, 44(5), 2020.
- [8] R. Campbell. Intentional Fires. Report, National Fire Protection Association, July 2017.
- [9] J. Floyd. Comparison of CFAST and FDS for Fire Simulation with the HDR T51 and T52 Tests. NISTIR 6866, National Institute of Standards and Technology, Gaithersburg, Maryland, March 2002.
- [10] G. Rein, A. Bar-Ilan, A.C. Fernandez-Pello, and N. Alvarez. A Comparison of Three Models in the Simulations of Accidental Fires. *Journal of Fire Protection Engineering*, 2005.
- [11] K. Hill, J. Dreisbach, F. Joglar, B. Najafi, K. McGrattan, R. Peacock, and A. Hamins. Verification and Validation of Selected Fire Models for Nuclear Power Plant Applications. NUREG-1824, United States Nuclear Regulatory Commission, Washington, DC, 2007.
- [12] N. Iqbal and M. Salley. Fire Dynamics Tools (FDTs): Quantitative Fire Hazard Analysis Methods for the U.S. Nuclear Regulatory Commission Fire Protection Inspection Program. NUREG-1805, United States Nuclear Regulatory Commission, Washington, DC, 2004.
- [13] F. Joglar. Verification and Validation of Selected Fire Models for Nuclear Power Plant Applications Volume 4: Fire-Induced Vulnerability Evaluation (FIVE-Rev1). NUREG-1824, United States Nuclear Regulatory Commission, Washington, DC, 2007.

- [14] K.J. Overholt. Verification and Validation of Commonly Used Empirical Correlations for Fire Scenarios. NIST Special Publication 1169, National Institute of Standards and Technology, Gaithersburg, Maryland, 2014.
- [15] M.H. Salley and A. Lindeman. Verification and Validation of Selected Fire Models for Nuclear Power Plant Applications. NUREG-1824, Supplement 1, United States Nuclear Regulatory Commission, Washington, DC, 2016.
- [16] M.L. Janssens, D.M. Ewan, C. Gomez, M.M. Hirschler, J.P. Huczek, R.L. Mason, K.J. Overholt, and J.M. Sharp. Reducing Uncertainty of Quantifying the Burning Rate of Upholstered Furniture. Technical report, SwRI Project No. 0.1.15998, Award No. 2010-DN-BX-K221, for National Institute of Justice, 2012.
- [17] R.A. Bryant and G. Mullholland. A guide to characterizing heat release rate measurement uncertainty for full-scale fire tests. *Fire and Materials*, 32:121–139, 2008.
- [18] W.M. Pitts, A.V. Murthy, J.L. de Ris, J. Filtz, K. Nygård, D. Smith, and I. Wetterlund. Round robin study of total heat flux gauge calibration at fire laboratories. *Fire Safety Journal*, 41(6):459–475, 2006.
- [19] R.A. Bryant. A comparison of gas velocity measurements in a full-scale enclosure fire. *Fire Safety Journal*, 44:793–800, 2009.
- [20] L.G. Blevins. Behavior of bare and aspirated thermocouples in compartment fires. In *National Heat Transfer Conference, 33rd Proceedings*, pages 15–17, 1999.
- [21] W.M. Pitts, E. Braun, R. Peacock, H. Mitler, E. Johnson, P. Reneke, and L.G. Blevins. Temperature uncertainties for bare-bead and aspirated thermocouple measurements in fire environments. *ASTM Special Technical Publication*, 1427:3–15, 2003.
- [22] A. Lock, M. Bundy, E.L. Johnsson, A. Hamins, G.H. Ko, C. Hwang, P. Fuss, and R. Harris. Experimental study of the effects of fuel type, fuel distribution, and vent size on full-scale underventilated compartment fires in an ISO 9705 room. NIST Technical Note 1603, National Institute of Standards and Technology, Gaithersburg, MD, 2008.
- [23] J. Willi and D. Madrzykowski. Examination of Fire Dynamics Analysis Techniques: Compartment Fire Experiments. Technical report, UL Firefighter Safety Research Institute, Columbia, Maryland, April 2021.
- [24] ASTM International. *Standard E 779: Standard Test Method for Determining Air Leakage Rate by Fan Pressurization*, 2010.
- [25] Wanyu R. Chan, Jeffrey Joh, and Max H. Sherman. Analysis of air leakage measurements of us houses. *Energy and Buildings*, 66:616 – 625, 2013.
- [26] M.L. Janssens and H.C. Tran. Data Reduction of Room Tests for Zone Model Validation. *Journal of Fire Science*, 10:528–555, 1992.

- [27] K. McGrattan, S. Hostikka, J. Floyd, R. McDermott, and M. Vanella. *Fire Dynamics Simulator, Technical Reference Guide Volume 3: Validation*. National Institute of Standards and Technology, Gaithersburg, Maryland, USA, and VTT Technical Research Centre of Finland, Espoo, Finland, sixth edition, September 2019.
- [28] B.J. McCaffrey, J.G. Quintiere, and M.F. Harkelroad. Estimating Room Temperatures and the Likelihood of Flashover Using Fire Test Data Correlations. *Fire Technology*, 17(2):98–119, 1981.
- [29] C. Beyler. Analysis of Compartment Fires with Overhead Forced Ventilation. In *Fire Safety Science – Proceedings of the Third International Symposium*, pages 291–300. International Association for Fire Safety Science, 1991.
- [30] Takeyoshi Tanaka and Toshio Yamana. Smoke Control in Large Scale Spaces (Part 1: Analytic Theories For Simple Smoke Control Problems). *Fire Science and Technology*, 5(1):31–40, 1985.
- [31] Toshio Yamana and Takeyoshi Tanaka. Smoke Control in Large Scale Spaces (Part 2: Smoke Control Experiments In A Large Storage Space). *Fire Science and Technology*, 5(1):41–54, 1985.
- [32] P.H. Thomas. The size of flames from natural fires. *Symposium (International) on Combustion*, 9(1):844 – 859, 1963.
- [33] G. Heskestad. Luminous Heights of Turbulent Diffusion Flames. *Fire Safety Journal*, 5:103–108, 1983.
- [34] G. Heskestad. Flame Heights of Fuel Arrays with Combustion in Depth. In *Fire Safety Science – Proceedings of the Fifth International Symposium*, pages 427–438. International Association for Fire Safety Science, 1997.
- [35] M.A. Delichatsios. Flame heights in turbulent wall fires with significant flame radiation. *Combustion Science and Technology*, 39:195–214, 1984.
- [36] T. Ahmad and G.M. Faeth. Turbulent wall fires. *Symposium (International) on Combustion*, 17(1):1149 – 1160, 1979. Seventeenth Symposium (International) on Combustion.
- [37] Y. Hasemi and T. Tokunaga. Some Experimental Aspects of Turbulent Diffusion Flames and Buoyant Plumes from Fire Sources Against a Wall and in a Corner of Walls. *Combustion Science and Technology*, 40(1-4):1–17, 1984.
- [38] C. Beyler. *SFPE Handbook of Fire Protection Engineering*, chapter Chapter 66 - Fire Hazard Calculations for Large, Open Hydrocarbon Fires. Springer, Bethesda, MD, 2016.
- [39] M. Shokri and C.L. Beyler. Radiation from large pool fires. *Journal of Fire Protection Engineering*, 1(4):141–149, 1989.
- [40] Gunnar Heskestad. Engineering relations for fire plumes. *Fire Safety Journal*, 7(1):25 – 32, 1984.

- [41] J.G. Quintiere and C.A. Wade. *SFPE Handbook of Fire Protection Engineering*, chapter Chapter 29 - Compartment Fire Modeling. Springer, Bethesda, MD, 2016.
- [42] R. D. Peacock, K. B. McGrattan, G. P. Forney, and P. A. Reneke. CFAST – Consolidated Model of Fire Growth and Smoke Transport (Version 7) Volume 1: Technical Reference Guide. Technical Note 1889v1, National Institute of Standards and Technology, Gaithersburg, Maryland, June 2020.
- [43] G.P. Forney. Smokeview, A Tool for Visualizing Fire Dynamics Simulation Data, Volume I: User’s Guide. NIST Special Publication 1017-1, National Institute of Standards and Technology, Gaithersburg, Maryland, January 2017.
- [44] K. McGrattan, S. Hostikka, J. Floyd, R. McDermott, and M. Vanella. *Fire Dynamics Simulator, User’s Guide*. National Institute of Standards and Technology, Gaithersburg, Maryland, USA, and VTT Technical Research Centre of Finland, Espoo, Finland, Sixth edition, September 2019.
- [45] K. McGrattan, S. Hostikka, J. Floyd, R. McDermott, and M. Vanella. *Fire Dynamics Simulator, Technical Reference Guide Volume 1: Mathematical Model*. National Institute of Standards and Technology, Gaithersburg, Maryland, USA, and VTT Technical Research Centre of Finland, Espoo, Finland, sixth edition, September 2019.
- [46] K. McGrattan, S. Hostikka, J. Floyd, R. McDermott, and M. Vanella. *Fire Dynamics Simulator, Technical Reference Guide, Volume 2: Verification*. National Institute of Standards and Technology, Gaithersburg, Maryland, USA, and VTT Technical Research Centre of Finland, Espoo, Finland, sixth edition, January 2017.
- [47] R. McDermott, K. McGrattan, and J. Floyd. A simple reaction time scale for under-resolved fire dynamics. In *Fire Safety Science – Proceedings of the 10th International Symposium*, pages 809–820, University of Maryland, College Park, Maryland, USA, 2011.
- [48] McDermott R. Vaari J., Floyd J. CFD Simulations of Co-Flow Diffusion Flames. In *Proceedings of the International Symposium of Fire Safety Science*, volume 10, pages 781–794, College Park, MD, June 2011. International Association for Fire Safety Science.
- [49] BNZ Materials, Inc. Marinite I. Technical report, North Billerica, MA, 2013.
- [50] M.K. Kumaran, J.C. Lackey, N. Normandin, F. Tariku, and D. van Reenan. A Thermal and Moisture Transport Property Database for Common Building and Insulating Materials: Final Report from ASHRAE Research Project 1018-RP. Technical report, American Society of Heating, Refrigerating, and Air-Conditioning Engineers, Inc., Atlanta, GA, 2002.
- [51] K. Ghazi Wakili, E. Hugi, L. Wullschleger, and T.H. Frank. Gypsum Board in Fire – Modeling and Experimental Validation. *Journal of Fire Sciences*, 25(3):267–282, 2007.
- [52] V. Kodur, D. Dwaikat, and R. Fike. High-Temperature Properties of Steel for Fire Resistance Modeling of Structures. *Journal of Materials in Civil Engineering*, 22(5):423–434, 2010.

- [53] V.K.R. Kodur and M.A. Sultan. Effect of Temperature on Thermal Properties of High-Strength Concrete. *Journal of Materials in Civil Engineering*, 15(2):101–107, March/April 2003.
- [54] M. Hurley, editor. *SFPE Handbook of Fire Protection Engineering*. Springer, New York, 5th edition, 2016.
- [55] H. Brohus, P.V. Nielsen, A.J. Petersen, and K. Sommerlund-Larsen. Sensitivity Analysis of Fire Dynamics Simulation. In *Proceedings of Roomvent*, pages 1341–1352, June 2007. Helsinki.
- [56] R. Upadhyay and O. Ezekoye. Treatment of design fire uncertainty using Quadrature Method of Moments. *Fire Science Journal*, 43:127–139, 2008.
- [57] W. Jahn, G. Rein, and J. Torrero. The Effect of Model Parameters on the Simulation of Fire Dynamics. In *Fire Safety Science – Proceedings of the Ninth International Symposium*, pages 1341–1352, September 2008. Karlsruhe, Germany.
- [58] R. D. Peacock, G. P. Forney, and P. A. Reneke. CFAST – Consolidated Model of Fire Growth and Smoke Transport (Version 7) Volume 3: Verification and Validation Guide. Technical Note 1889v3, National Institute of Standards and Technology, Gaithersburg, Maryland, February 2021.

# Appendix A Detailed Results

## A.1 Compartment Experiments

This section presents comparisons of the experimental data and model predictions for the compartment experiments. In each figure, data that was measured with the fuel package in each location are presented along with the corresponding model predictions using the FDT methods, CFAST, and FDS. The data collected with the door open and closed are presented separately in each of the following sections.

### A.1.1 Gas Temperature

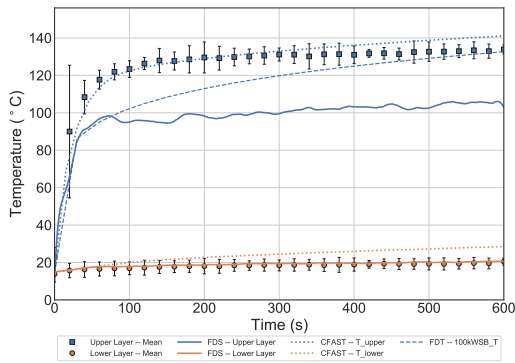
#### Open Door

A comparison of the layer temperature data collected in the experiments with the 0.3 m Burner and a HRR of 100 kW is presented in Figure A.1. The FDT method tended to underpredict the upper layer temperature, but gradually increased as the measured temperature reached a steady state, effectively decreasing the error over time. FDS tended to underpredict the steady upper layer temperature, but accurately predicted the lower layer temperature. CFAST predicted the upper layer temperature remarkably well, but tended to slightly overpredict the lower layer temperature. There was no significant difference based on the location of the burner in each experiment.

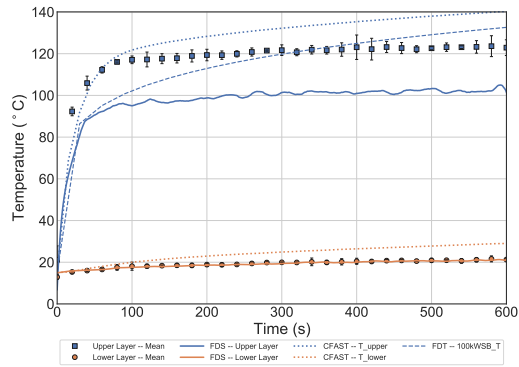
A comparison of the layer interface elevation collected in the experiments with the 0.3 m Burner and a HRR of 100 kW is presented in Figure A.2. The FDT method predicted a rapid descent of the layer interface, but was limited by the door height, so a true comparison is unavailable. FDS tended to overpredict the descent of the upper layer and CFAST tended to underpredict the descent of the upper layer. There was no significant difference in the data or predictions based on the location of the burner in each experiment.

A comparison of the layer temperature data collected in the experiments with the 0.6 m Burner and a HRR of 100 kW is presented in Figure A.3. The FDT method tended to underpredict the upper layer temperature, but gradually increased as the measured temperature reached a steady state, effectively decreasing the error over time. FDS tended to underpredict the steady upper layer temperature, but accurately predicted the lower layer temperature. CFAST slightly underpredicted the upper layer temperature and tended to overpredict the lower layer temperature. There was no significant difference based on the location of the burner in each experiment.

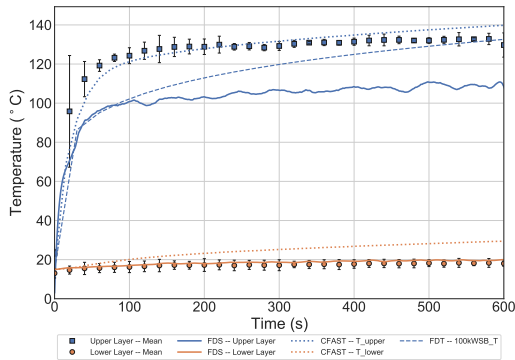
A comparison of the layer interface elevation collected in the experiments with the 0.6 m Burner and a HRR of 100 kW is presented in Figure A.4. The FDT method predicted a rapid descent of the layer interface, but was limited by the door height, so a true comparison is unavailable. FDS



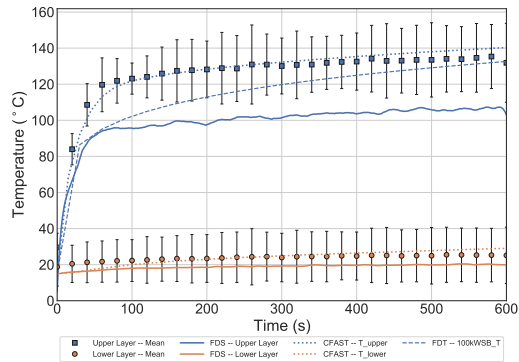
(a) Center Position



(b) Back Position



(c) Corner Position

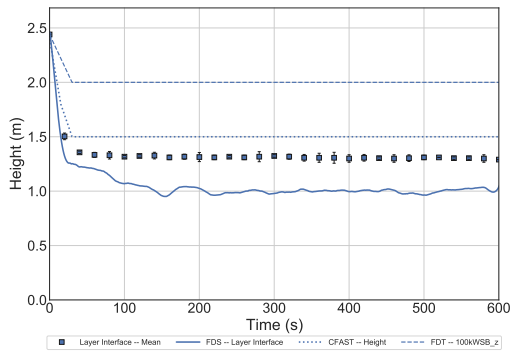


(d) Side Position

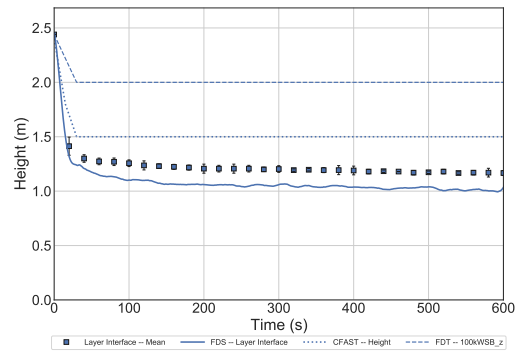
Figure A.1: Comparison of the Layer Temperatures in 0.3 m Burner, 100 kW Experiments with Door Open

tended to slightly overpredict the descent of the upper layer and CFAST tended to underpredict the descent of the upper layer. There was no significant difference in the data or predictions based on the location of the burner in each experiment.

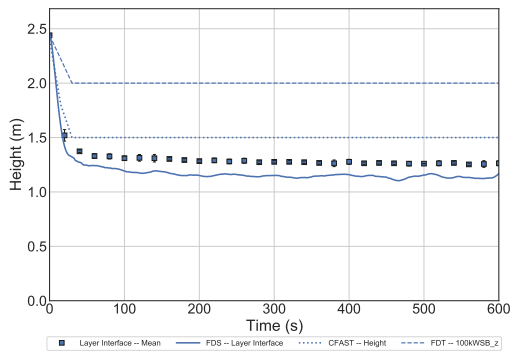
A comparison of the layer temperature data collected in the experiments with the 0.6 m Burner and a HRR of 500 kW is presented in Figure A.5. The FDT method tended to underpredict the upper layer temperature, but gradually increased as the measured temperature reached a steady state, effectively decreasing the error over time. FDS tended to underpredict the steady upper layer temperature, and slightly underpredicted the lower layer temperature. CFAST accurately predicted the upper layer temperature, but continued increasing as the experimental data reached a steady state, effectively increasing the error between the two. CFAST tended to overpredict the lower layer temperature. There was no significant difference based on the location of the burner in each experiment.



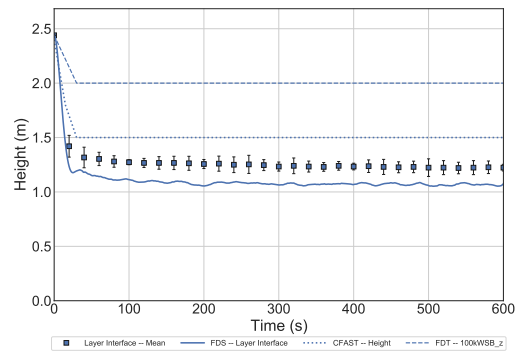
(a) Center Position



(b) Back Position



(c) Corner Position

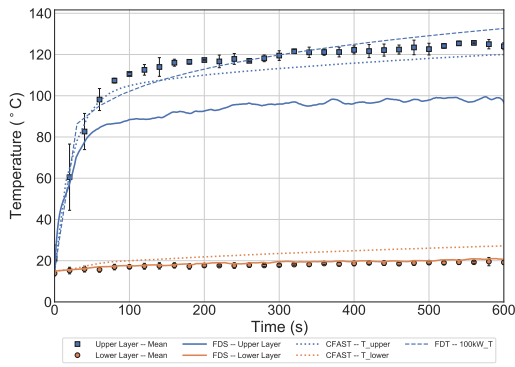


(d) Side Position

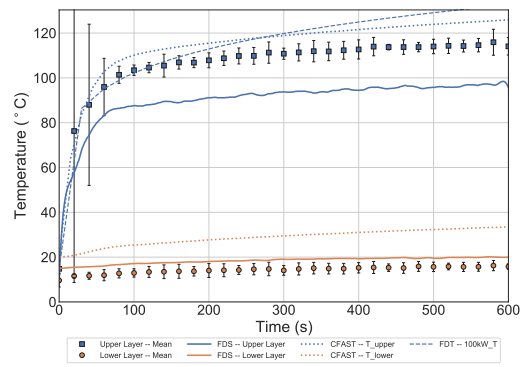
Figure A.2: Comparison of the Layer Interface Elevation in 0.3 m Burner, 100 kW Experiments with Door Open

A comparison of the layer interface elevation collected in the experiments with the 0.6 m Burner and a HRR of 500 kW is presented in Figure A.6. The FDT method predicted a rapid descent of the layer interface, but was limited by the door height, so a true comparison is unavailable. FDS accurately predicted the elevation of the upper layer interface and CFAST accurately predicted the descent of the upper layer until approximately 150 s, at which point CFAST predicted a rise in the interface that was not observed. There was no significant difference in the data or predictions based on the location of the burner in each experiment.

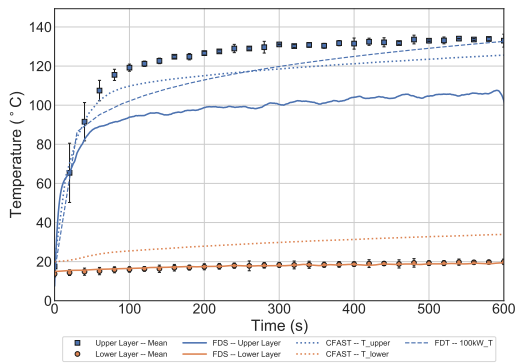
A comparison of the layer temperature data collected in the experiments with the Red Accent Chair is presented in Figure A.7. The FDT method was developed for a constant HRR fire source away from the walls of the compartment and does not account for a growth period or decay period. The maximum upper and low layer temperature was highest when the chair was in the back position. In this case, the upper layer temperature predicted with the FDT method using the maximum HRR was comparable to the measured maximum in the range of 400 s to 800 s, but the same prediction



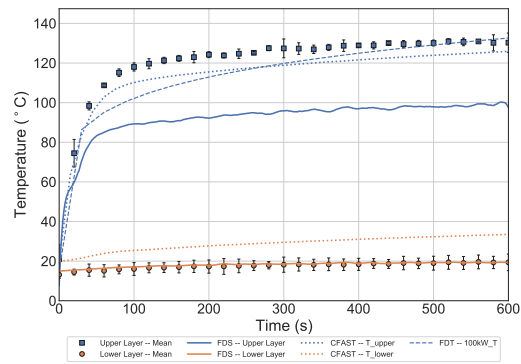
(a) Center Position



(b) Back Position



(c) Corner Position

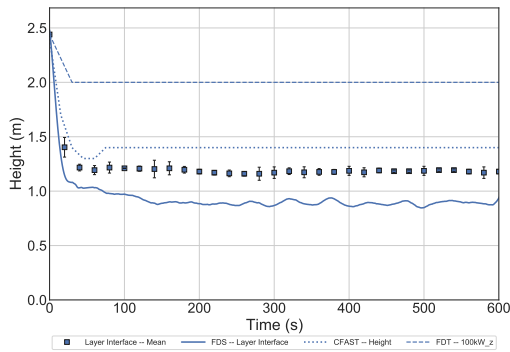


(d) Side Position

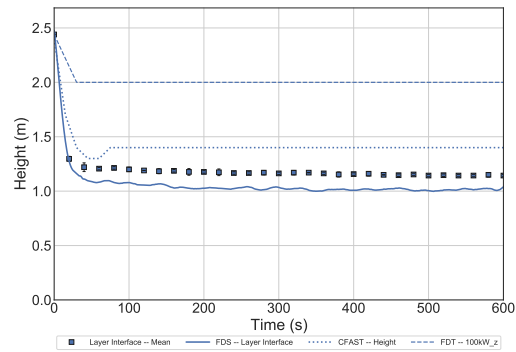
Figure A.3: Comparison of the Layer Temperatures in 0.6 m Burner, 100 kW Experiments with Door Open

was high for the corner and center positions. The FDT predictions made using the mean and steady HRRs accurately described the approximate mean and steady upper layer temperatures. The upper and lower gas layer temperatures predicted with FDS and CFAST generally agreed with each other. FDS and CFAST accurately represented the upper layer temperature, but neither captured the maximum temperature in the lower layer.

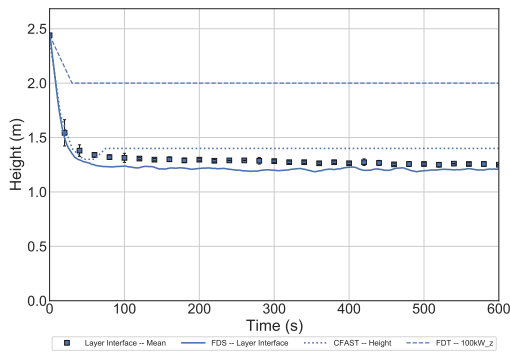
A comparison of the layer interface elevation collected in the experiments with the Red Accent Chair is presented in Figure A.6. The FDT method predicted a rapid descent of the layer interface, but was limited by the door height, so a true comparison is unavailable. FDS accurately predicted the elevation of the upper layer interface from approximately 200 s to the end of the experiment and the CFAST predictions tracked with the FDS prediction until approximately 200 s, after which CFAST predicted the interface height was at a higher elevation than measured. There was no significant difference in the data or predictions based on the location of the burner in each experiment.



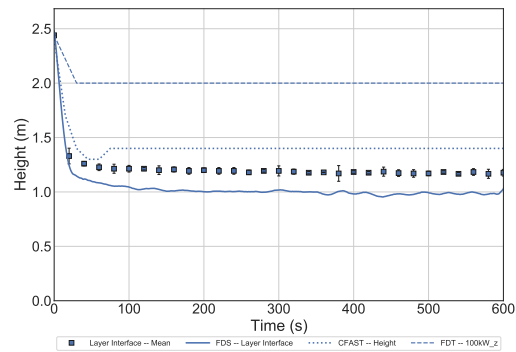
(a) Center Position



(b) Back Position



(c) Corner Position

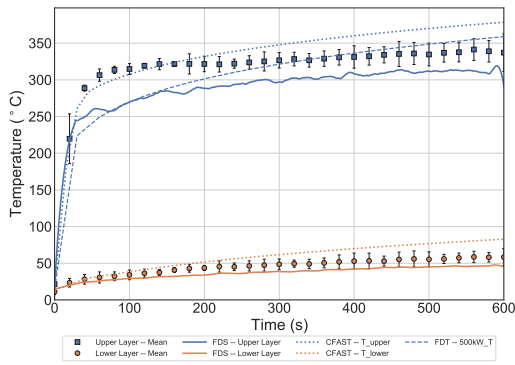


(d) Side Position

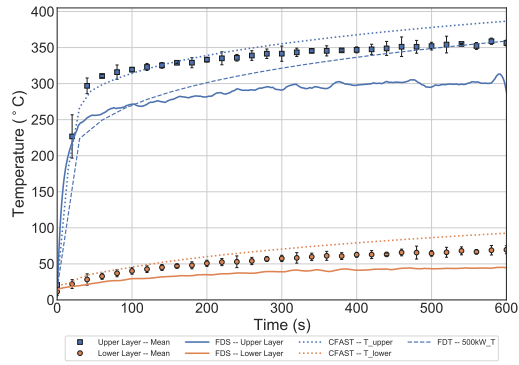
Figure A.4: Comparison of the Layer Interface Elevation in 0.6 m Burner, 100 kW Experiments with Door Open

A comparison of the layer temperature data collected in the experiments with the Overstuffed Sofa is presented in Figure ???. The maximum upper layer temperature over the 200 s to 400 s range was accurately predicted by the FDT method using the maximum HRR. The FDT prediction calculated with the mean HRR accurately represented the approximate mean temperature for the upper gas layer. The FDS and CFAST predictions of the upper and lower layer temperatures were qualitatively similar to the measured upper and lower layer temperature profiles, but CFAST generally accurately represented the maximum upper layer temperature and FDS underpredicted the maximum upper layer temperature. CFAST and FDS both underpredicted the maximum lower layer temperature.

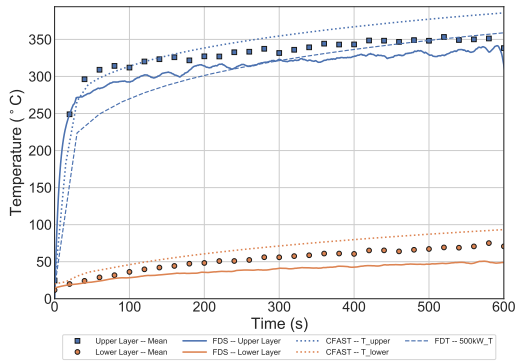
A comparison of the layer interface elevation collected in the experiments with the Overstuffed Sofa is presented in Figure A.10. The FDT method predicted a rapid descent of the layer interface, but was limited by the door height, so a true comparison is unavailable. FDS accurately predicted the elevation of the layer interface from approximately 200 s to the end of the experiment in the



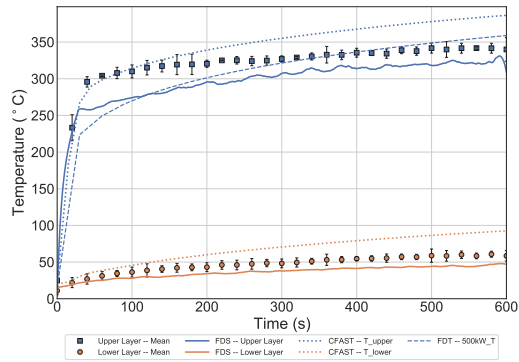
(a) Center Position



(b) Back Position



(c) Corner Position

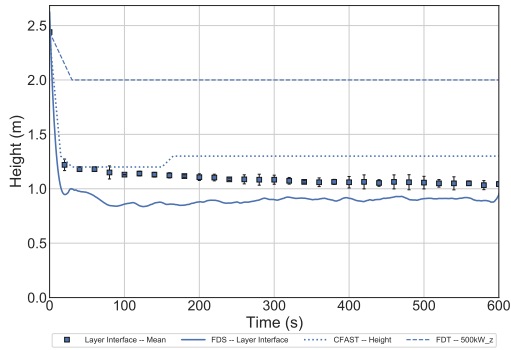


(d) Side Position

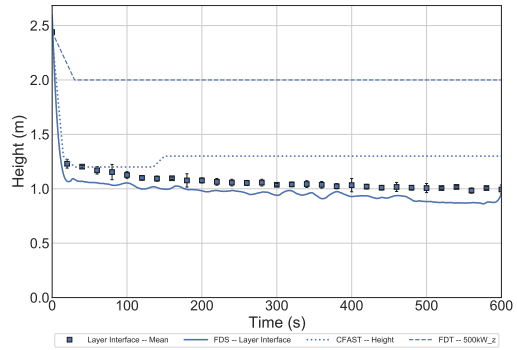
Figure A.5: Comparison of the Layer Temperatures in 0.6 m Burner, 500 kW Experiments with Door Open

Corner and Back positions, but underpredicted the descent of the layer in the center position. CFAST underpredicted the descent of the layer interface in all positions.

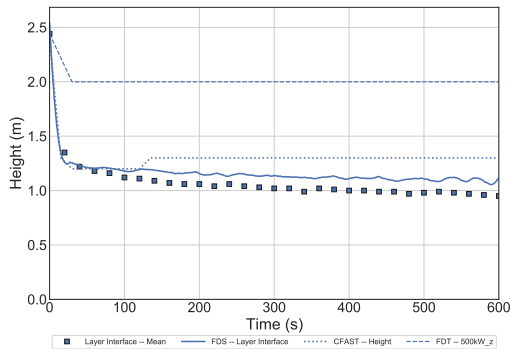
Although the MQH correlation, presented as the FDT method for the open door experiment comparisons, was only formulated to predict temperatures up to  $600^{\circ}\text{C}$  with fuel sources away from the walls and corners of the compartment, the predictions made using the maximum HRR yielded conservative results for the maximum upper layer temperature and those calculated with the mean HRR yielded a reasonable estimate for the mean upper layer temperature over the duration of the experiment. The location of the fuel package did not significantly affect the accuracy of these predictions.



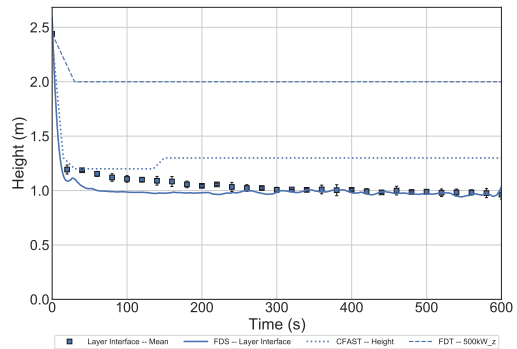
(a) Center Position



(b) Back Position

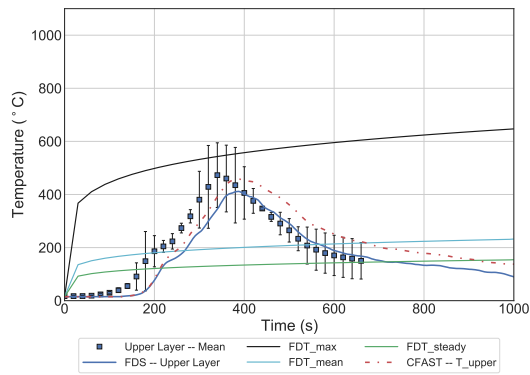


(c) Corner Position

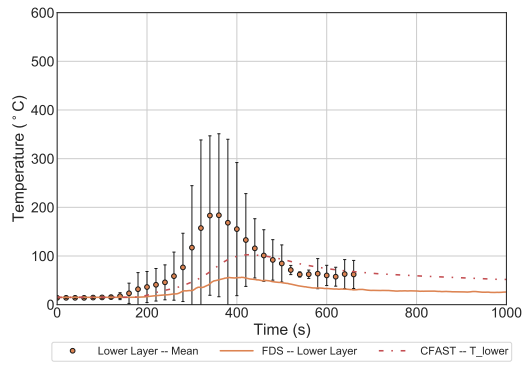


(d) Side Position

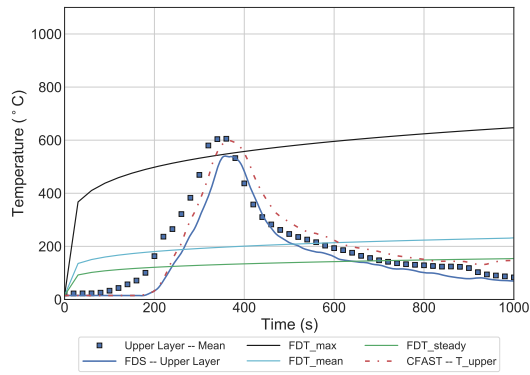
Figure A.6: Comparison of the Layer Interface Elevation in 0.6 m Burner, 500 kW Experiments with Door Open



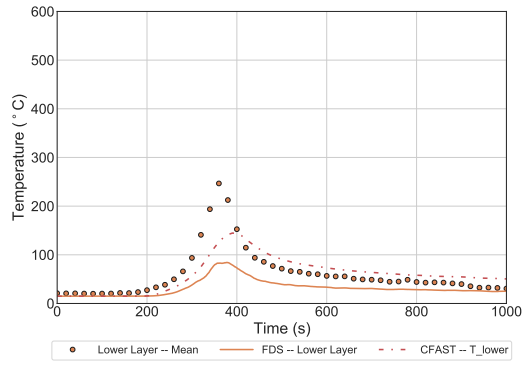
(a) Center Position Upper Layer Temperature



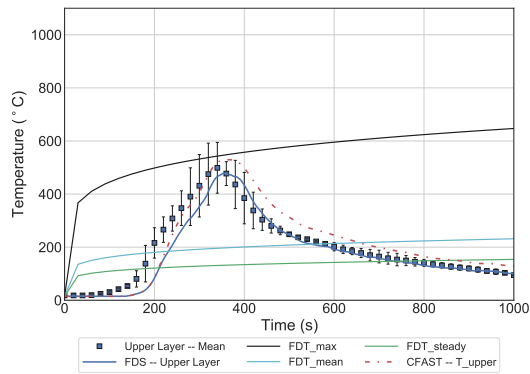
(b) Center Position Lower Layer Temperature



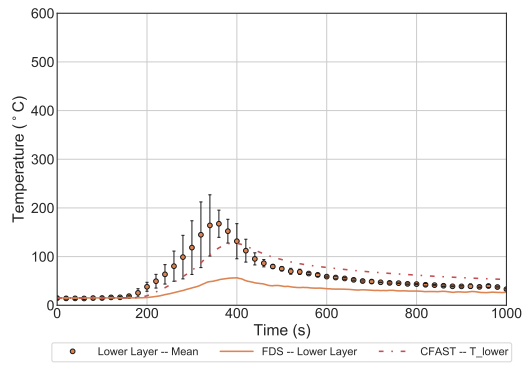
(c) Back Position Upper Layer Temperature



(d) Back Position Lower Layer Temperature

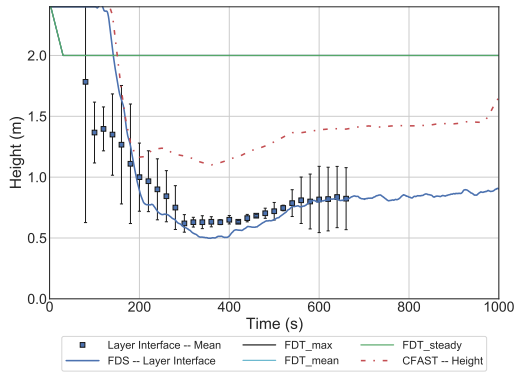


(e) Corner Position Upper Layer Temperature

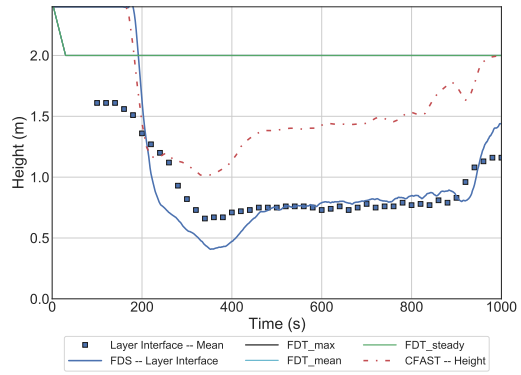


(f) Corner Position Lower Layer Temperature

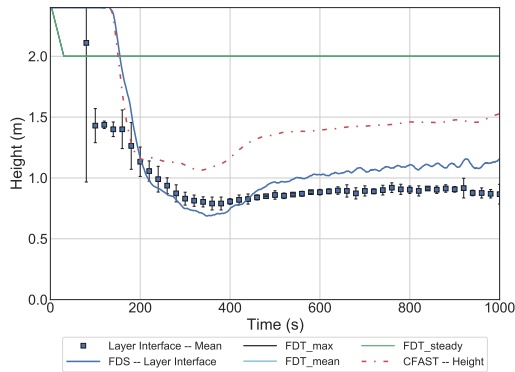
Figure A.7: Comparison of the Layer Temperatures in the Red Accent Chair Experiments with the Door Open



(a) Center Position

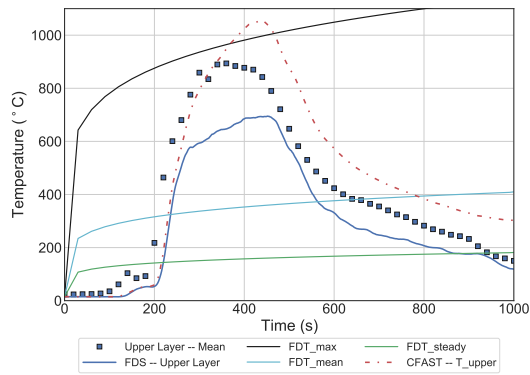


(b) Back Position

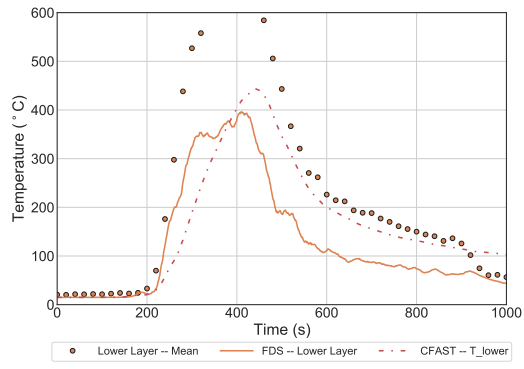


(c) Corner Position

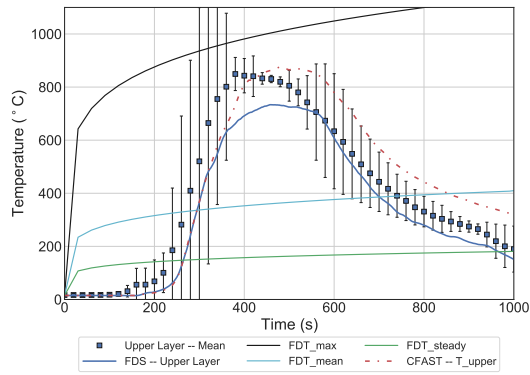
Figure A.8: Comparison of the Layer Interface Elevation in Red Accent Chair with the Door Open



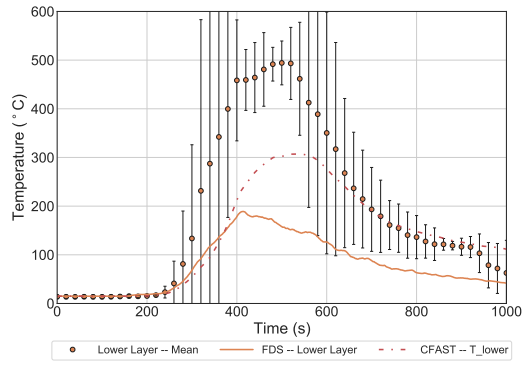
(a) Center Position Upper Layer Temperature



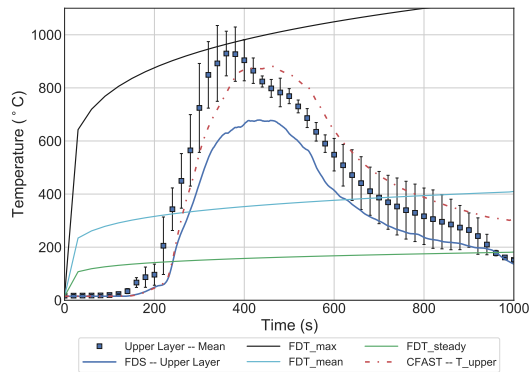
(b) Center Position Lower Layer Temperature



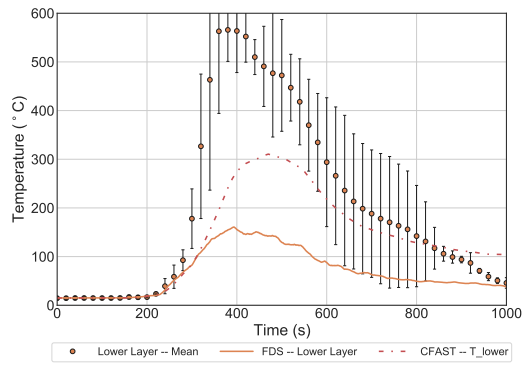
(c) Back Position Upper Layer Temperature



(d) Back Position Lower Layer Temperature

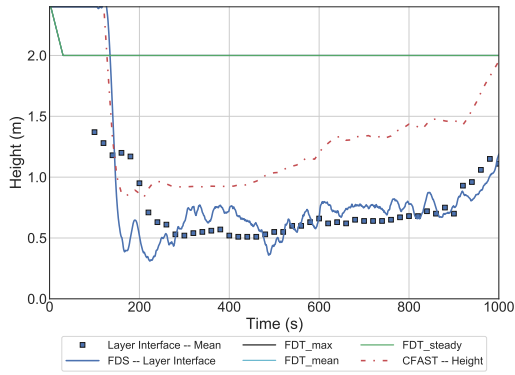


(e) Corner Position Upper Layer Temperature

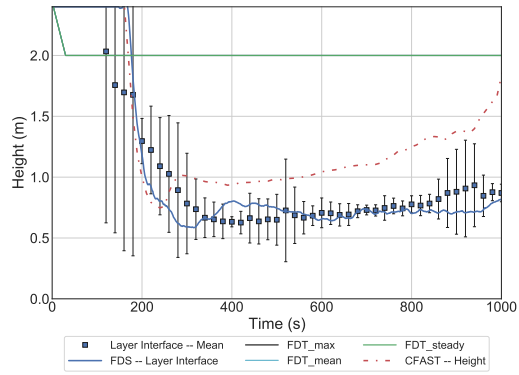


(f) Corner Position Lower Layer Temperature

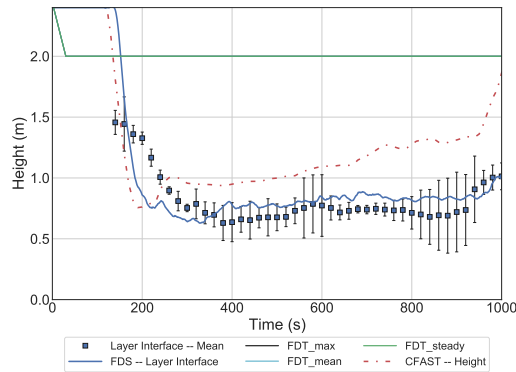
Figure A.9: Comparison of the Layer Temperatures in the Overstuffed Sofa Experiments with the Door Open



(a) Center Position



(b) Back Position

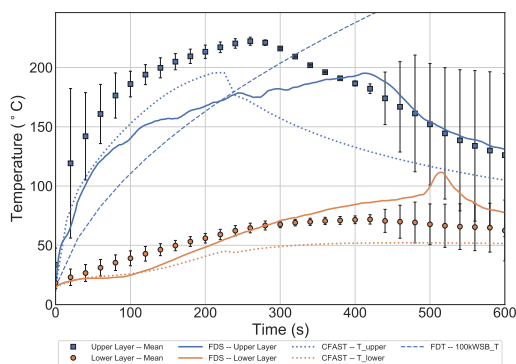


(c) Corner Position

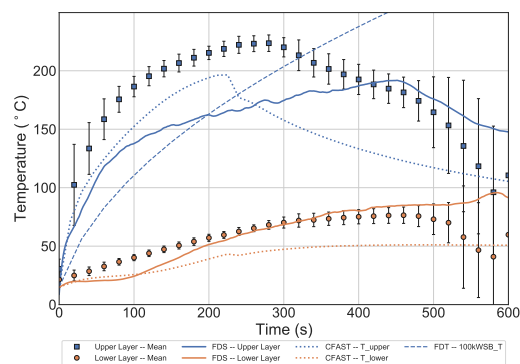
Figure A.10: Comparison of the Layer Interface Elevation in Overstuffed Sofa with the Door Open

## Closed Door

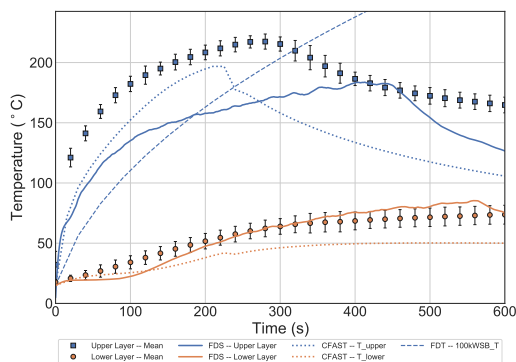
A comparison of the layer temperature data collected in the experiments with the 0.3 m Burner and a HRR of 100 kW is presented in Figure A.11. The FDT method tended to underpredict the upper layer temperature until approximately 300 s, at which point the HRR and temperatures measured with the burner in all locations presumably decreased due to a lack of ventilation. The CFAST predictions for upper and lower gas layer temperatures followed the same qualitative trend as the experimental data, but underpredicted the temperatures throughout the experiment. FDS generally predicted the qualitative shape of the temperature curves, but underpredicted the upper layer temperature and overpredicted the lower layer temperature.



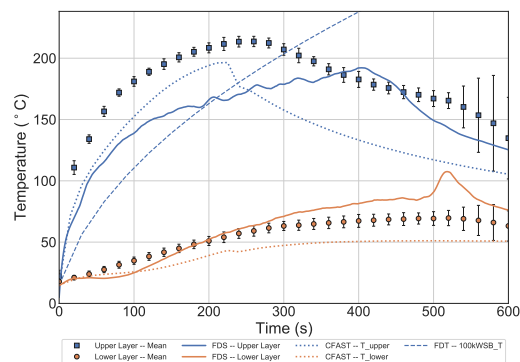
(a) Center Position



(b) Back Position



(c) Corner Position

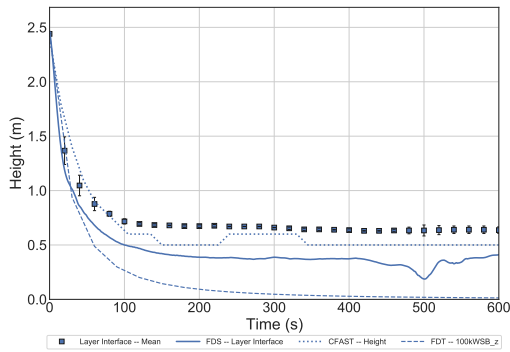


(d) Side Position

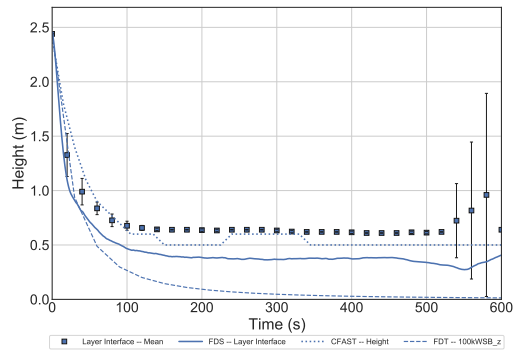
Figure A.11: Comparison of the Layer Temperatures in 0.3 m Burner, 100 kW Experiments with Door Closed

A comparison of the layer interface elevation collected in the experiments with the 0.3 m Burner and a HRR of 100 kW is presented in Figure A.12. The FDT method predicted the hot gas layer would descend to the floor of the compartment by approximately 300 s, which was a conservative

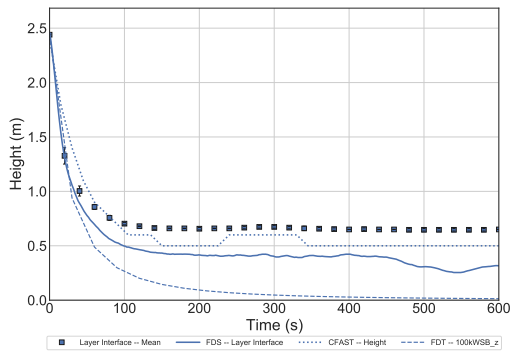
estimate as the experimentally observed hot gas layer descended to approximately 0.7 m above the floor. CFAST accurately predicted the elevation of the layer interface throughout the experiments. FDS tended to overpredict the descent of the layer interface in all positions.



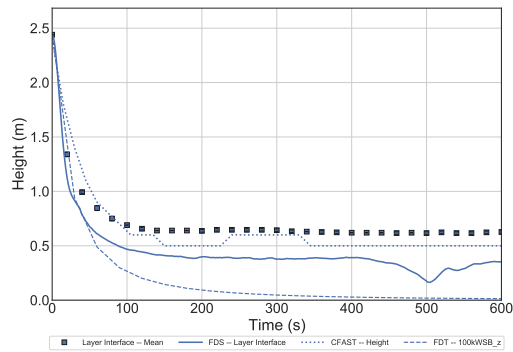
(a) Center Position



(b) Back Position



(c) Corner Position



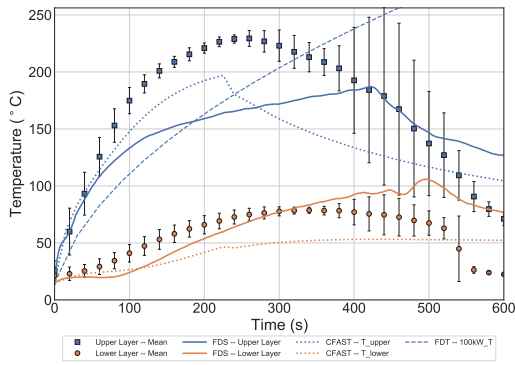
(d) Side Position

Figure A.12: Comparison of the Layer Interface Elevation in 0.3 m Burner, 100 kW Experiments with Door Closed

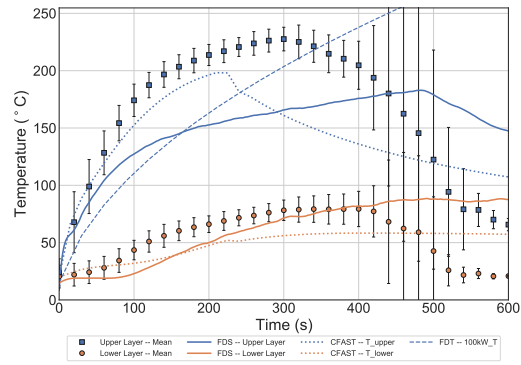
A comparison of the layer temperature data collected in the experiments with the 0.6 m Burner and a HRR of 100 kW is presented in Figure A.13. The trends in the experimental data and model predictions for the 0.6 m Burner were generally the same as those in the 0.3 m Burner experiments. FDS tended to accurately predict the lower layer temperatures until approximately 400 s in the 0.6 m Burner experiments.

A comparison of the layer interface elevation collected in the experiments with the 0.6 m Burner and a HRR of 100 kW is presented in Figure A.14. The trends in the 0.6 m Burner case were identical to those in the 0.3 m Burner case with a HRR of 100 kW.

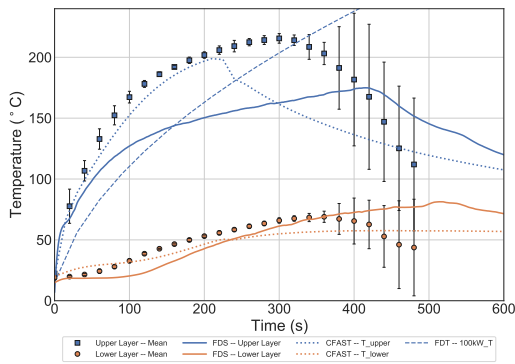
A comparison of the layer temperature data collected in the experiments with the 0.6 m Burner



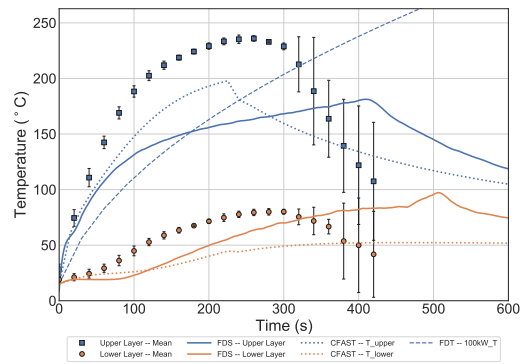
(a) Center Position



(b) Back Position



(c) Corner Position

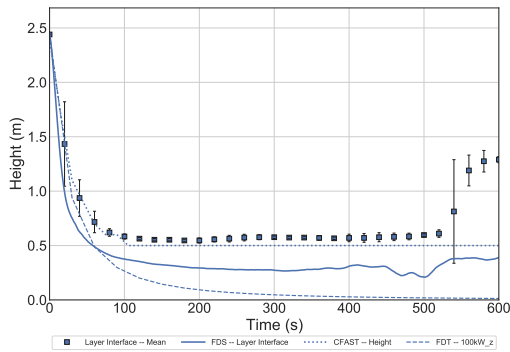


(d) Side Position

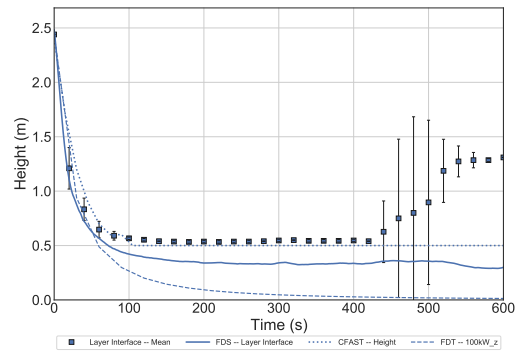
Figure A.13: Comparison of the Layer Temperatures in 0.6 m Burner, 100 kW Experiments with Door Closed

and a HRR of 500 kW is presented in Figure A.15. The FDT method predicted the rise in upper layer temperature to its peak at approximately 50 s. CF-FAST accurately predicted the upper layer temperature, but underpredicted the lower layer temperature throughout the experiment. FDS generally predicted the qualitative shape of the temperature curves, but erroneously predicted a local maximum in the upper and lower layer temperatures.

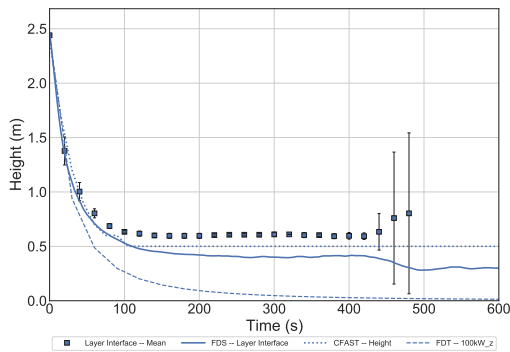
A comparison of the layer interface elevation collected in the experiments with the 0.3 m Burner and a HRR of 100 kW is presented in Figure A.14. The FDT method predicted the hot gas layer would descend to the floor of the compartment by approximately 300 s, which was a conservative estimate as the experimentally observed hot gas layer descended to approximately 0.6 m above the floor. CF-FAST accurately predicted the elevation of the layer interface throughout the experiments. FDS tended to overpredict the descent of the layer interface in all positions. The layer interface elevation increased after approximately 300 s and none of the models predicted the increase.



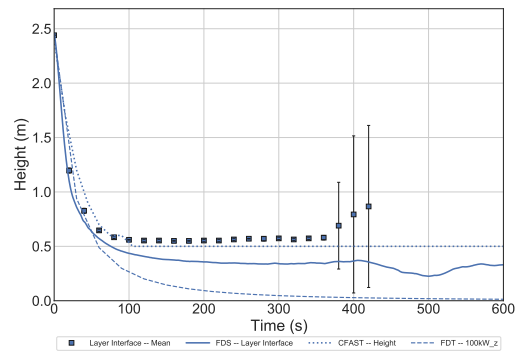
(a) Center Position



(b) Back Position



(c) Corner Position

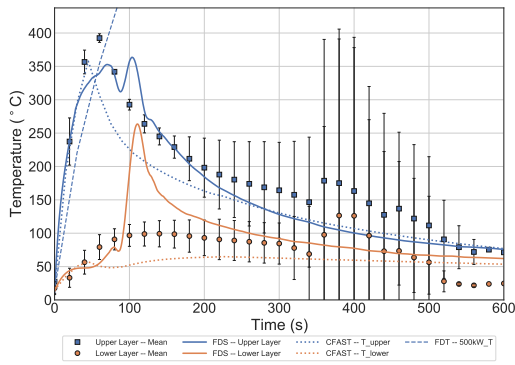


(d) Side Position

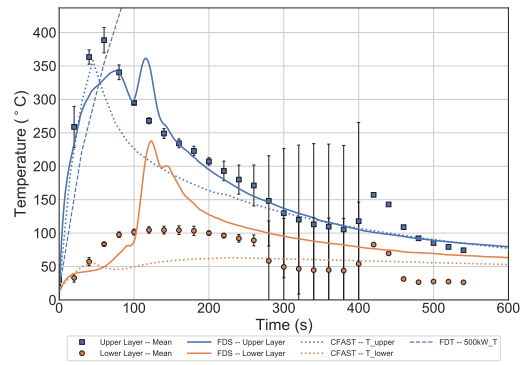
Figure A.14: Comparison of the Layer Interface Elevation in 0.6 m Burner, 100 kW Experiments with Door Closed

A comparison of the layer temperature data collected in the experiments with the Red Accent Chair is presented in Figure A.17. The FDT method calculated with the maximum, mean, and steady HRR from the experiments significantly overpredicted the hot gas layer temperatures. The CFAST prediction for upper layer temperature qualitatively matched the experimental data, although the upper and lower layer temperatures were underpredicted. FDS slightly overpredicted the maximum upper and lower layer temperatures and accurately predicted the temperatures in the growth and decay phases. The location of the fuel package did not significantly affect the experimental data or predictions.

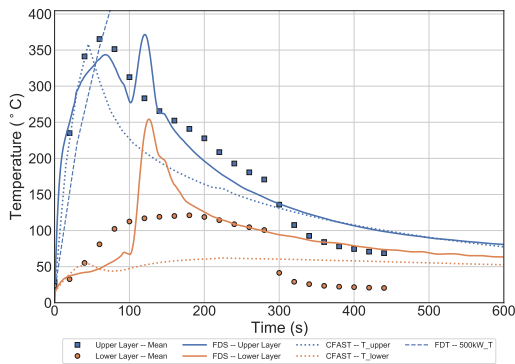
A comparison of the layer interface elevation measured in the experiments with the Red Accent Chair is presented in Figure A.18. The FDT method predicted the hot gas layer would rapidly descend to the floor of the compartment within 100 s, which was a conservative estimate as the experimentally observed hot gas layer descended to approximately 0.6 m above the floor by approximately 200 s. CFAST and FDS qualitatively predicted the rate of descent of the layer interface



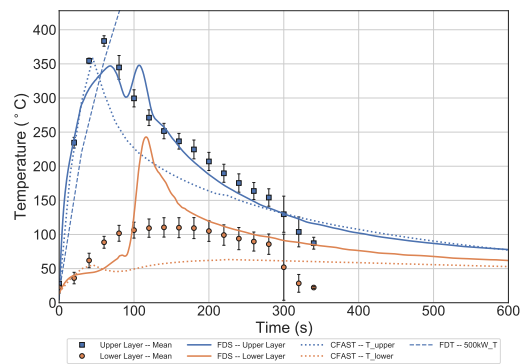
(a) Center Position



(b) Back Position



(c) Corner Position



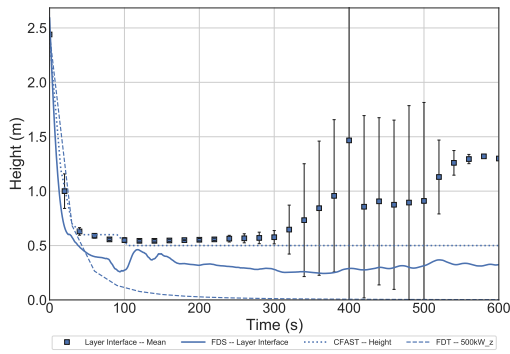
(d) Side Position

Figure A.15: Comparison of the Layer Temperatures in 0.6 m Burner, 500 kW Experiments with Door Closed

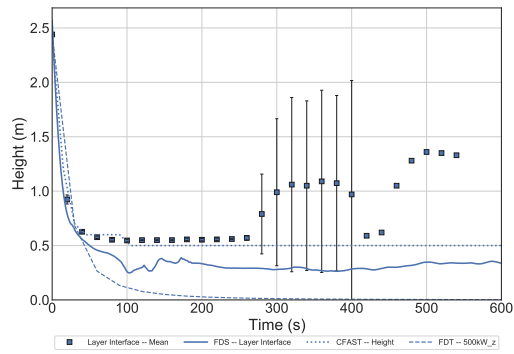
and slightly overpredicted the descent of the layer at steady state.

A comparison of the layer temperature data collected in the experiments with the Overstuffed Sofa is presented in Figure A.19. The FDT method calculated with the maximum, mean, and steady HRR from the experiments significantly overpredicted the hot gas layer temperatures. The CFAST prediction for upper layer temperature qualitatively matched the experimental data and generally predicted the maximum upper layer temperature, although the lower layer temperatures were underpredicted. FDS accurately predicted the temperatures in growth period, overpredicted the maximum upper and lower layer temperatures, and underpredicted the temperatures in the decay phases. The location of the fuel package did not significantly affect the experimental data or predictions.

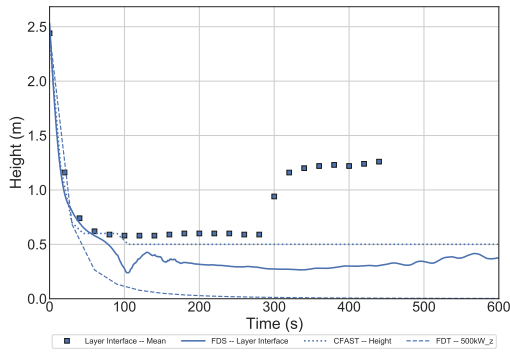
A comparison of the layer interface elevation measured in the experiments with the Overstuffed Sofa is presented in Figure A.20. The FDT method predicted the hot gas layer would rapidly



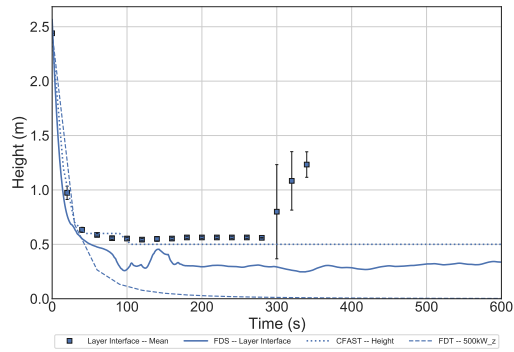
(a) Center Position



(b) Back Position



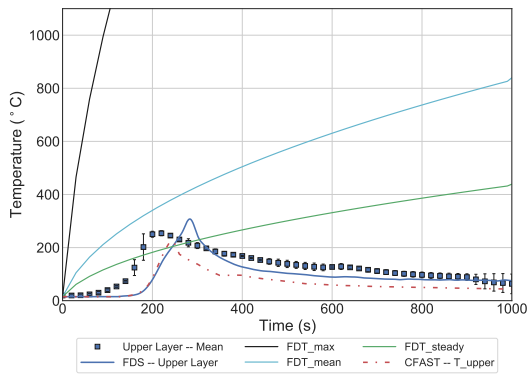
(c) Corner Position



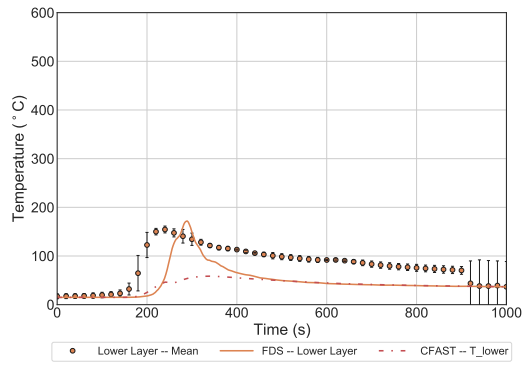
(d) Side Position

Figure A.16: Comparison of the Layer Interface Elevation in 0.6 m Burner, 500 kW Experiments with Door Closed

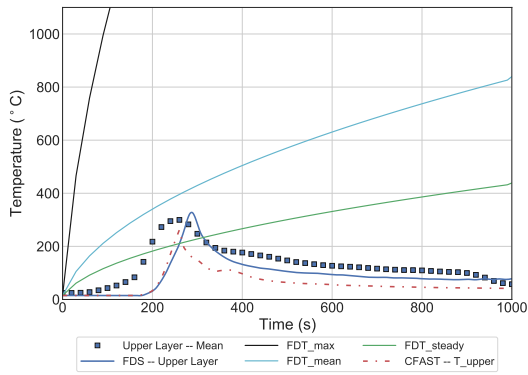
descend to the floor of the compartment within 100 s, which was a conservative estimate as the experimentally observed hot gas layer interface descended to a steady state of approximately 0.6 m above the floor in the range of 200 s to 400 s. CFAST and FDS qualitatively predicted the rate of descent of the layer interface. CFAST accurately predicted the steady interface elevation and FDS tended to predict a higher elevation for the steady interface height.



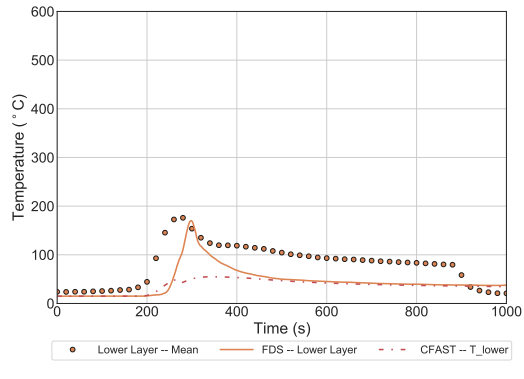
(a) Center Position Upper Layer Temperature



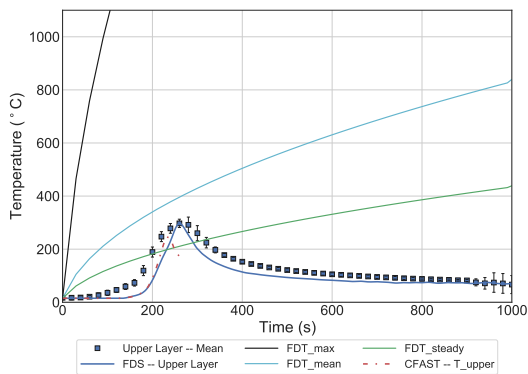
(b) Center Position Lower Layer Temperature



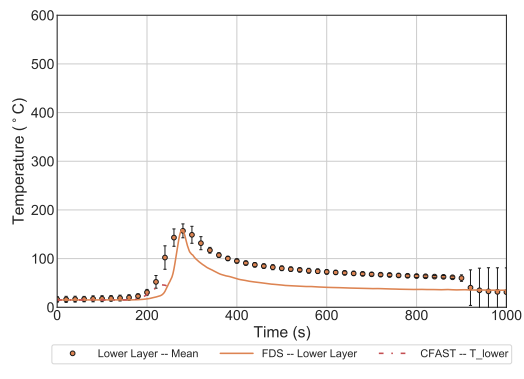
(c) Back Position Upper Layer Temperature



(d) Back Position Lower Layer Temperature

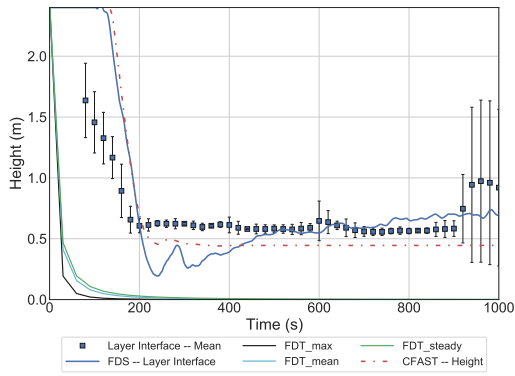


(e) Corner Position Upper Layer Temperature

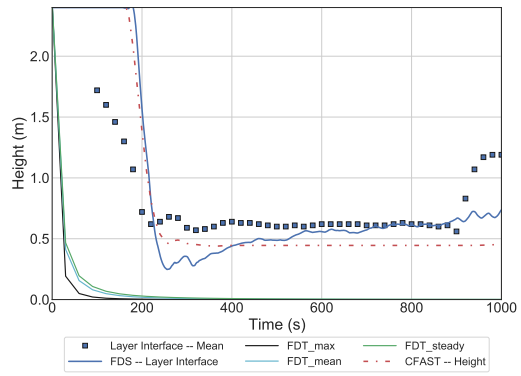


(f) Corner Position Lower Layer Temperature

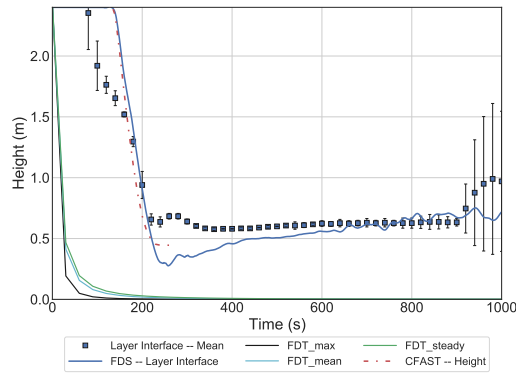
Figure A.17: Comparison of the Layer Temperatures in the Red Accent Chair Experiments with the Door Closed



(a) Center Position

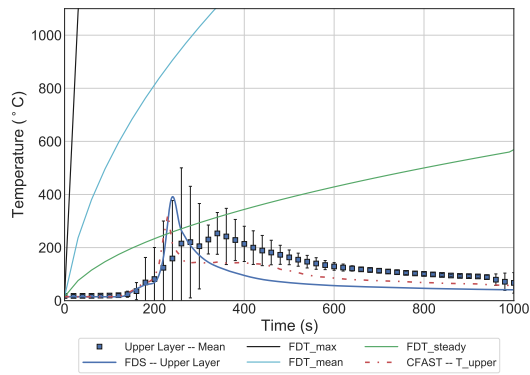


(b) Back Position

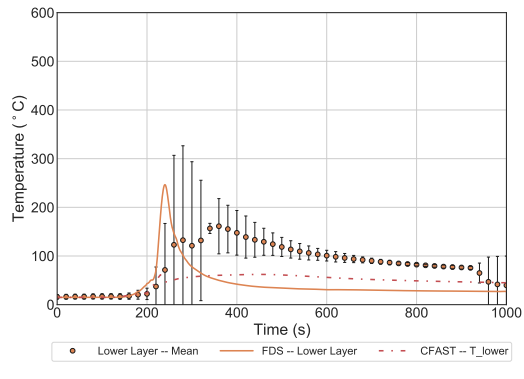


(c) Corner Position

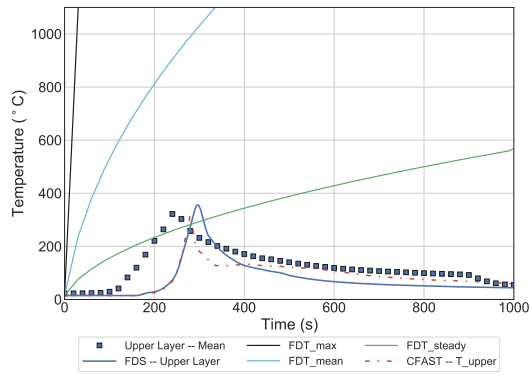
Figure A.18: Comparison of the Layer Interface Elevation in Red Accent Chair with the Door Closed



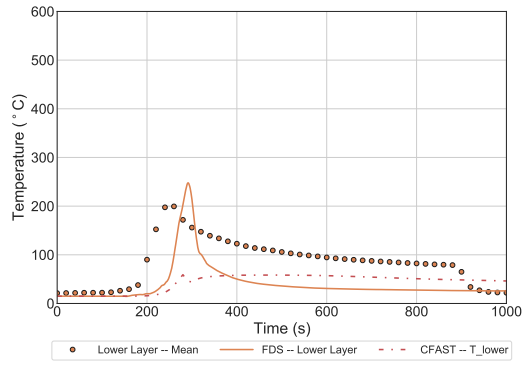
(a) Center Position Upper Layer Temperature



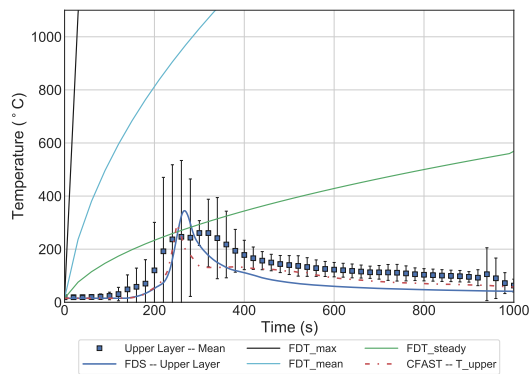
(b) Center Position Lower Layer Temperature



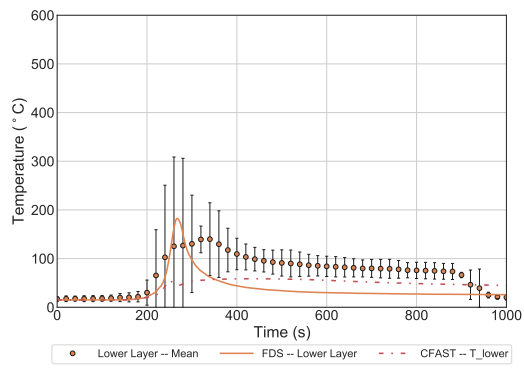
(c) Back Position Upper Layer Temperature



(d) Back Position Lower Layer Temperature

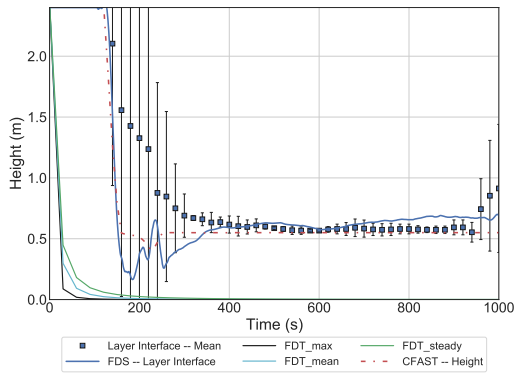


(e) Corner Position Upper Layer Temperature

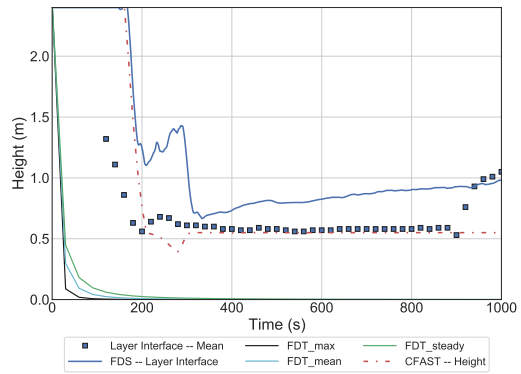


(f) Corner Position Lower Layer Temperature

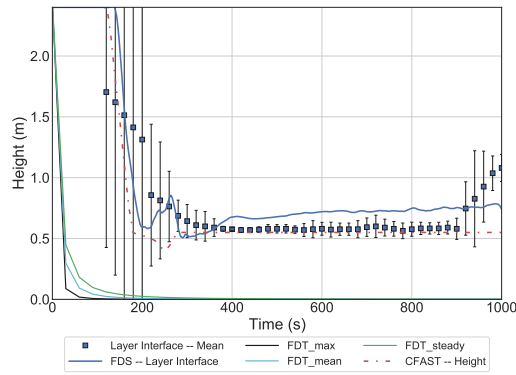
Figure A.19: Comparison of the Layer Temperatures in the Overstuffed Sofa Experiments with the Door Closed



(a) Center Position



(b) Back Position



(c) Corner Position

Figure A.20: Comparison of the Layer Interface Elevation in Overstuffed Sofa with the Door Closed

## A.1.2 Plume Temperature and Velocity

### Open Door

A comparison of the plume temperatures measured in the experiments with the 0.3 m Burner with a HRR of 100 kW is presented in Figure A.21. The experimental data were consistent when the burner was located in the back and corner position but significantly lower when the burner was in the side position. The FDT correlations tended to overpredict the plume temperatures for both measurement elevations with the burner in all of the positions. The plume temperature predicted with FDS were significantly lower than the measured temperatures.

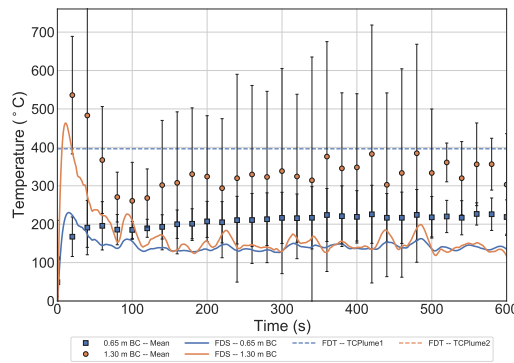
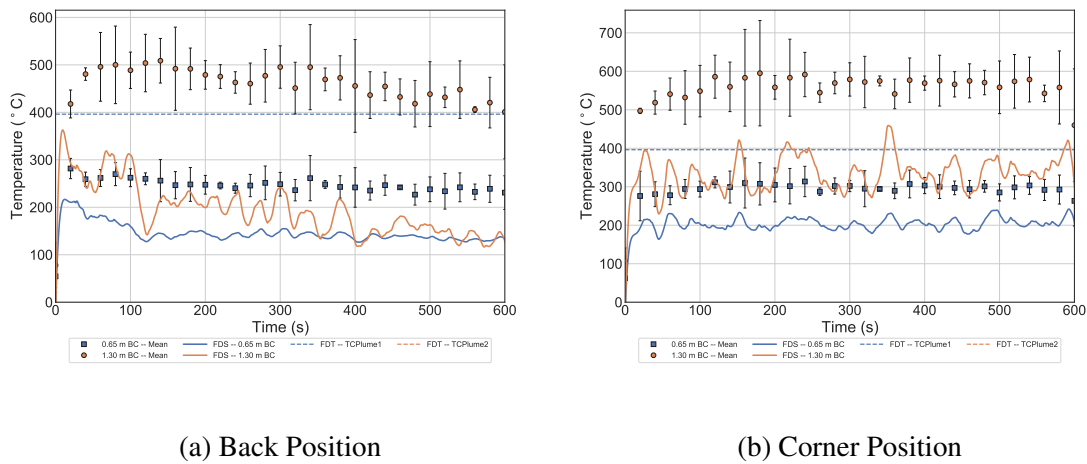
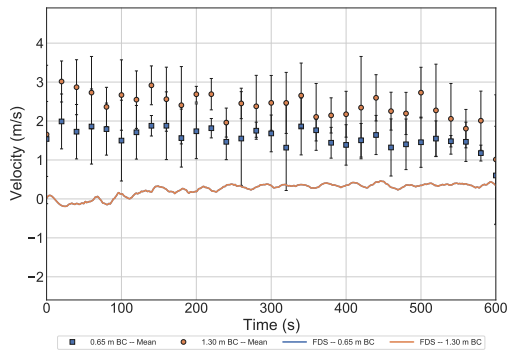
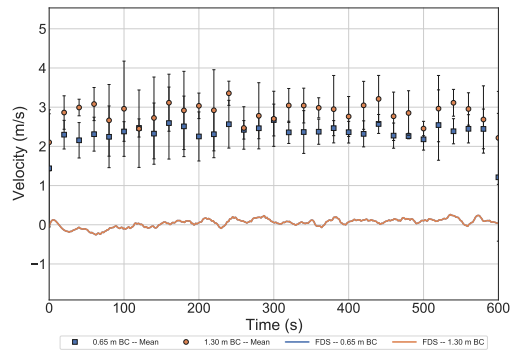


Figure A.21: Comparison of the Plume Temperature in the 0.3 m Burner, 100 kW Experiments with Door Open

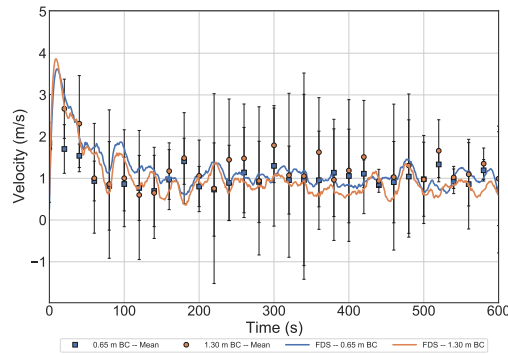
A comparison of the plume temperatures measured in the experiments with the 0.6 m Burner and a HRR of 100 kW is presented in Figure A.23. The experimental data were consistent when the



(a) Back Position



(b) Corner Position



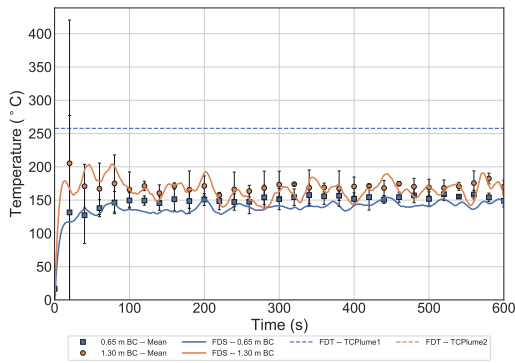
(c) Side Position

Figure A.22: Comparison of the Plume Velocity in the 0.3 m Burner, 100 kW Experiments with Door Open

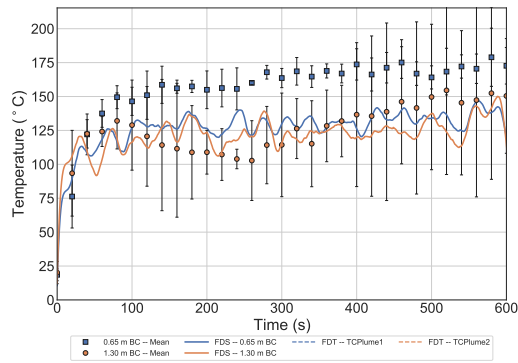
burner was located in the back and corner position but significantly higher when the burner was in the side position. The FDT correlations tended to overpredict the plume temperatures for both measurement elevations with the burner in all the positions, although the steady temperature at the higher elevation was well characterized by the FDT correlation in the side position. The plume temperatures predicted with FDS were accurate for the back and corner position and significantly underpredicted the measured temperatures in the side position.

A comparison of the plume temperatures measured in the experiments with the 0.6 m Burner with a HRR of 500 kW is presented in Figure A.25. The FDT correlations tended to overpredict the plume temperatures for both measurement elevations with the burner in all the positions. All the plume temperatures were underpredicted by FDS.

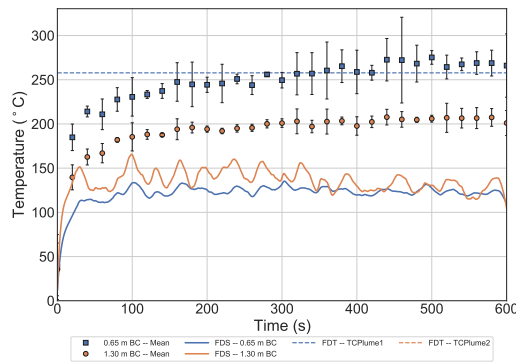
A comparison of the plume temperatures measured in the experiments with the Red Accent Chair is presented in Figure A.27. The FDT correlation calculated with the maximum HRR overpre-



(a) Back Position



(b) Corner Position



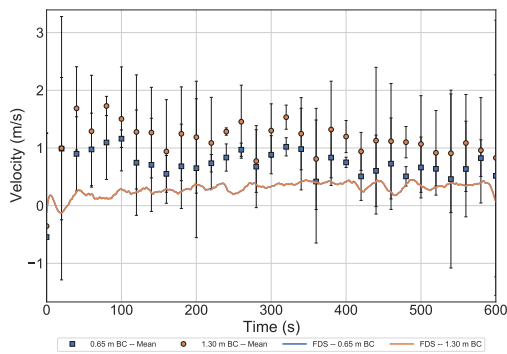
(c) Side Position

Figure A.23: Comparison of the Plume Temperature in the 0.6 m Burner, 100 kW Experiments with Door Open

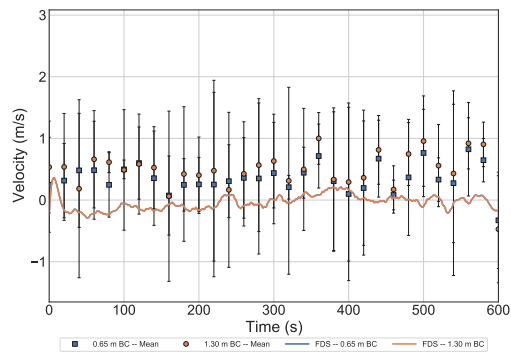
dicted the plume temperature measured at both elevations while the temperature calculated with the mean and steady HRRs accurately predicted the the approximate mean and steady temperatures at the higher elevation measurement. FDS predicted the qualitative shape of the plume temperature measurements, but underpredicted the temperature during the growth phase and underpredicted the maximum temperature for both elevations.

A comparison of the plume velocities measured in the experiments with the Red Accent Chair is presented in Figure ???. FDS accurately predicted the maximum plume velocity when the chair was in the back position, but underpredicted the velocity throughout the experiment when the chair was in the corner position.

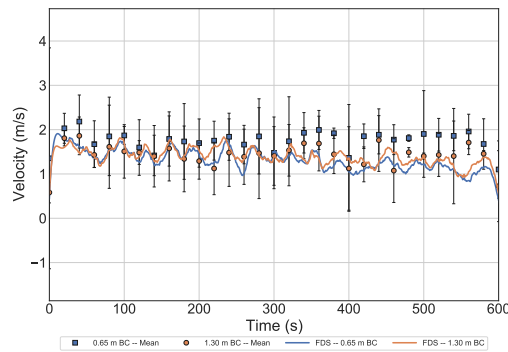
A comparison of the plume temperatures measured in the experiments with the Overstuffed Sofa is presented in Figure A.29. The FDT correlation calculated with the maximum HRR overpredicted the plume temperature measured at both elevations while the temperature calculated with



(a) Back Position



(b) Corner Position

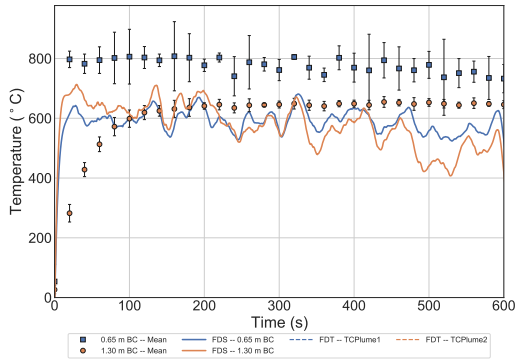


(c) Side Position

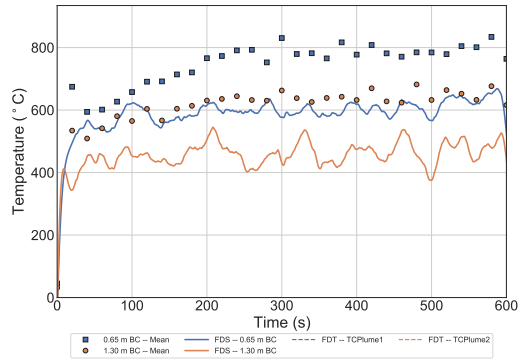
Figure A.24: Comparison of the Plume Velocity in the 0.6 m Burner, 100 kW Experiments with Door Open

the steady HRR accurately predicted the approximate steady temperature at the higher elevation measurement. FDS predicted the qualitative shape of the plume temperature measurements, but underpredicted the temperature during the growth phase and underpredicted the maximum temperature for both elevations.

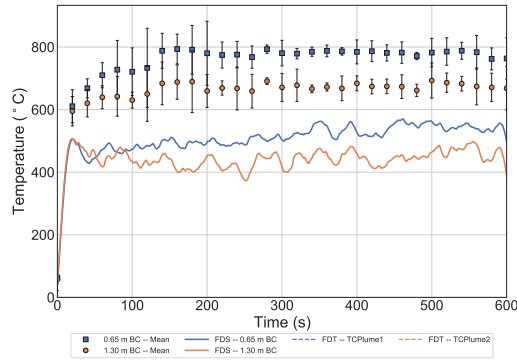
A comparison of the plume velocities measured in the experiments with the Overstuffed Sofa is presented in Figure A.30. FDS accurately predicted the maximum plume velocity when the sofa was in both positions, but did not capture the qualitative shape of either velocity curve.



(a) Back Position

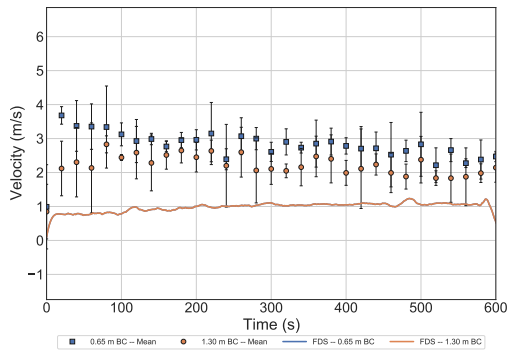


(b) Corner Position

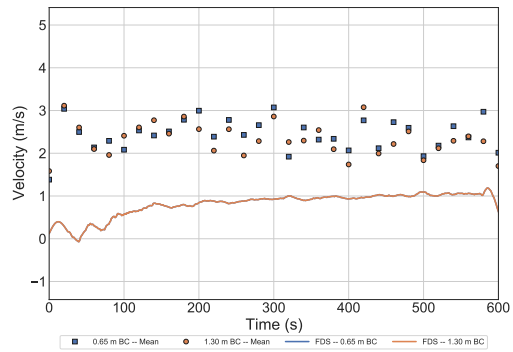


(c) Side Position

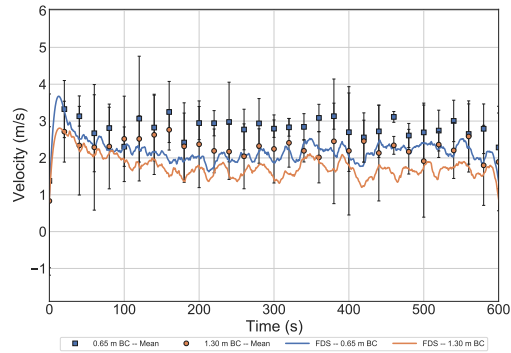
Figure A.25: Comparison of the Plume Temperature in the 0.6 m Burner, 500 kW Experiments with Door Open



(a) Back Position

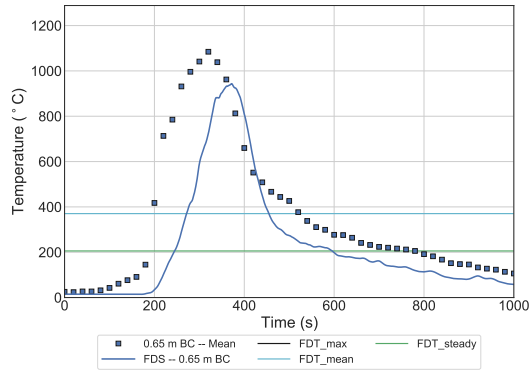


(b) Corner Position

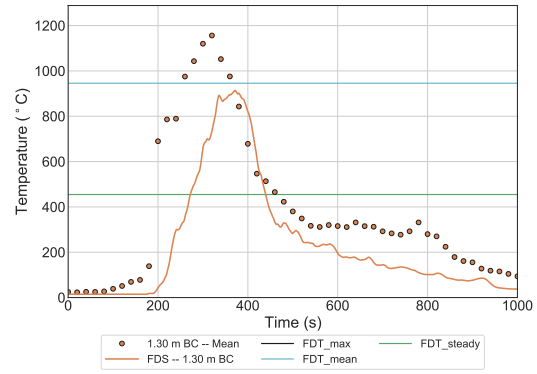


(c) Side Position

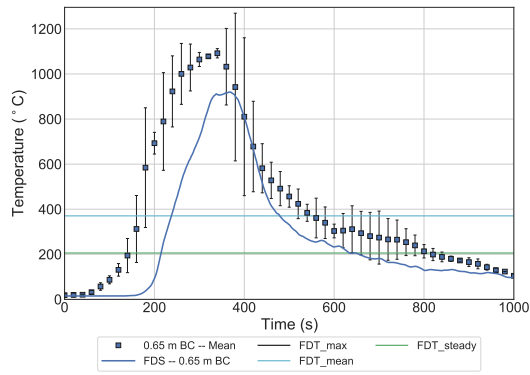
Figure A.26: Comparison of the Plume Velocity in the 0.6 m Burner, 500 kW Experiments with Door Open



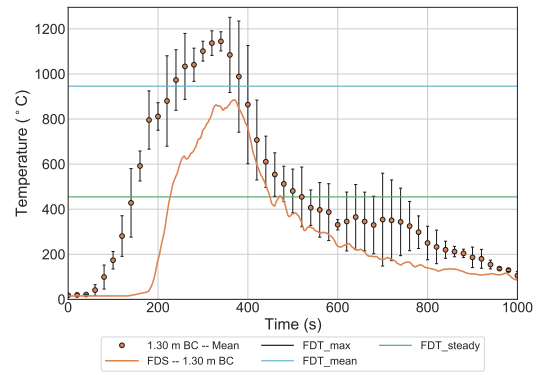
(a) Back Position Plume TC1



(b) Corner Position Plume TC2

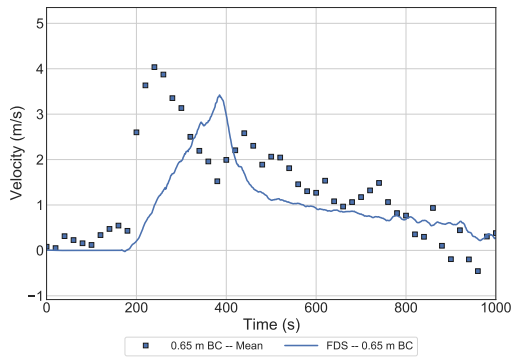


(c) Corner Position Plume TC1

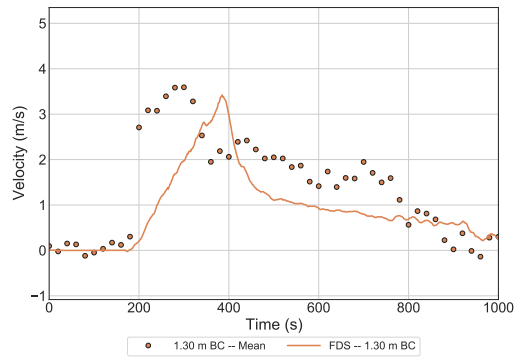


(d) Corner Position Plume TC2

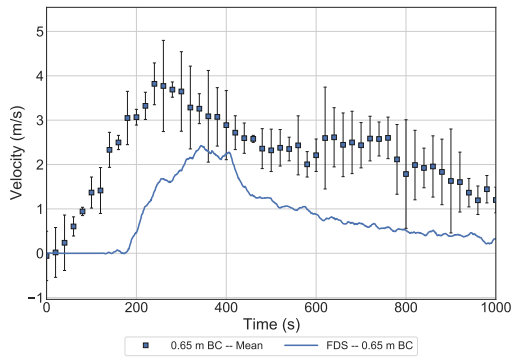
Figure A.27: Comparison of the Plume Temperature in the Red Accent Chair Experiments with the Door Open



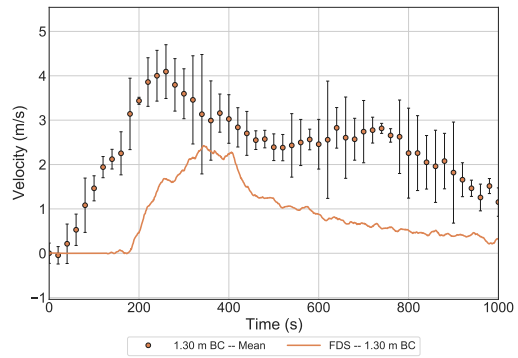
(a) Back Position Plume BDP1



(b) Back Position Plume BDP2

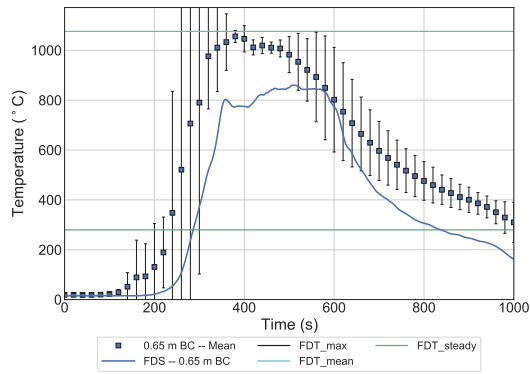


(c) Corner Position Plume BDP1

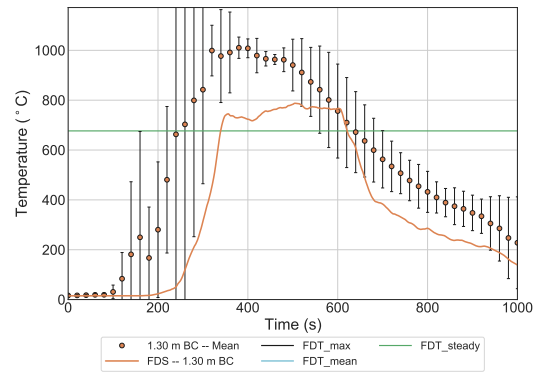


(d) Corner Position Plume BDP2

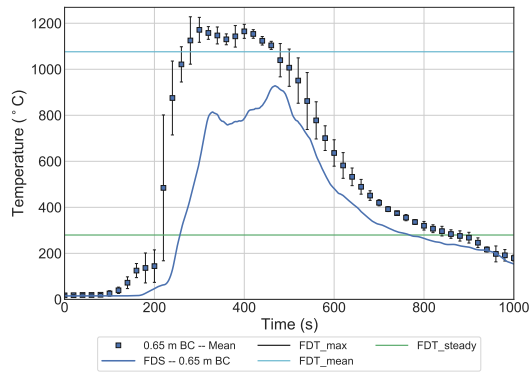
Figure A.28: Comparison of the Plume Velocity in the Red Accent Chair Experiments with the Door Open



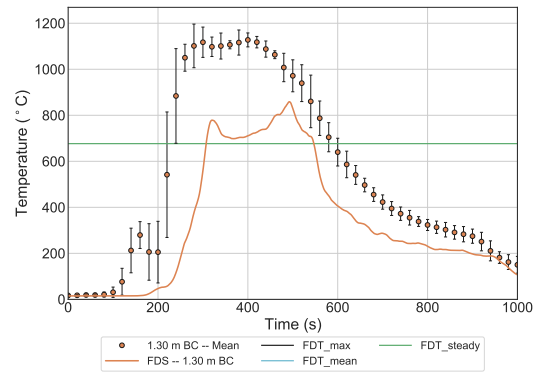
(a) Back Position Plume TC1



(b) Corner Position Plume TC2

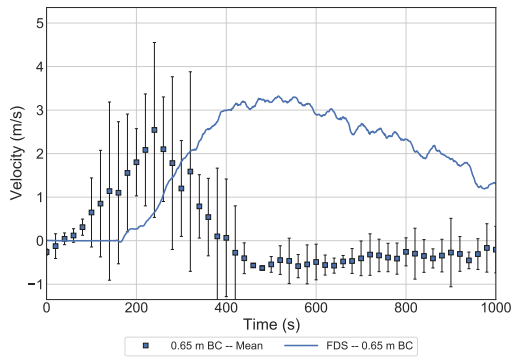


(c) Corner Position Plume TC1

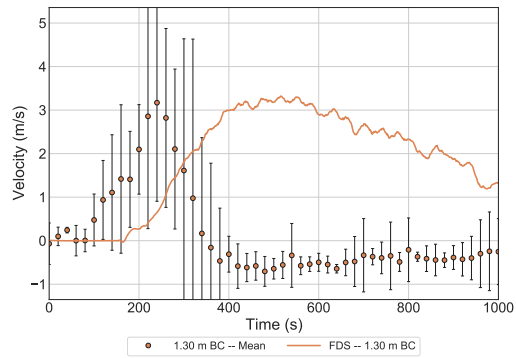


(d) Corner Position Plume TC2

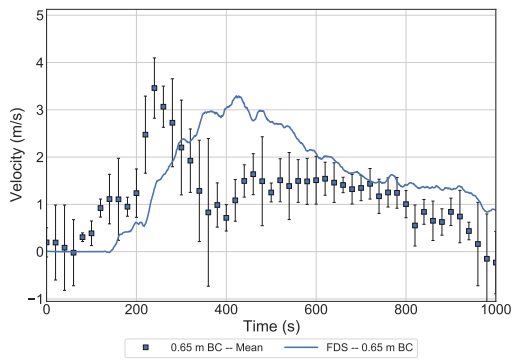
Figure A.29: Comparison of the Plume Temperature in the Overstuffed Sofa Experiments with the Door Open



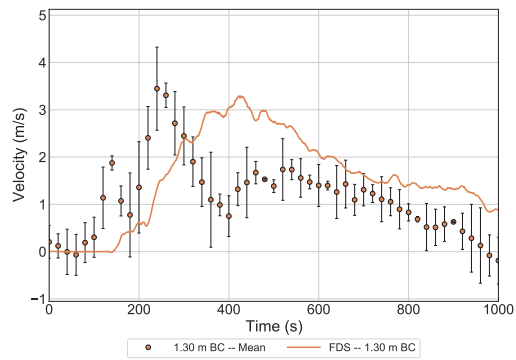
(a) Back Position Plume BDP1



(b) Back Position Plume BDP2



(c) Corner Position Plume BDP1

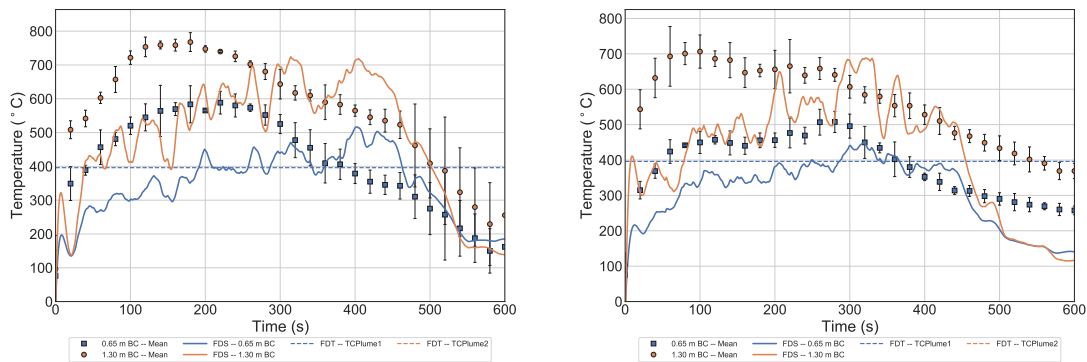


(d) Corner Position Plume BDP2

Figure A.30: Comparison of the Plume Velocity in the Overstuffed Sofa Experiments with the Door Open

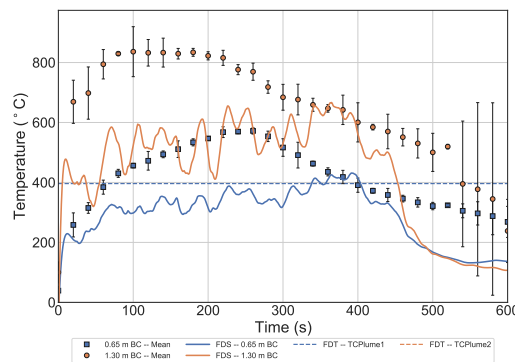
## Closed Door

A comparison of the plume temperatures measured in the experiments with the 0.3 m Burner with a HRR of 100 kW is presented in Figure A.21. The FDT correlation overpredicted the lower elevation plume temperature measurement and accurately represented the approximate mean temperature measured at the higher elevation location. The plume temperature predicted with FDS were generally lower than the measured temperatures and FDS did not qualitatively capture the shape of the curves.



(a) Back Position

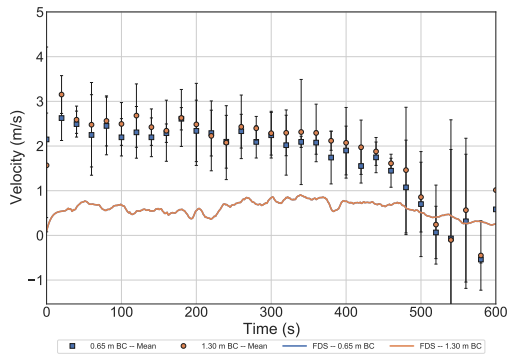
(b) Corner Position



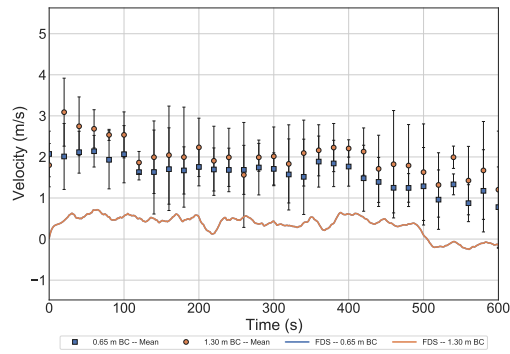
(c) Side Position

Figure A.31: Comparison of the Plume Temperature in the 0.3 m Burner, 100 kW Experiments with Door Closed

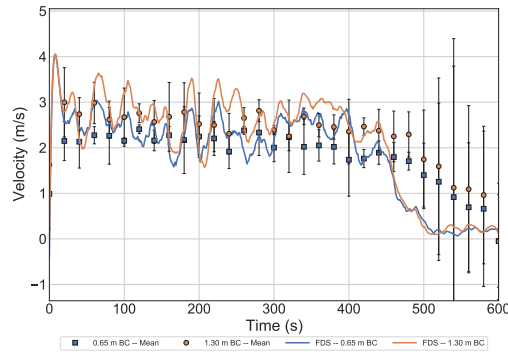
A comparison of the plume temperatures measured in the experiments with the 0.6 m Burner with a HRR of 100 kW is presented in Figure A.23. The FDT correlation overpredicted the lower elevation plume temperature measurement and accurately represented the approximate mean temperature measured at the higher elevation location when the burner was in the back and corner positions. The plume temperature predicted with FDS were generally lower than the measured



(a) Back Position



(b) Corner Position



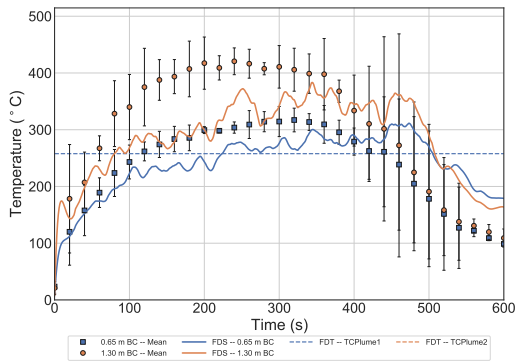
(c) Side Position

Figure A.32: Comparison of the Plume Velocity in the 0.3 m Burner, 100 kW Experiments with Door Closed

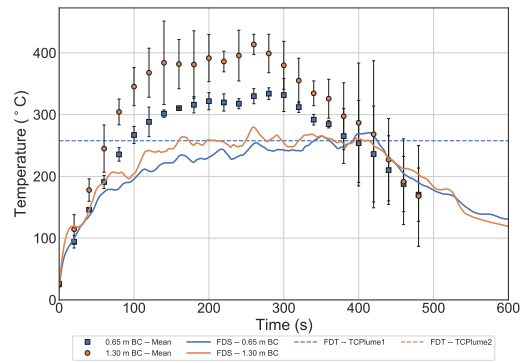
temperatures and FDS did not qualitatively capture the shape of the curves.

A comparison of the plume temperatures measured in the experiments with the 0.6 m Burner with a HRR of 500 kW is presented in Figure A.25. The FDT correlation overpredicted the plume temperatures. FDS was generally able to predict the qualitative shape of the plume temperature data although the magnitudes were underpredicted throughout the experiments.

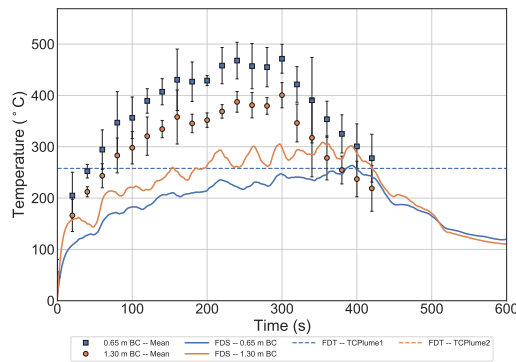
A comparison of the plume temperatures measured in the experiments with the Red Accent Chair is presented in Figure A.37. The FDT correlation calculated with the maximum HRR overpredicted the plume temperature measured at both elevations while the temperature calculated with the steady HRR approximated the mean temperature measured at the higher elevation. FDS predicted the qualitative shape of the plume temperature measurements, but underpredicted the temperature during the growth phase and underpredicted the maximum temperature for both elevations.



(a) Back Position



(b) Corner Position



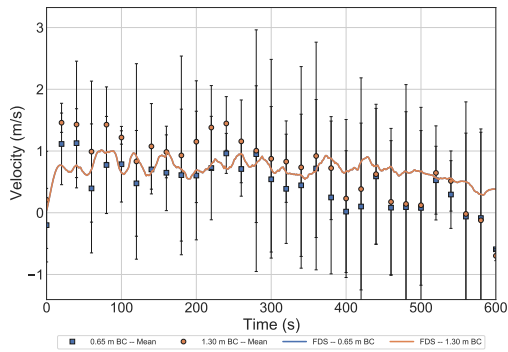
(c) Side Position

Figure A.33: Comparison of the Plume Temperature in the 0.6 m Burner, 100 kW Experiments with Door Closed

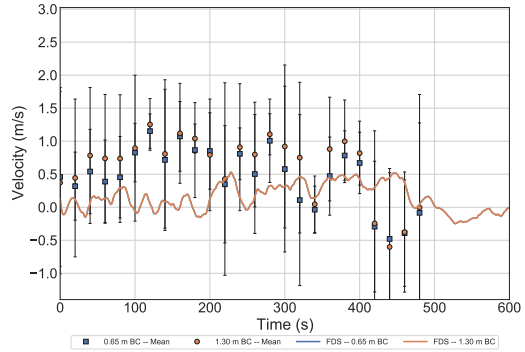
A comparison of the plume velocities measured in the experiments with the Red Accent Chair is presented in Figure A.38. FDS generally underpredicted the plume velocity at both elevations throughout the experiment.

A comparison of the plume temperatures measured in the experiments with the Overstuffed Sofa is presented in Figure A.39. The FDT correlation overpredicted all the temperatures. FDS predicted the qualitative shape of the plume temperature measurements, and accurately predicted the maximum temperature in the higher elevation measurement position, but underpredicted the temperatures during the growth and decay phases.

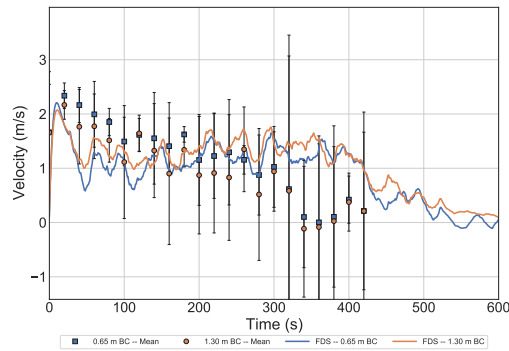
A comparison of the plume velocities measured in the experiments with the overstuffed Sofa is presented in Figure A.38. FDS generally underpredicted the plume velocity at both elevations when the sofa was in the back position and accurately predicted the maximum velocity measured when the sofa was in the corner position.



(a) Back Position

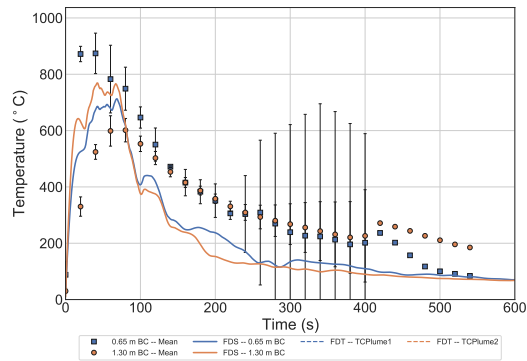


(b) Corner Position

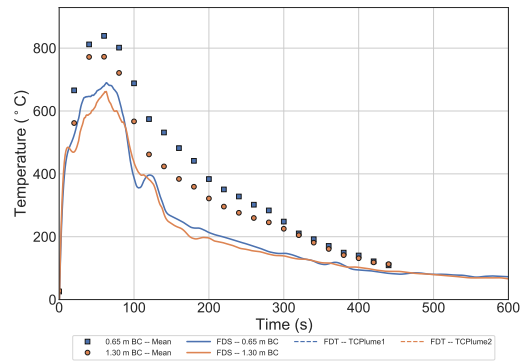


(c) Side Position

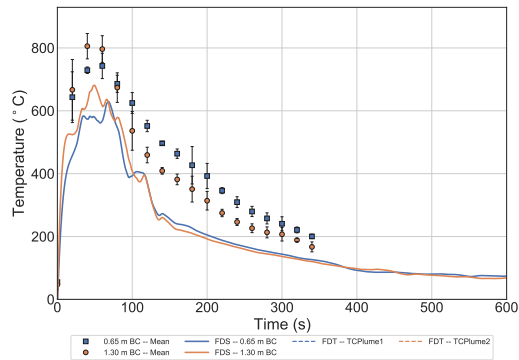
Figure A.34: Comparison of the Plume Velocity in the 0.6 m Burner, 100 kW Experiments with Door Closed



(a) Back Position

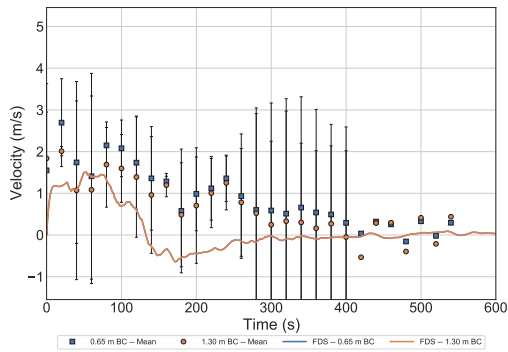


(b) Corner Position

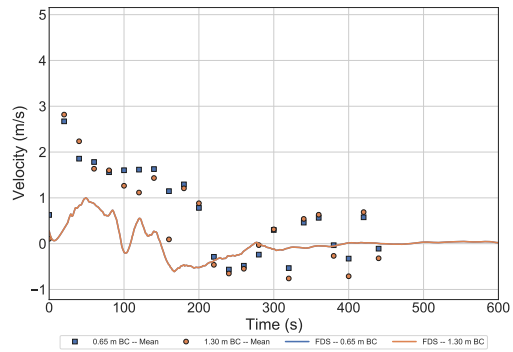


(c) Side Position

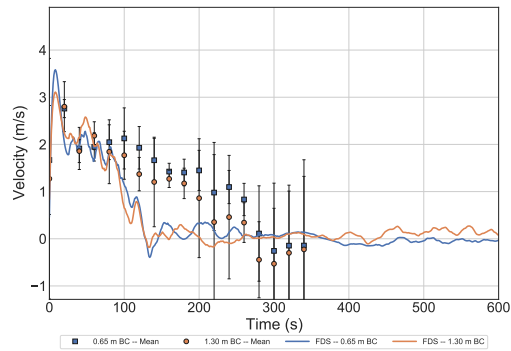
Figure A.35: Comparison of the Plume Temperature in the 0.6 m Burner, 500 kW Experiments with Door Closed



(a) Back Position

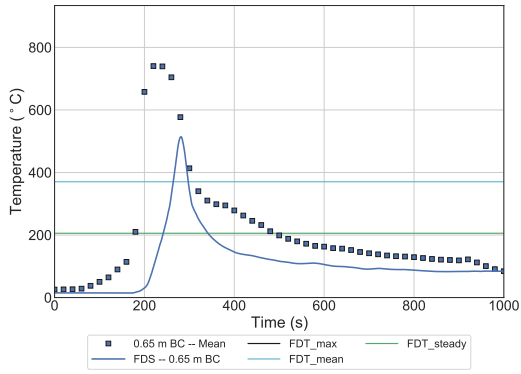


(b) Corner Position

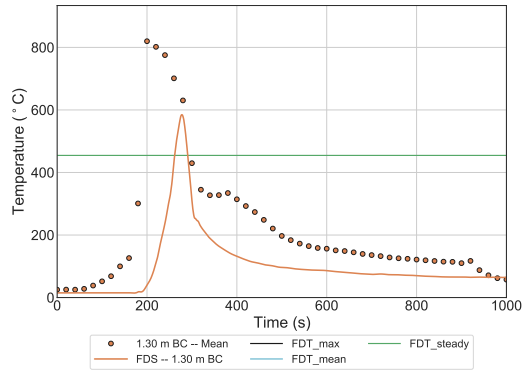


(c) Side Position

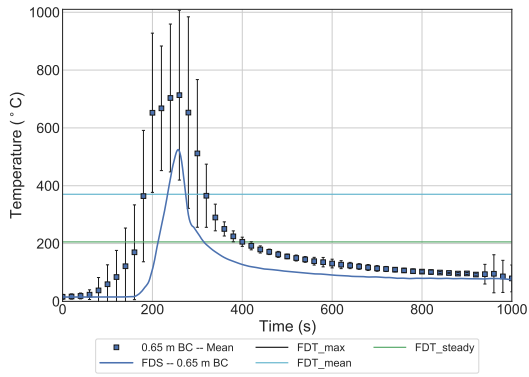
Figure A.36: Comparison of the Plume Velocity in the 0.6 m Burner, 500 kW Experiments with Door Closed



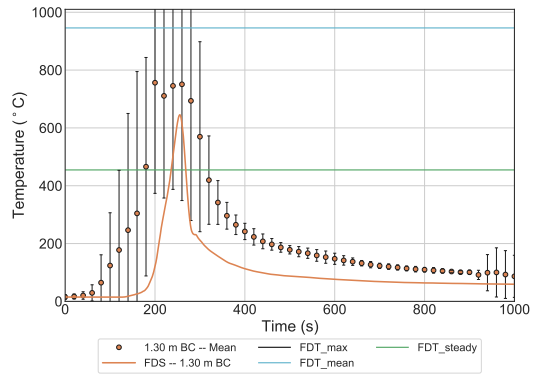
(a) Back Position Plume TC1



(b) Corner Position Plume TC2

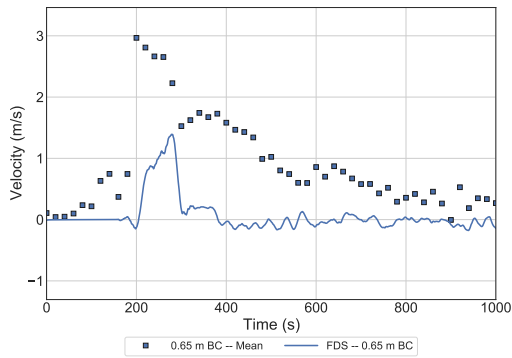


(c) Corner Position Plume TC1

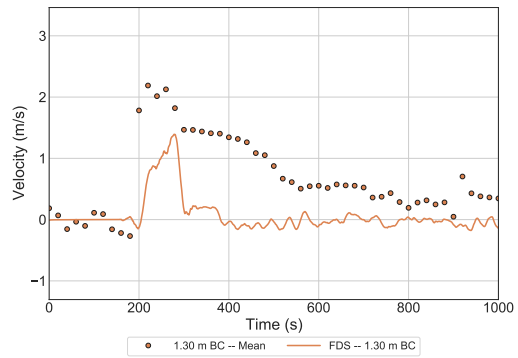


(d) Corner Position Plume TC2

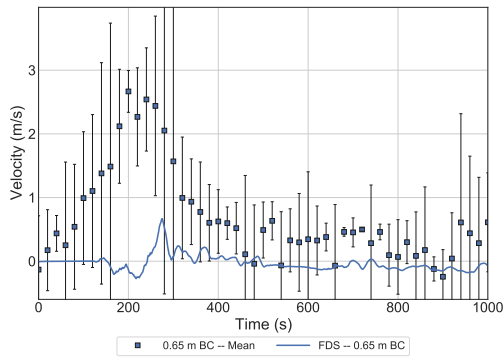
Figure A.37: Comparison of the Plume Temperature in the Red Accent Chair Experiments with the Door Closed



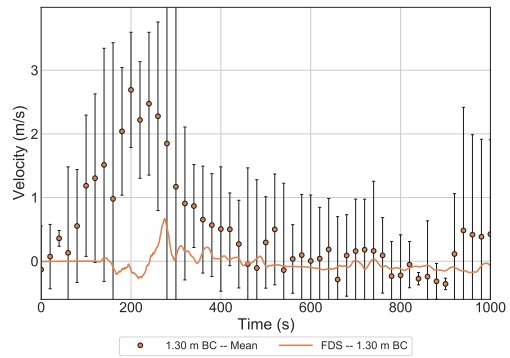
(a) Back Position Plume BDP1



(b) Back Position Plume BDP2

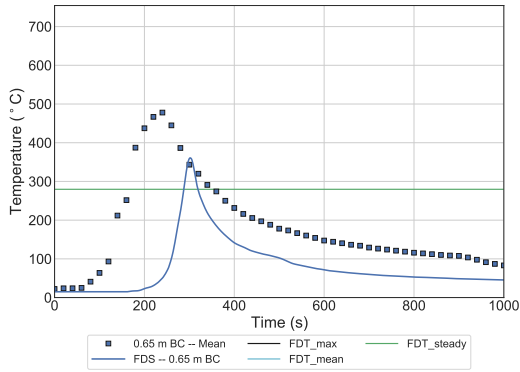


(c) Corner Position Plume BDP1

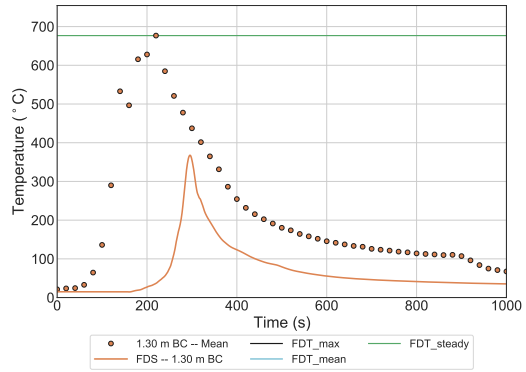


(d) Corner Position Plume BDP2

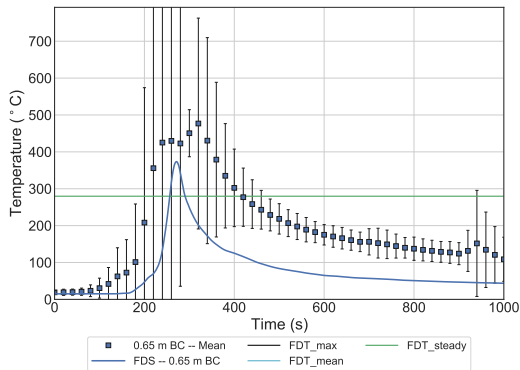
Figure A.38: Comparison of the Plume Velocity in the Red Accent Chair Experiments with the Door Closed



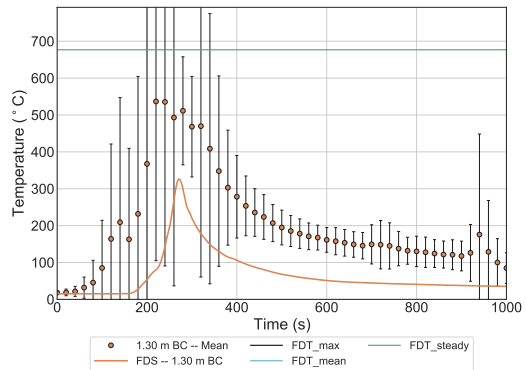
(a) Back Position Plume TC1



(b) Corner Position Plume TC2

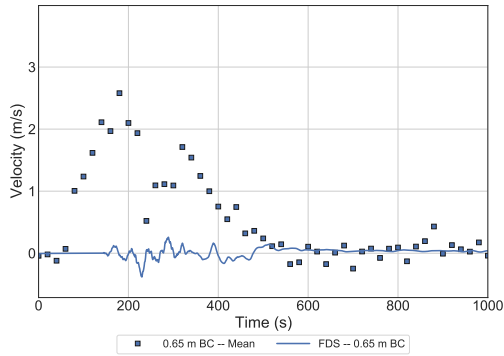


(c) Corner Position Plume TC1

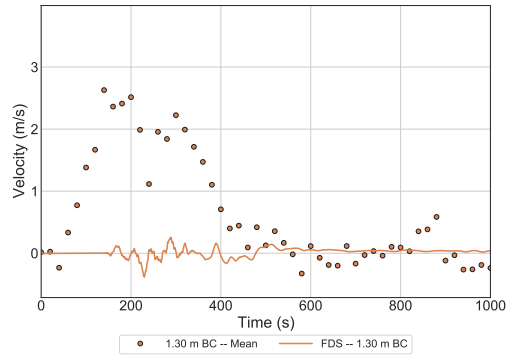


(d) Corner Position Plume TC2

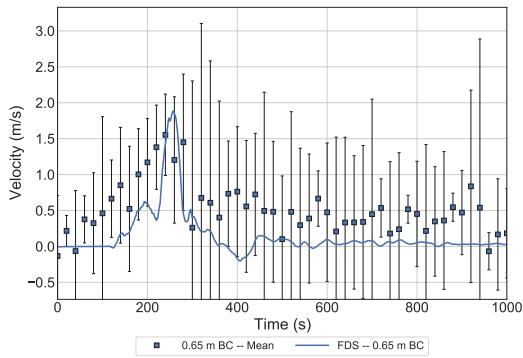
Figure A.39: Comparison of the Plume Temperature in the Overstuffed Sofa Experiments with the Door Closed



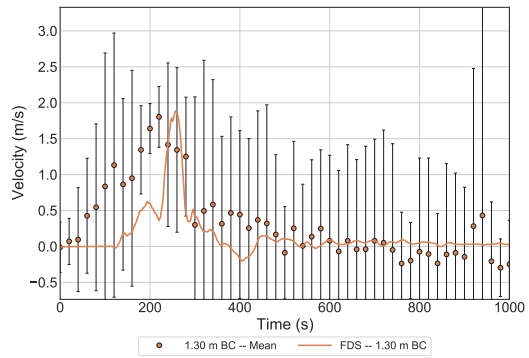
(a) Back Position Plume BDP1



(b) Back Position Plume BDP2



(c) Corner Position Plume BDP1



(d) Corner Position Plume BDP2

Figure A.40: Comparison of the Plume Velocity in the Overstuffed Sofa Experiments with the Door Closed

### A.1.3 Flame Height

#### Open Door

Figure A.41 displays the measured and predicted mean flame heights for the 0.3 m Burner experiments with the 100 kW HRR. The experimental flame height does not appear to be influenced by the location of the burner for this HRR or burner size. FDS and CFAST accurately predicted the flame height when the burner was in all positions. In the center position, the Heskestad correlation provided a better prediction than the Thomas correlation. The FDT correlation for the flame height in the back and side positions overpredicted the measured flame heights, although the correlation for the corner provided a good prediction of the measured flame height.

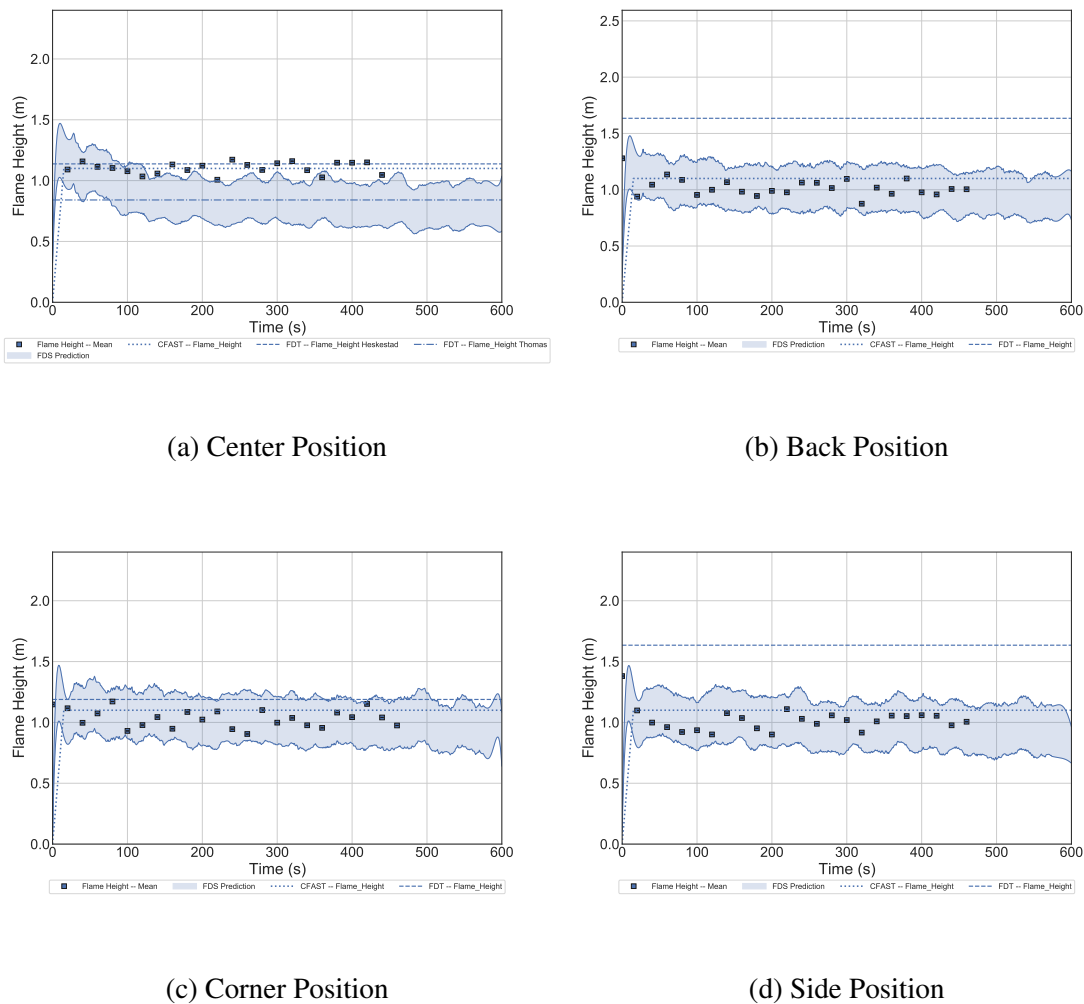


Figure A.41: Comparison of the Mean Flame Height in the 0.3 m Burner, 100 kW Experiments with Door Open

Figure A.42 displays the measured and predicted mean flame heights for the 0.6 m Burner experiments with the 100 kW HRR. The experimental flame height was slightly larger when the burner

was in the corner position relative to when the burner was in the back and side positions. FDS accurately predicted the flame height when the burner was in all positions. CFAST accurately predicted the flame height in the corner, but overpredicted the flame height at the side and back. The FDT correlations for the flame height in each position overpredicted the measurement.

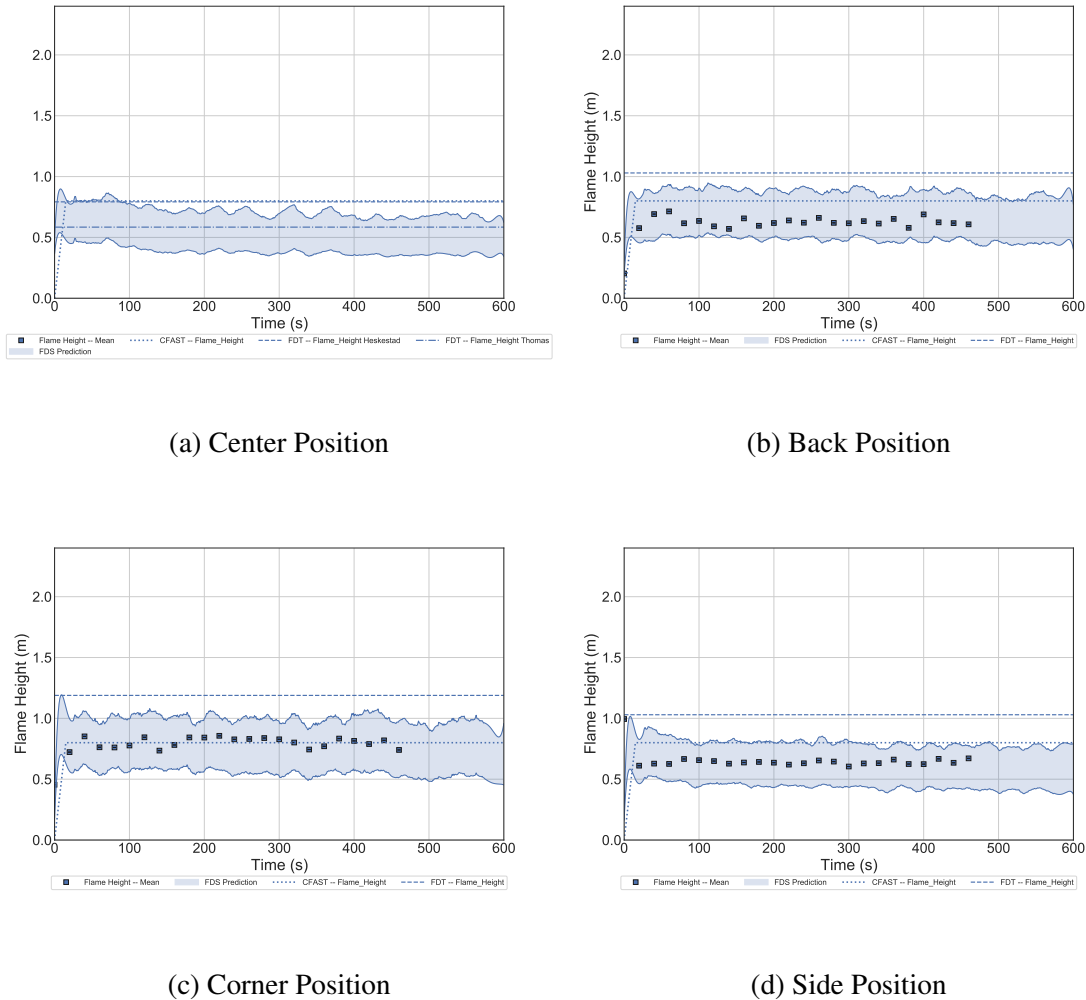
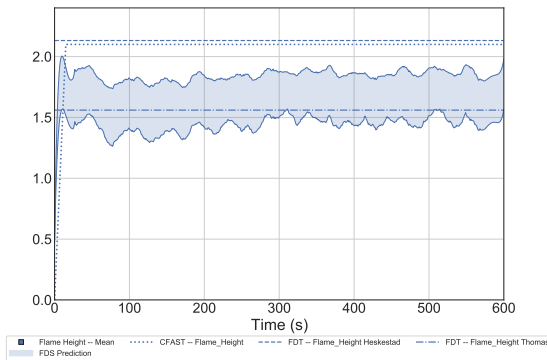


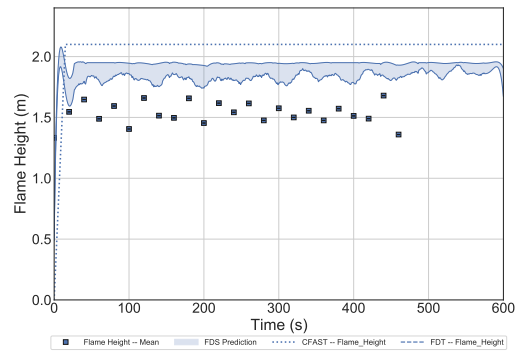
Figure A.42: Comparison of the Mean Flame Height in the 0.6 m Burner, 100 kW Experiments with Door Open

Figure A.43 displays the measured and predicted mean flame heights for the 0.6 m Experiments with the 500 kW HRR. CFAST and FDS predicted that the mean flame height was consistent with the ceiling height when the burner was in all the positions. The FDT correlations were not limited by the flame height and predicted that the flame height was larger than the ceiling height, so they do not appear in the plots. The experimental data reached a maximum at approximately 1.6 m.

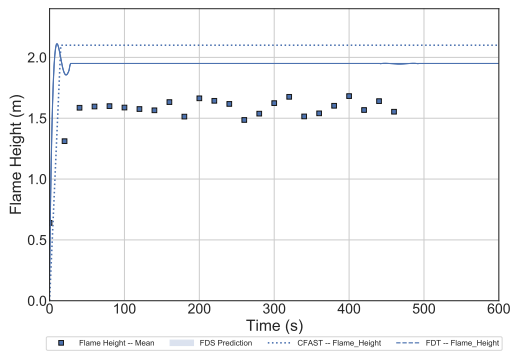
Figure A.44 displays the measured and predicted mean flame heights for the Red Accent Chair. CFAST and FDS predicted that the mean flame height was consistent with the ceiling height when the burner was in all the positions. The FDT correlations were not limited by the flame height and predicted that the flame height calculated with the maximum HRR was larger than the ceiling



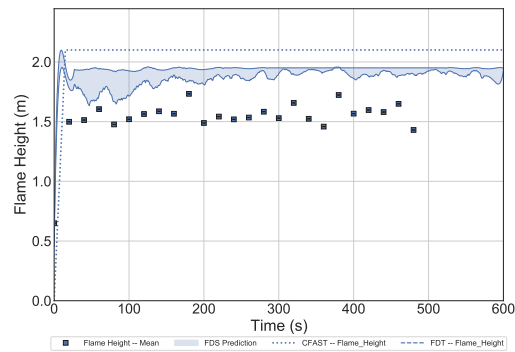
(a) Center Position



(b) Back Position



(c) Corner Position

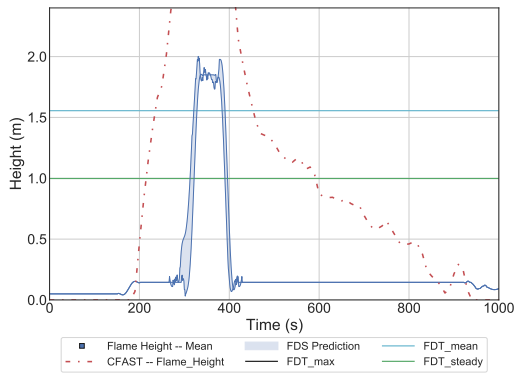


(d) Side Position

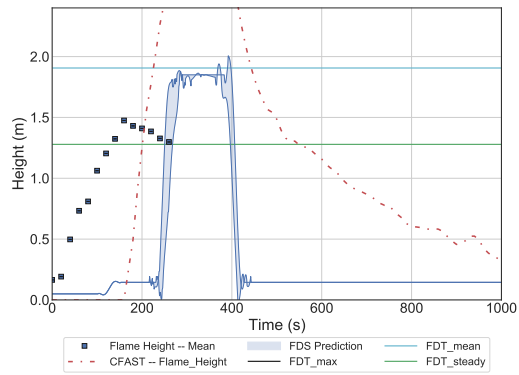
Figure A.43: Comparison of the Mean Flame Height in the 0.6 m Burner, 500 kW Experiments with Door Open

height, so they do not appear in the plots. The flame FDT correlations calculated with the mean and steady HRRs also overpredicted the respective flame heights. The experimental data reached a maximum at approximately 1.5 m before data collection stopped.

Figure A.45 displays the measured and predicted mean flame heights for the Overstuffed Sofa. CFAST and FDS predicted that the mean flame height was consistent with the ceiling height when the burner was in all the positions. The FDT correlations were not limited by the flame height and predicted that the flame height calculated with the maximum HRR was larger than the ceiling height, so they do not appear in the plots. The flame FDT correlations calculated with the mean and steady HRRs also overpredicted the respective flame heights. The experimental data reached a maximum at approximately 1.4 m before data collection stopped.

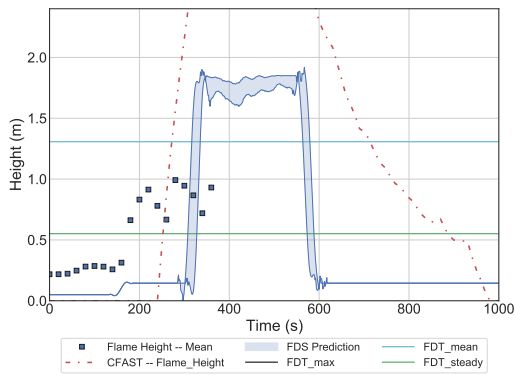


(a) Back Position

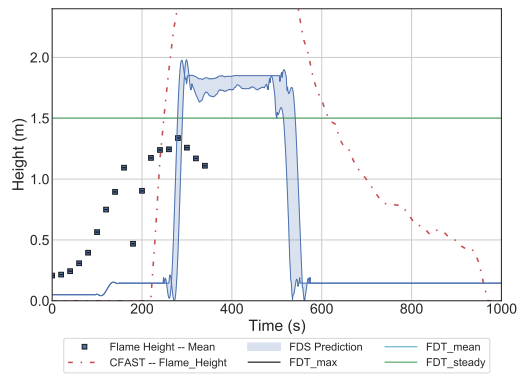


(b) Corner Position

Figure A.44: Comparison of the Mean Flame Height in the Red Accent Chair Experiments with the Door Open



(a) Back Position



(b) Corner Position

Figure A.45: Comparison of the Mean Flame Height in the Overstuffed Sofa Experiments with the Door Open

### Closed Door

Figure A.46 displays the measured and predicted mean flame heights for the 0.3 m Burner experiments with the 100 kW HRR. CFAST accurately predicted the the flame height and the qualitative trends as the compartment transitioned to a ventilation-limited condition. The FDS predictions were accurate up to approximately 200 s at which point the prediction and experimental data diverged. The FDT correlations for the flame height in the back and side positions overpredicted the measured flame heights throughout the experiments, although the correlation for the corner provided a good prediction of the measured flame height up to 200 s.

Figure A.47 displays the measured and predicted mean flame heights for the 0.6 m Burner experi-

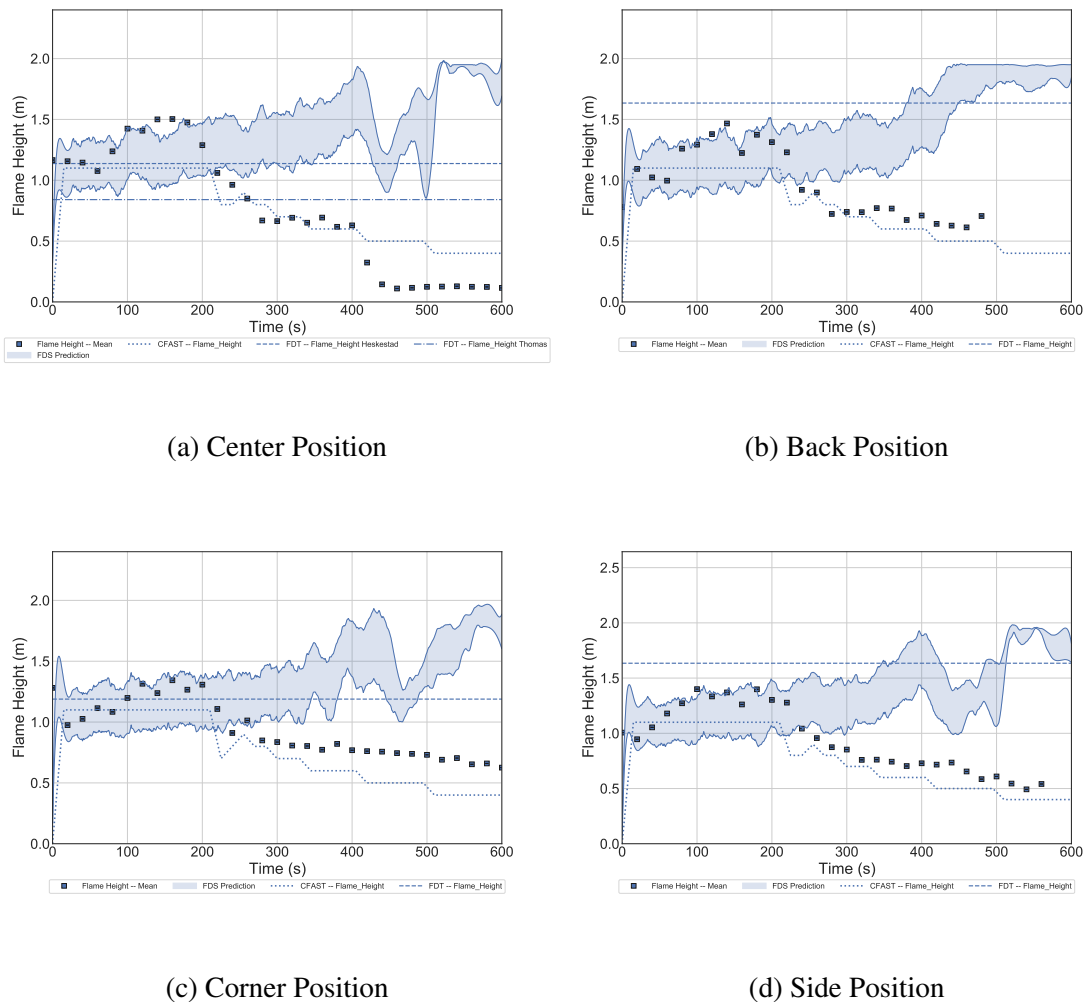
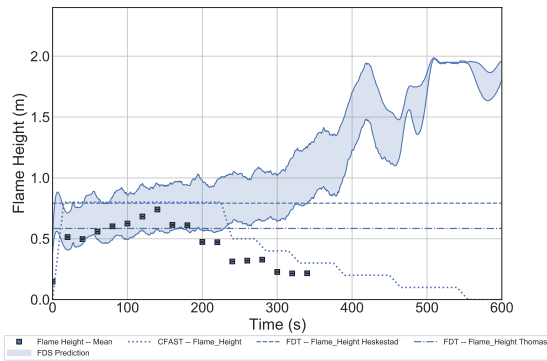


Figure A.46: Comparison of the Mean Flame Height in the 0.3 m Burner, 100 kW Experiments with Door Closed

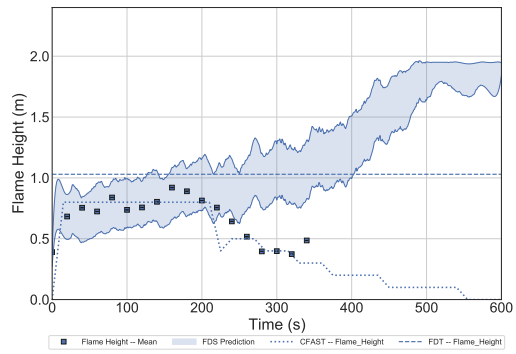
ments with a HRR of 100 kW. CFAST accurately predicted the the flame height and the qualitative trends as the compartment transitioned to a ventilation-limited condition. The FDS predictions were accurate up to approximately 200 s, at which point the prediction and experimental data diverged. The FDT correlations for the flame height in the back, corner, and side positions over-predicted the measured flame heights throughout the experiments, although the Thomas correlation for the center provided a good prediction of the measured flame height up to 200 s.

Figure A.49 displays the measured and predicted mean flame heights for the Red Accent Chair experiments. The FDS and CFAST predictions agreed well with each other and qualitatively with the experimental data, but overpredicted the peak mean flame height magnitude and timing.

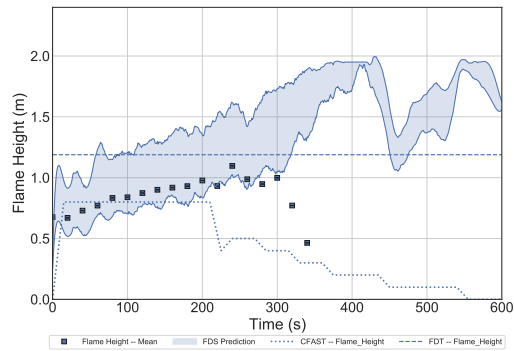
Figure A.50 displays the measured and predicted mean flame heights for the Overstuffed Sofa experiments. The FDS and CFAST predictions agreed with each other and qualitatively with the experimental data, but overpredicted the peak mean flame height magnitude and timing.



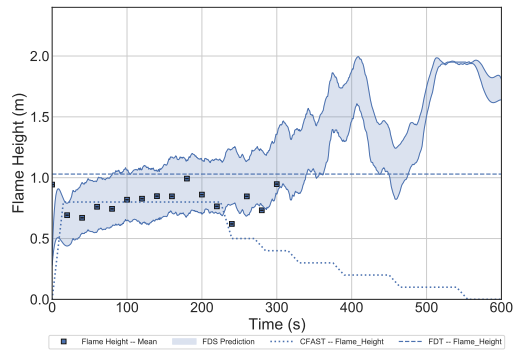
(a) Center Position



(b) Back Position

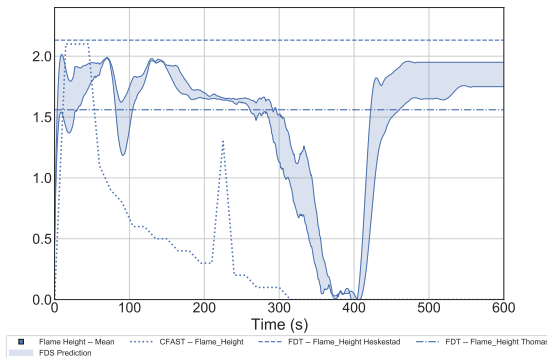


(c) Corner Position

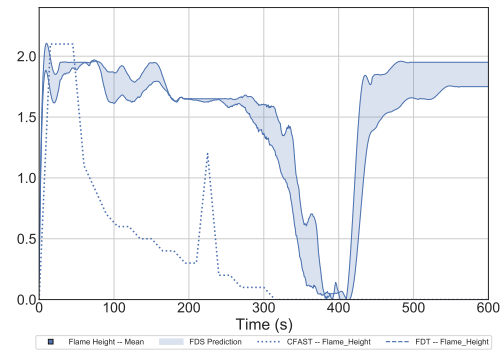


(d) Side Position

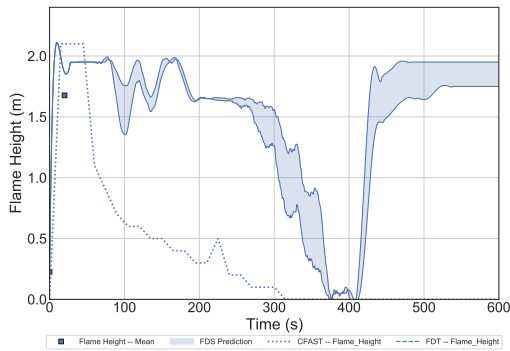
Figure A.47: Comparison of the Mean Flame Height in the 0.6 m Burner, 100 kW Experiments with Door Closed



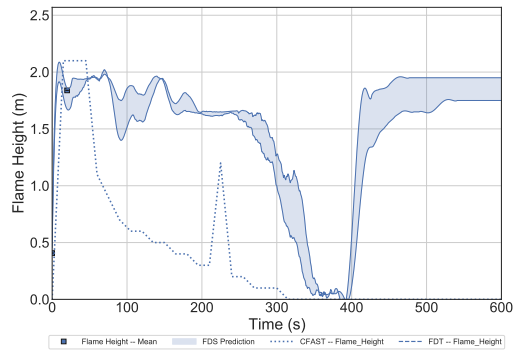
(a) Center Position



(b) Back Position

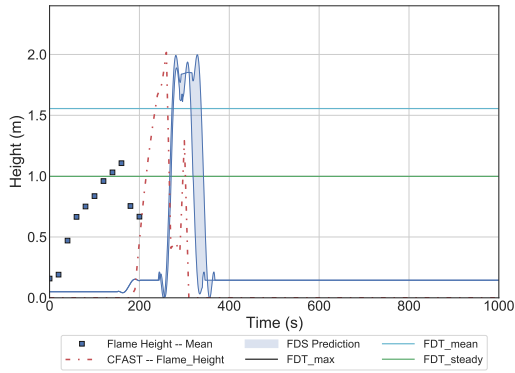


(c) Corner Position

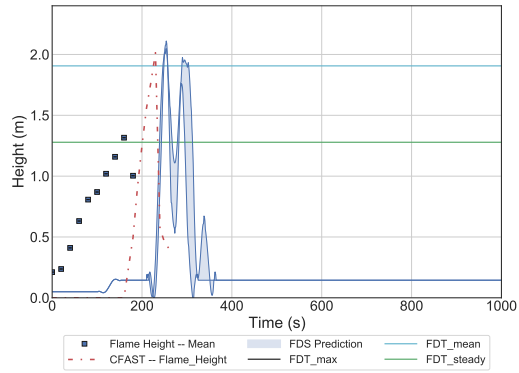


(d) Side Position

Figure A.48: Comparison of the Mean Flame Height in the 0.6 m Burner, 500 kW Experiments with Door Closed

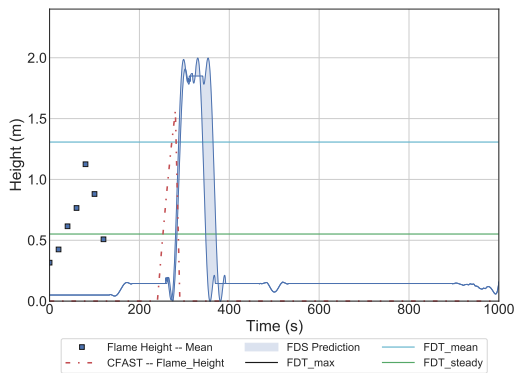


(a) Back Position

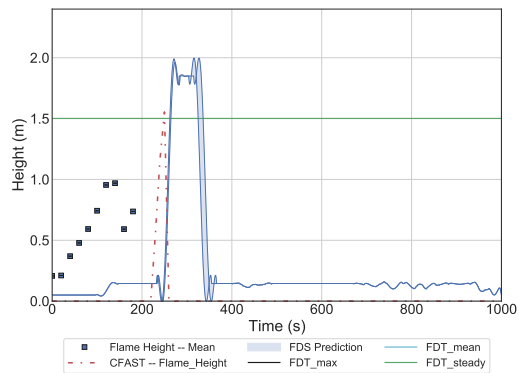


(b) Corner Position

Figure A.49: Comparison of the Mean Flame Height in the Red Accent Chair Experiments with the Door Closed



(a) Back Position



(b) Corner Position

Figure A.50: Comparison of the Mean Flame Height in the Overstuffed Sofa Experiments with the Door Closed

### A.1.4 Heat Flux

The following sections display the experimental total and radiative heat flux measurements from the experiments conducted in the compartment as well as the model predictions.

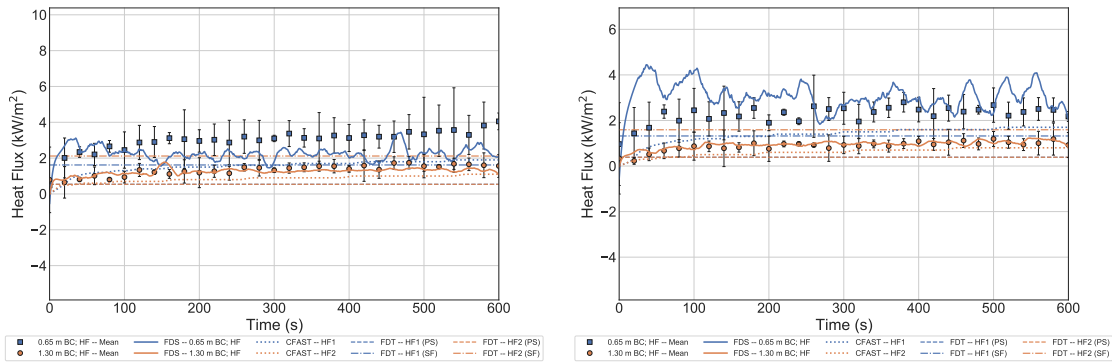
#### Open Door

A comparison of the measured and predicted heat fluxes to the right wall of the compartment for the 0.3 m Burner with a HRR of 100 kW is provided in Figure A.51. FDS and CFAST accurately predicted the heat flux to the lower elevation gauge while the point source method underpredicted and the solid flame correlation overpredicted the heat flux to the lower elevation gauge when the burner was in the center position. FDS accurately predicted the heat flux to the upper elevation gauge and the point source method, the solid flame method, and CFAST underpredicted the heat flux to the higher elevation gauge when the burner was in the center position. The same trends were evident when the burner was in the other positions except that all of the models, with the exception of the point source model yielded good predictions of the data measured at the lower elevation gauge.

A comparison of the measured and predicted heat fluxes to the back wall of the compartment for the 0.3 m Burner with a HRR of 100 kW is provided in Figure A.52. Although the heat flux between the right wall and the back wall from the burner placed in the center of the compartment should be identical in quiescent conditions, that is not evident in the figure. None of the models accurately predicted the heat fluxes to the back wall when the burner was in the center of the compartment. CFAST and FDS predicted the heat flux to the lower elevation gauge on the back wall when the burner was in the back position. FDS accurately predicted the heat fluxes when the burner was in the corner position and side position, and CFAST predicted the heat flux to the lower elevation gauge with the burner in the side position.

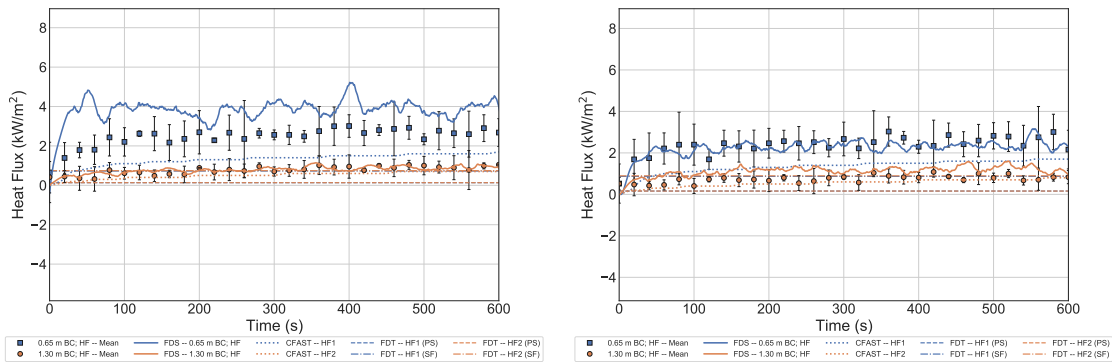
A comparison of the measured and predicted heat fluxes to the right wall of the compartment for the 0.6 m Burner with a HRR of 100 kW is provided in Figure A.53. FDS, CFAST, and the point source method accurately predicted the heat flux to the lower elevation gauge while the solid flame correlation overpredicted the heat flux to the lower elevation gauge when the burner was in the center position. FDS and the solid flame method accurately predicted the heat flux to the upper elevation gauge and the point source method and CFAST underpredicted the heat flux to the higher elevation gauge when the burner was in the center position. The same trends were evident when the burner was in the other positions except that all the models, with the exception of the point source model yielded good predictions of the data measured at the lower elevation gauge and only FDS predicted the heat flux to the higher elevation gauge.

A comparison of the measured and predicted heat fluxes to the right wall of the compartment for the 0.6 m Burner with a HRR of 100 kW is provided in Figure A.54. CFAST and the point source method accurately predicted the heat flux to the lower elevation gauge while the solid flame correlation and FDS overpredicted the heat flux to the lower elevation gauge when the burner was



(a) Center Position

(b) Back Position



(c) Corner Position

(d) Side Position

Figure A.51: Comparison of the Heat Flux to the Right Side Wall in the 0.3 m Burner, 100 kW Experiments with Door Open

in the center position. The solid flame method accurately predicted, FDS overpredicted, and the point source method and CFAST underpredicted the heat flux to the higher elevation gauge when the burner was in the center position. None of the models accurately predicted the heat flux to the back wall when the burner was in the back, corner, and side positions.

A comparison of the measured and predicted heat fluxes to the right wall of the compartment for the 0.6 m Burner with a HRR of 500 kW is provided in Figure A.55. The measured data does not appear to reach steady state in the 600 s displayed in the figure. The CFAST and FDS prediction qualitatively capture the continually increasing heat fluxes that were measured and FDS generally accurately predicted the heat flux at both elevations. CFAST predicted the lower elevation heat flux and underpredicted the higher elevation heat flux when the burner was in each position. The solid flame method predicted the approximate mean heat flux at the lower elevation gauge when the burner was in the center and the back positions, and the point source method underpredicted all heat fluxes.

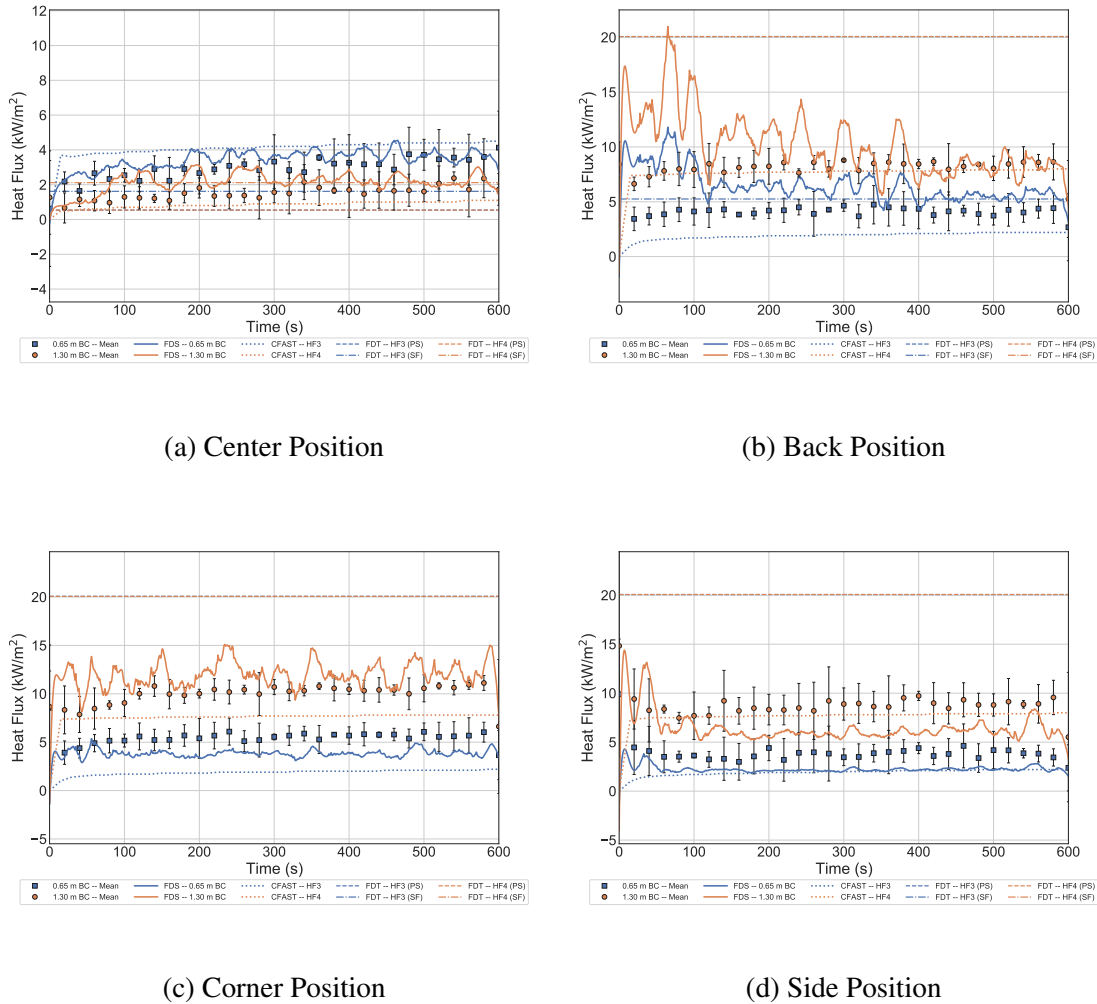
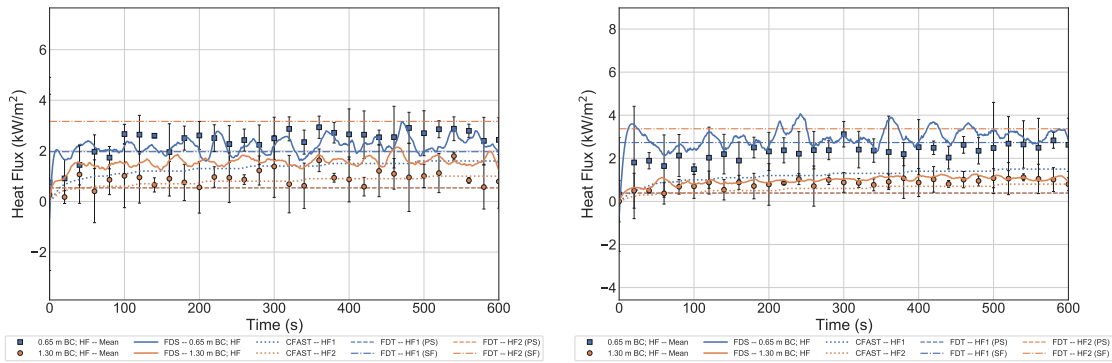


Figure A.52: Comparison of the Heat Flux to the Back Wall in the 0.3 m Burner, 100 kW Experiments with Door Open

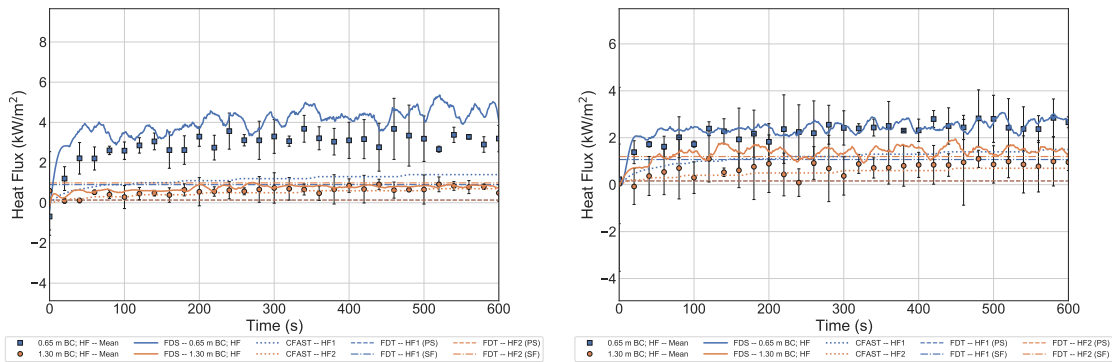
A comparison of the measured and predicted heat fluxes to the right wall of the compartment for the 0.6 m Burner with a HRR of 500 kW is provided in Figure A.56. When the burner was in the center position, FDS accurately predicted the higher elevation heat flux and CFAST provided the best approximation of the lower elevation heat flux, while all other models did provide accurate predictions of the measured heat fluxes. FDS also accurately predicted the higher elevation heat flux when the burner was in the corner and side positions. The error bars that represent the scatter in the experimental data for the lower elevation heat flux gauge in the side position are so large that they encompass the predictions from all the models.

A comparison of the measured and predicted heat fluxes to the right wall of the compartment for the Red Accent Chair is provided in Figure A.57. The point source and solid flame methods calculated with the maximum, mean, and steady HRRs significantly underpredicted the heat fluxes when the chair was in each position. FDS and CFAST captured the qualitative shape of the measured heat flux curve from all positions and FDS accurately predicted the maximum heat flux while CFAST



(a) Center Position

(b) Back Position



(c) Corner Position

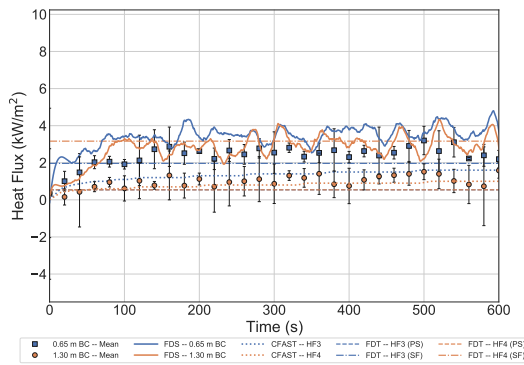
(d) Side Position

Figure A.53: Comparison of the Heat Flux to the Right Side Wall in the 0.6 m Burner, 100 kW Experiments with Door Open

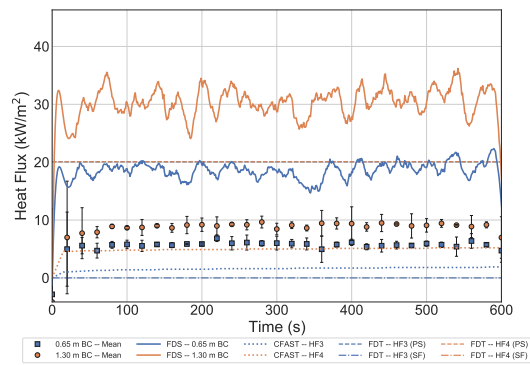
slightly underpredicted the maximum heat flux.

A comparison of the measured and predicted heat fluxes to the back wall of the compartment for the Red Accent Chair is provided in Figure A.58. The point source and solid flame methods calculated with the maximum, mean, and steady HRRs significantly underpredicted the heat fluxes when the chair was in each position. FDS and CFAST captured the qualitative shape of the measured heat flux curve from all positions and FDS slightly underpredicted the maximum heat flux while CFAST significantly underpredicted the maximum heat flux.

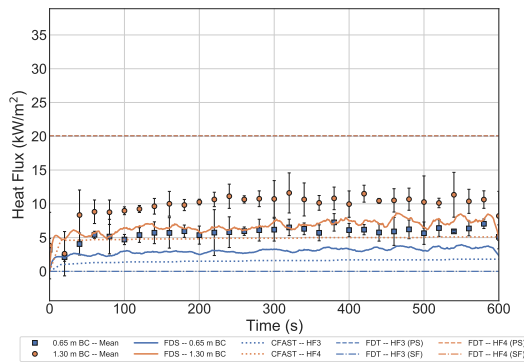
A comparison of the measured and predicted heat fluxes to the right wall of the compartment for the Overstuffed Sofa is provided in Figure A.59. The point source and solid flame methods calculated with the maximum, mean, and steady HRRs significantly underpredicted the heat fluxes when the sofa was in each position. FDS and CFAST captured the qualitative shape of the measured heat flux curve from all positions. FDS underpredicted the maximum heat flux measured with the sofa



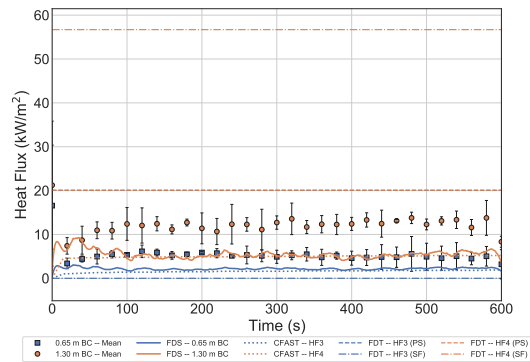
(a) Center Position



(b) Back Position



(c) Corner Position

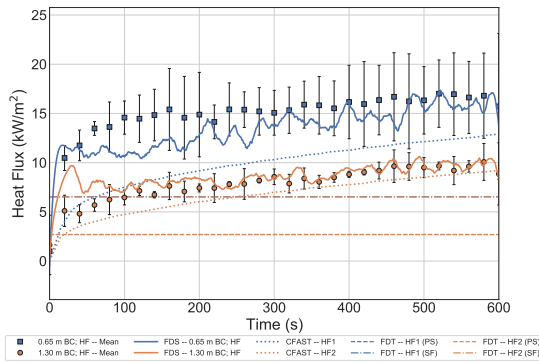


(d) Side Position

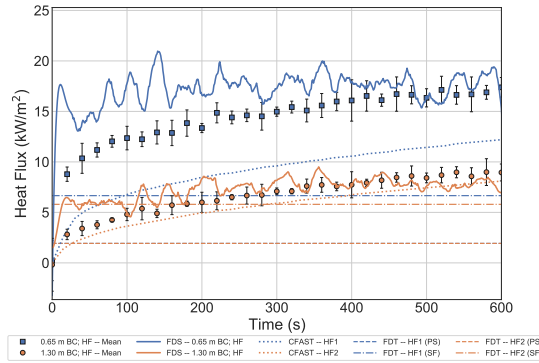
Figure A.54: Comparison of the Heat Flux to the Back Wall in the 0.6 m Burner, 100 kW Experiments with Door Open

in each position while CFAST overpredicted the maximum when the sofa was in the center position and back position, but underpredicted the maximum when the sofa was in the corner position.

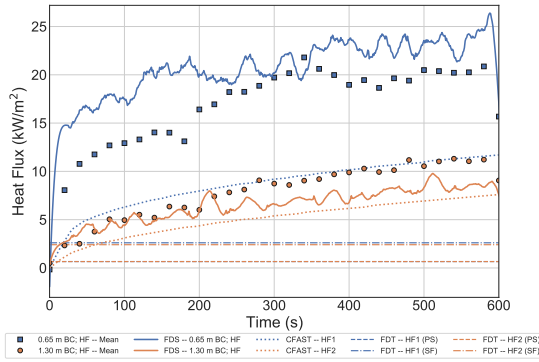
A comparison of the measured and predicted heat fluxes to the back wall of the compartment for the Overstuffed Sofa is provided in Figure A.59. The point source and solid flame methods calculated with the maximum, mean, and steady HRRs significantly underpredicted the heat fluxes when the sofa was in each position. FDS and CFAST generally represented the qualitative shape of the experimental data curves, although FDS significantly underpredicted the maximum heat flux when the sofa was in the corner and center positions and slightly underpredicted the maximum when the sofa was in the back position. CFAST overpredicted the heat fluxes to the back wall when the sofa was in the center position, accurately predicted the maximum heat fluxes in back position, and underpredicted the heat fluxes in the corner position.



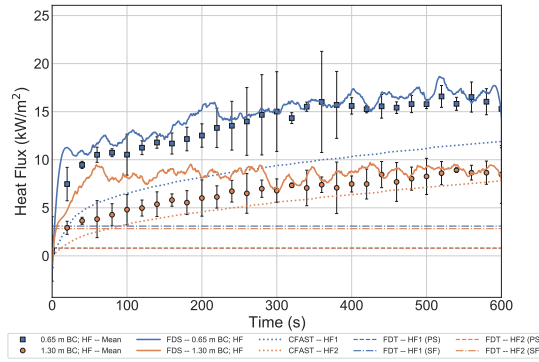
(a) Center Position



(b) Back Position

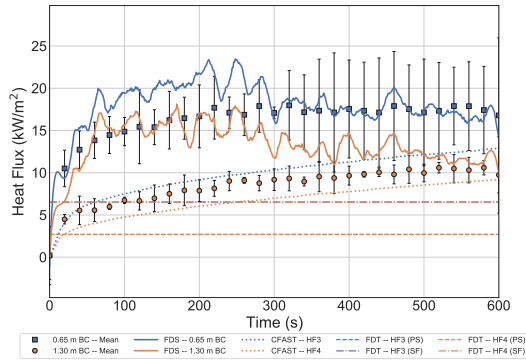


(c) Corner Position

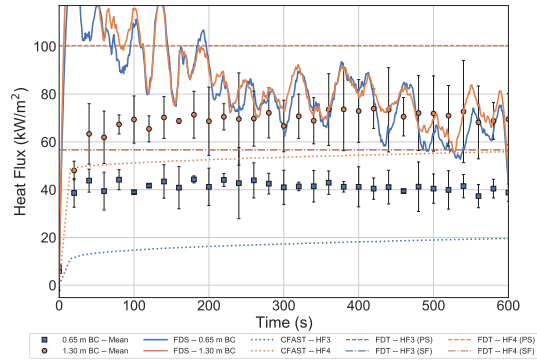


(d) Side Position

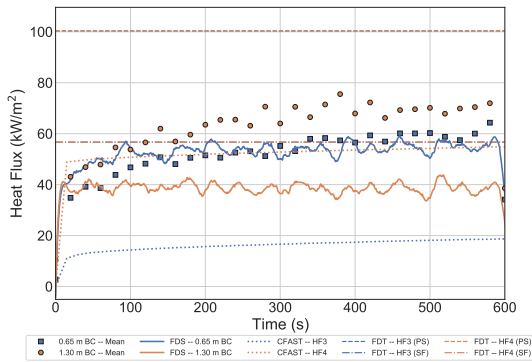
Figure A.55: Comparison of the Heat Flux to the Right Side Wall in the 0.6 m Burner, 500 kW Experiments with Door Open



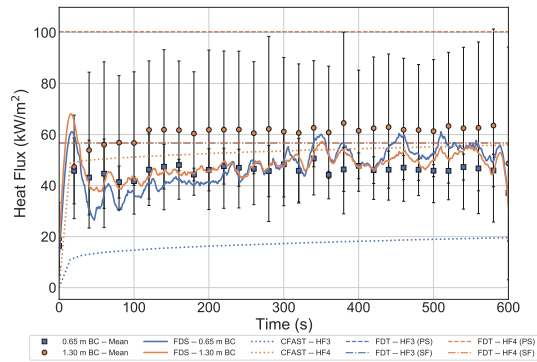
(a) Center Position



(b) Back Position

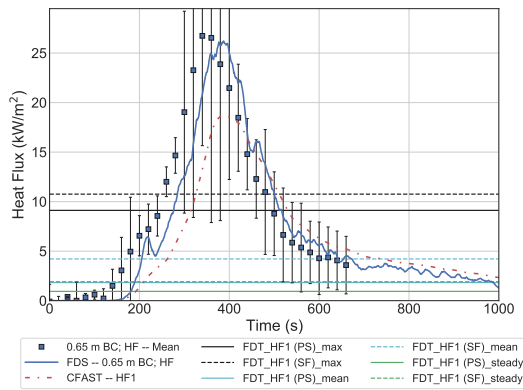


(c) Corner Position

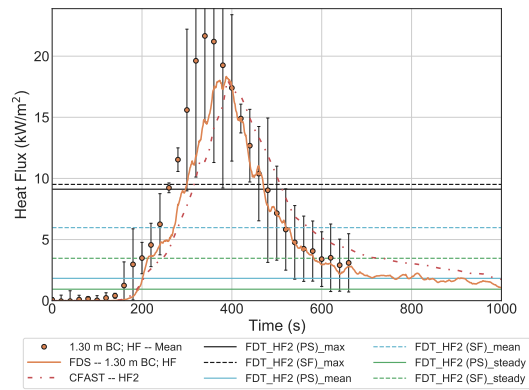


(d) Side Position

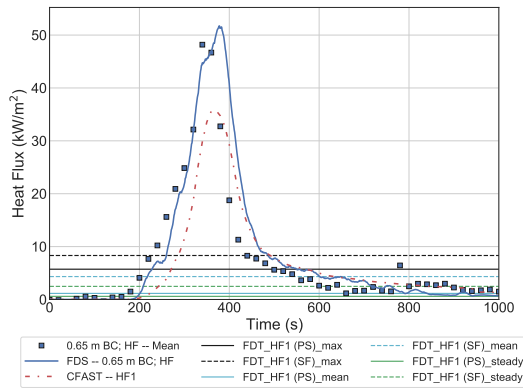
Figure A.56: Comparison of the Heat Flux to the Back Wall in the 0.6 m Burner, 500 kW Experiments with Door Open



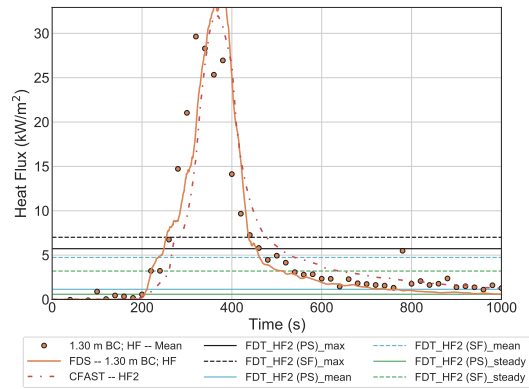
(a) Center Position, Heat Flux Gauge 1



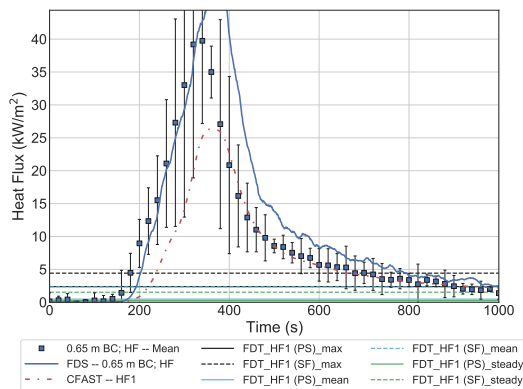
(b) Center Position, Heat Flux Gauge 2



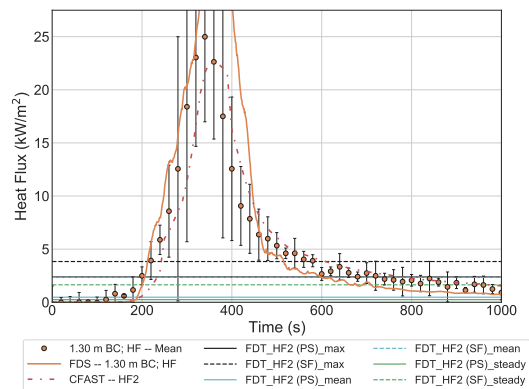
(c) Back Position, Heat Flux Gauge 1



(d) Back Position, Heat Flux Gauge 2

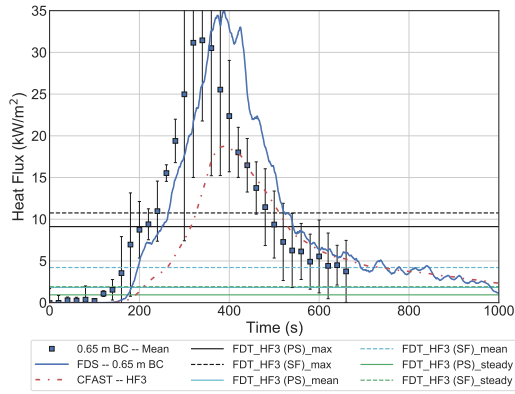


(e) Corner Position, Heat Flux Gauge 1

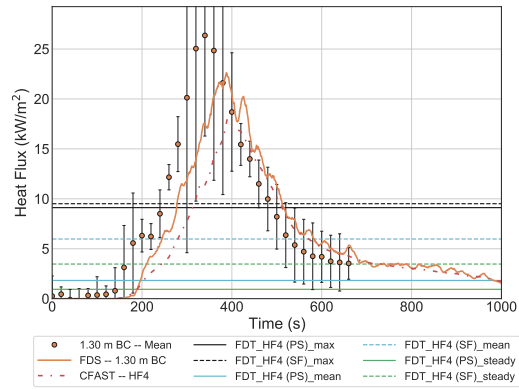


(f) Corner Position, Heat Flux Gauge 2

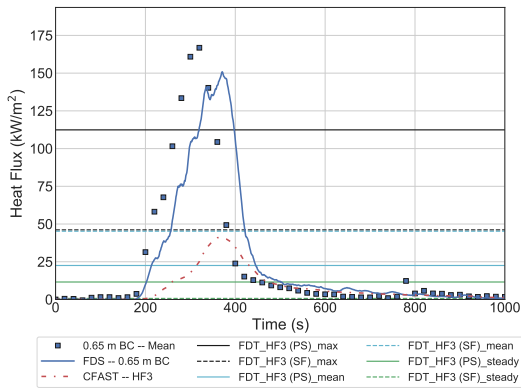
Figure A.57: Comparison of the Heat Flux to the Right Side Wall in the Red Accent Chair Experiments with the Door Open



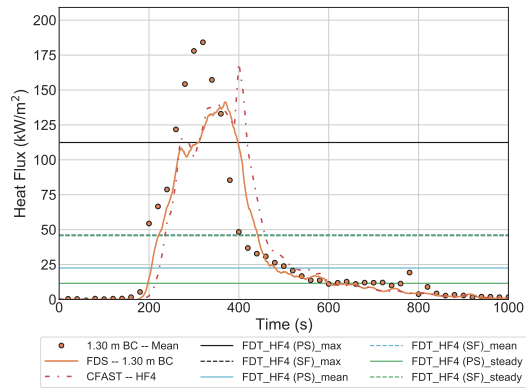
(a) Center Position, Heat Flux Gauge 3



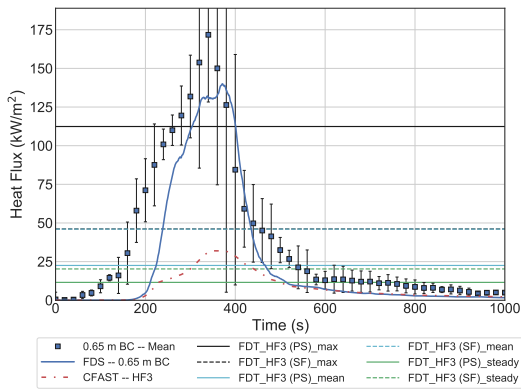
(b) Center Position, Heat Flux Gauge 4



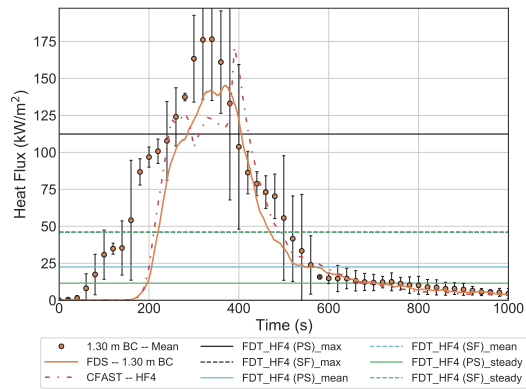
(c) Back Position, Heat Flux Gauge 3



(d) Back Position, Heat Flux Gauge 4

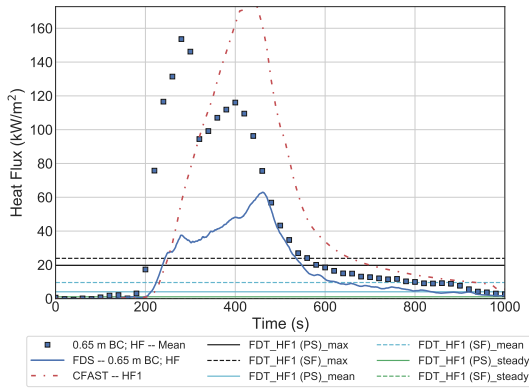


(e) Corner Position, Heat Flux Gauge 3

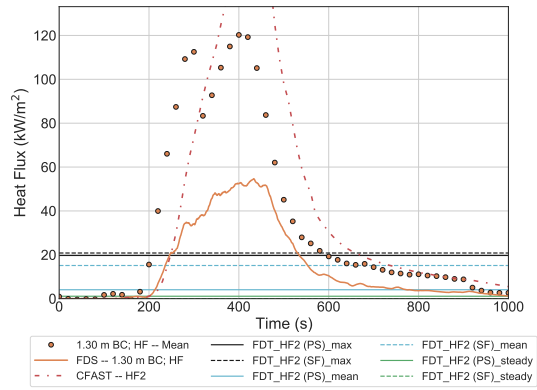


(f) Corner Position, Heat Flux Gauge 4

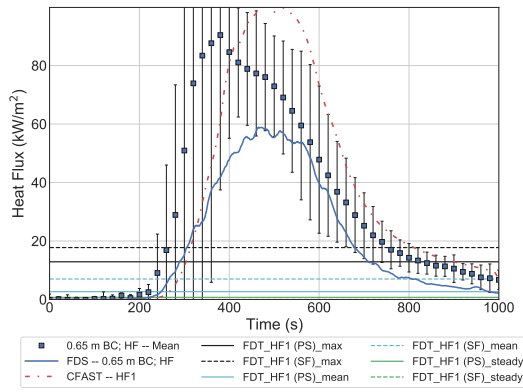
Figure A.58: Comparison of the Heat Flux to the Back Wall in the Red Accent Chair Experiments with the Door Open



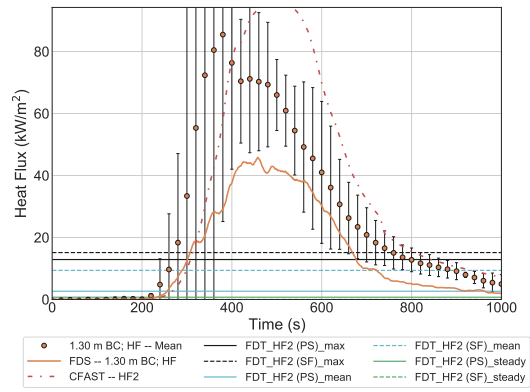
(a) Center Position, Heat Flux Gauge 1



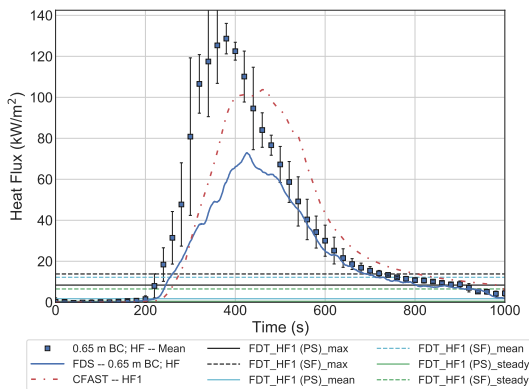
(b) Center Position, Heat Flux Gauge 2



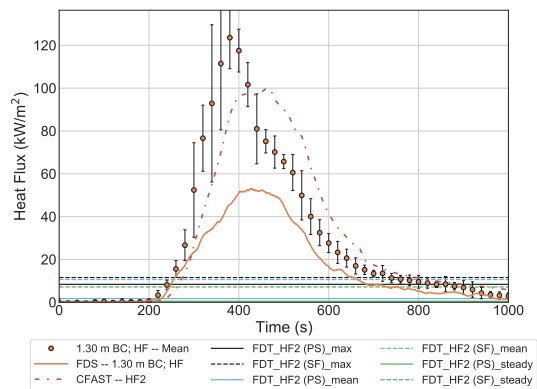
(c) Back Position, Heat Flux Gauge 1



(d) Back Position, Heat Flux Gauge 2

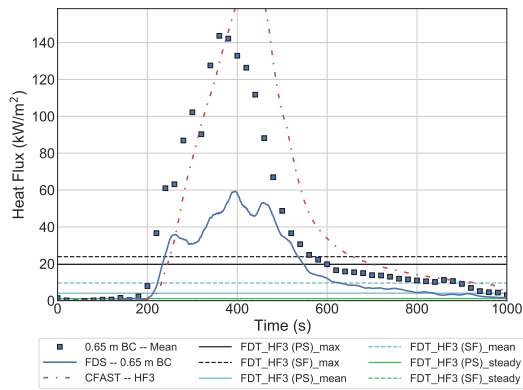


(e) Corner Position, Heat Flux Gauge 1

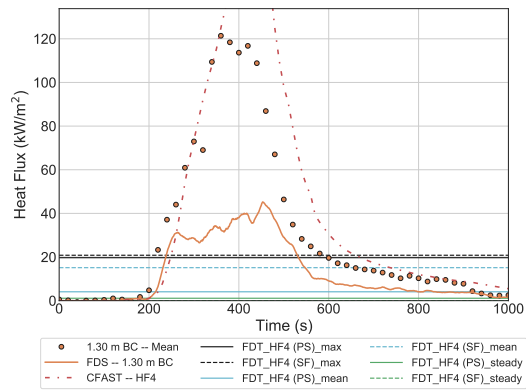


(f) Corner Position, Heat Flux Gauge 2

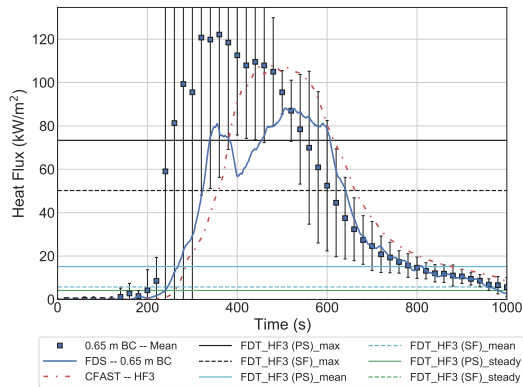
Figure A.59: Comparison of the Heat Flux to the Right Side Wall in the Overstuffed Sofa Experiments with the Door Open



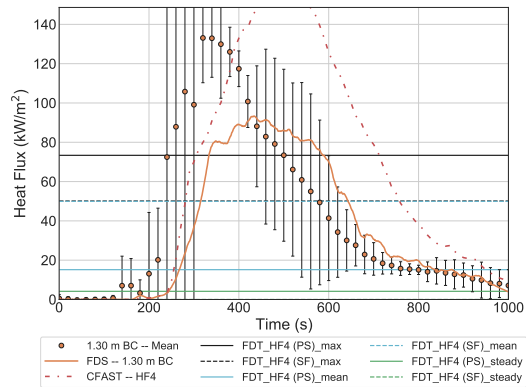
(a) Center Position, Heat Flux Gauge 3



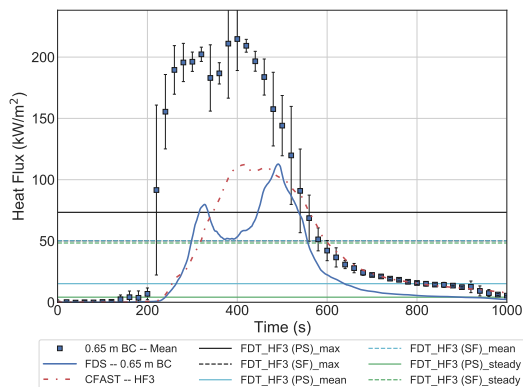
(b) Center Position, Heat Flux Gauge 4



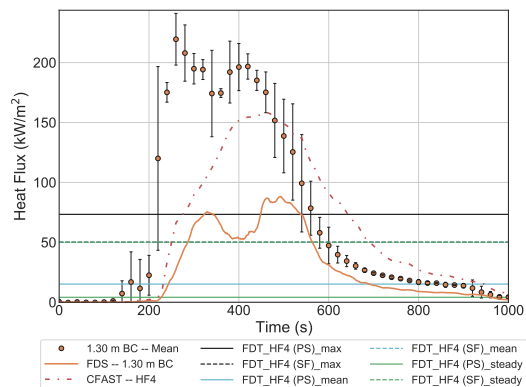
(c) Back Position, Heat Flux Gauge 3



(d) Back Position, Heat Flux Gauge 4



(e) Corner Position, Heat Flux Gauge 3



(f) Corner Position, Heat Flux Gauge 4

Figure A.60: Comparison of the Heat Flux to the Back Wall in the Overstuffed Sofa Experiments with the Door Open

## Closed Door

A comparison of the measured and predicted heat fluxes to the right wall of the compartment for the 0.3 m Burner with a HRR of 100 kW is provided in Figure A.61. FDS accurately predicted the heat fluxes when the burner was in the back, corner, and side positions. All other models underpredicted the heat flux to the right side wall for the experiments.

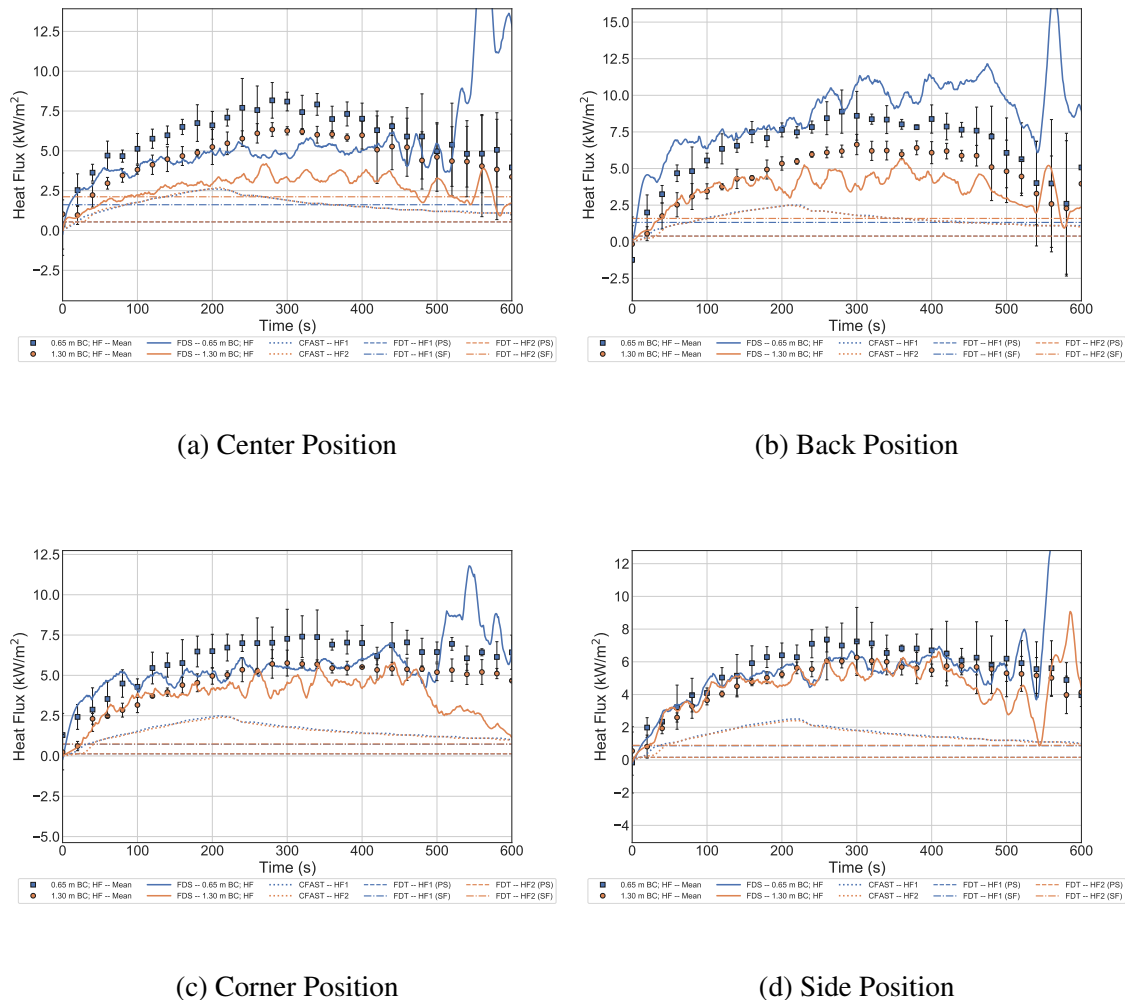
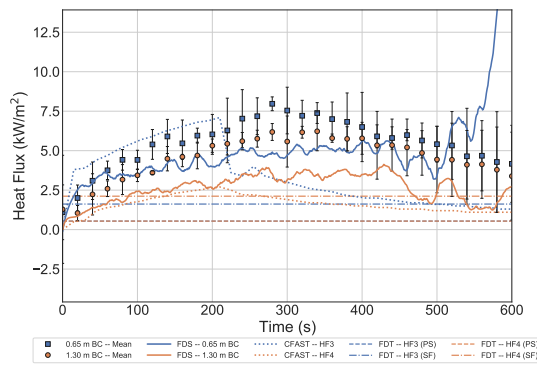
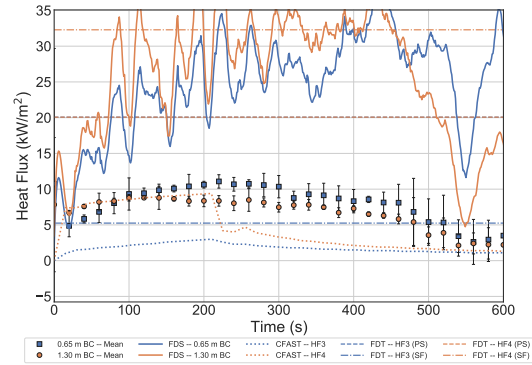


Figure A.61: Comparison of the Heat Flux to the Right Side Wall in the 0.3 m Burner, 100 kW Experiments with Door Closed

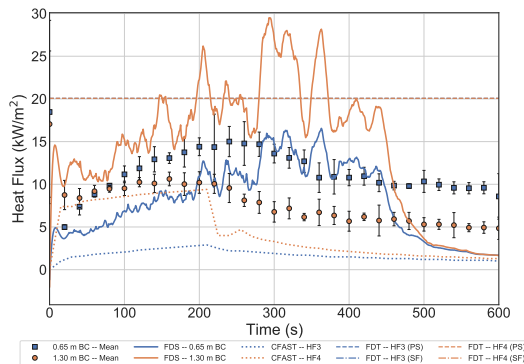
A comparison of the measured and predicted heat fluxes to the back wall of the compartment for the 0.3 m Burner with a HRR of 100 kW is provided in Figure A.62. CFAST accurately predicted the heat flux to the lower elevation gauge with the burner in the back, corner, and side positions and to the higher elevation gauge with the burner in the center position up to approximately 200 s, at which point the heat flux precipitously dropped due to the ventilation limitation, which was not accurately predicted.



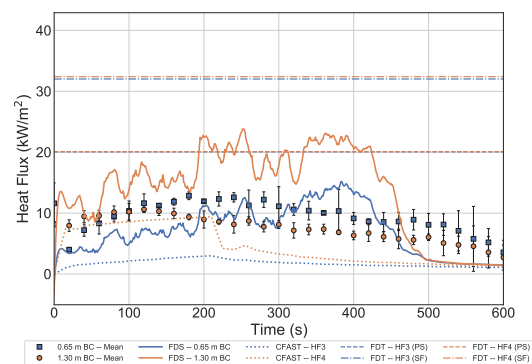
(a) Center Position



(b) Back Position



(c) Corner Position



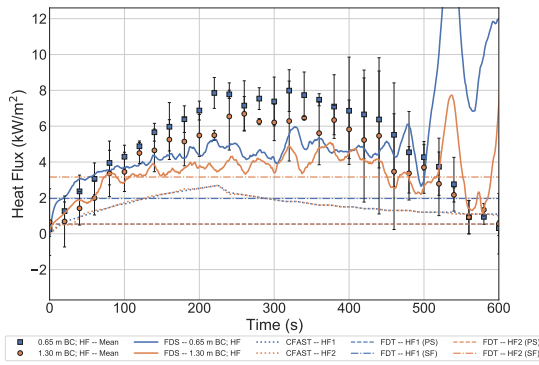
(d) Side Position

Figure A.62: Comparison of the Heat Flux to the Back Wall in the 0.3 m Burner, 100 kW Experiments with Door Closed

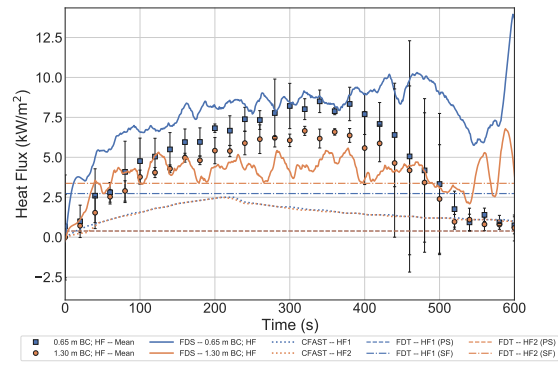
A comparison of the measured and predicted heat fluxes to the right wall of the compartment for the 0.6 m Burner with a HRR of 100 kW is provided in Figure A.63. FDS accurately predicted the heat fluxes when the burner was in the back, corner, and side positions. All other models underpredicted the heat flux to the right side wall for the experiments.

A comparison of the measured and predicted heat fluxes to the back wall of the compartment for the 0.3 m Burner with a HRR of 100 kW is provided in Figure A.64. None of the models systematically accurately predicted the magnitude of the heat fluxes to the back walls with the burner in any of the positions.

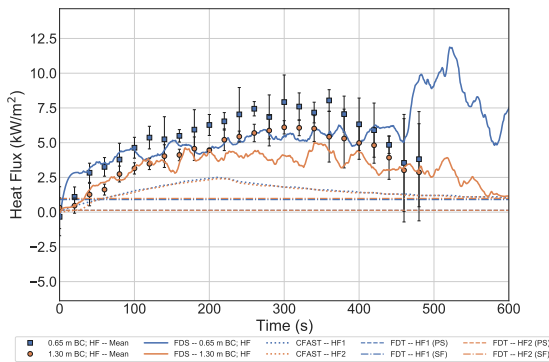
A comparison of the measured and predicted heat fluxes to the right wall of the compartment for the 0.6 m Burner with a HRR of 500 kW is provided in Figure A.65. FDS accurately predicted the heat fluxes when the burner was in all the positions. The solid flame model typically predicted the approximate mean heat flux when the burner was in the back and center positions. CFAST



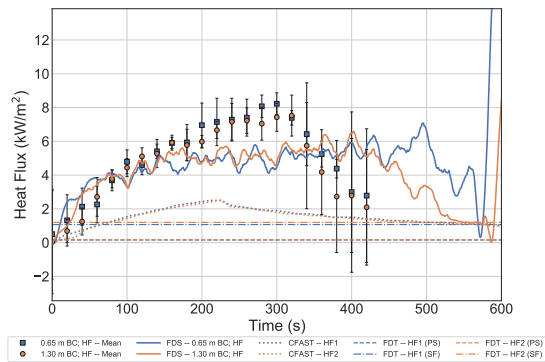
(a) Center Position



(b) Back Position



(c) Corner Position



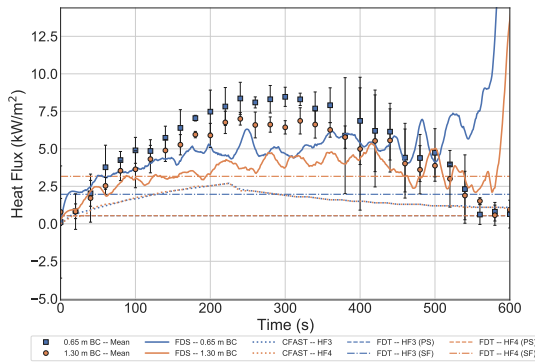
(d) Side Position

Figure A.63: Comparison of the Heat Flux to the Right Side Wall in the 0.6 m Burner, 100 kW Experiments with Door Closed

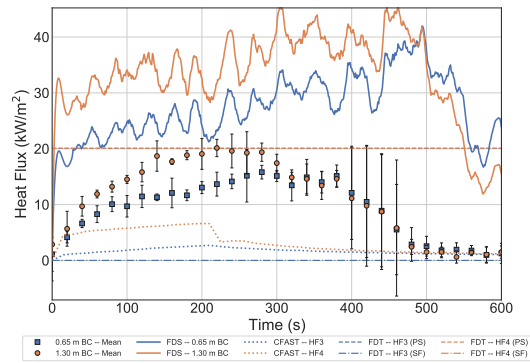
predicted the qualitative shape of the experimental heat flux curve, but significantly underpredicted the maximum measured heat fluxes.

A comparison of the measured and predicted heat fluxes to the back wall of the compartment for the 0.6 m Burner with a HRR of 500 kW is provided in Figure A.66. FDS accurately predicted the heat fluxes when the burner was in the center, corner, and side positions, but overpredicted the heat flux when the burner was in the back position. The solid flame method provided an accurate representation of the approximately steady heat flux after the growth phase.

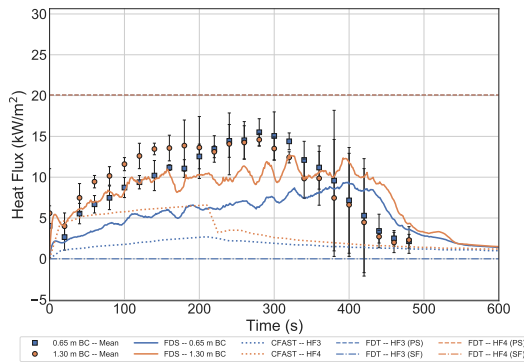
A comparison of the measured and predicted heat fluxes to the right wall of the compartment for the Red Accent Chair is provided in Figure A.67. The point source method provided a reasonable prediction of the maximum heat flux when the chair was in the center position. FDS overpredicted the maximum heat flux and underpredicted the heat flux in the decay phase when the chair was in all the positions and CFAST underpredicted the heat flux when the chair was in all the positions.



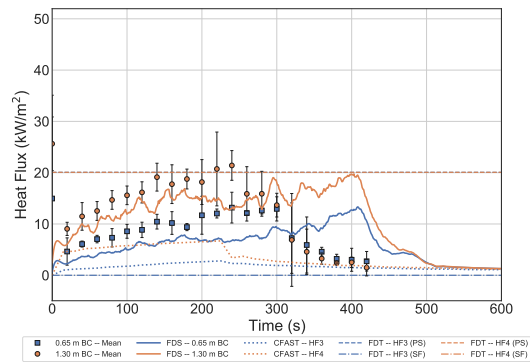
(a) Center Position



(b) Back Position



(c) Corner Position

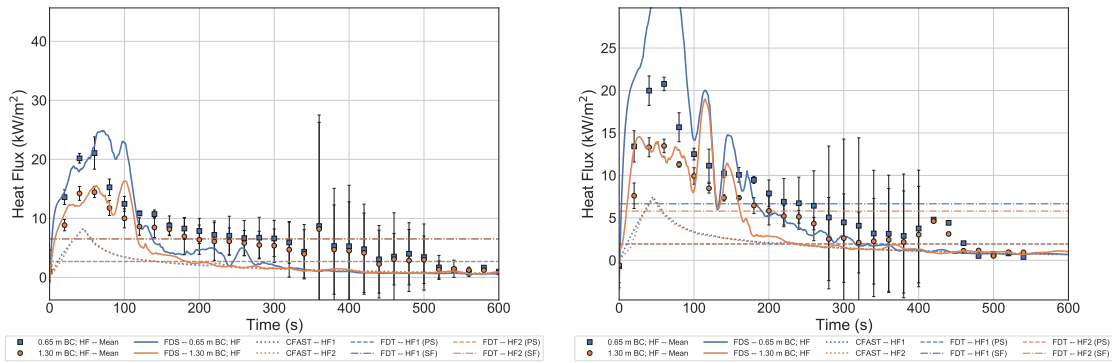


(d) Side Position

Figure A.64: Comparison of the Heat Flux to the Back Wall in the 0.6 m Burner, 100 kW Experiments with Door Closed

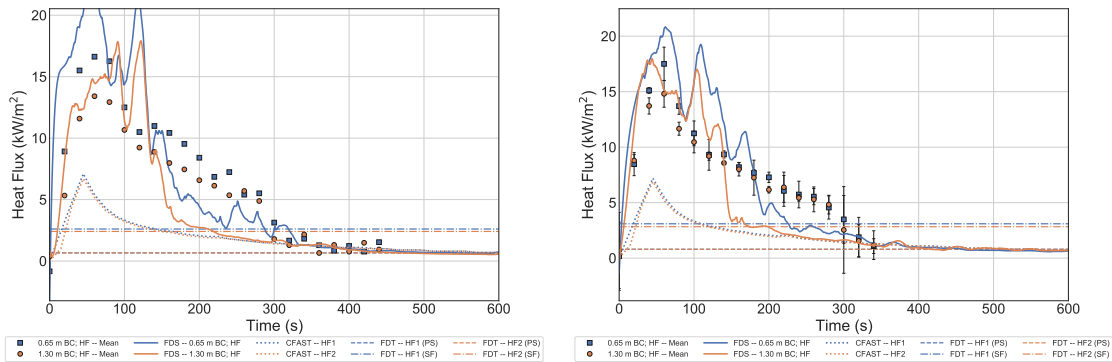
A comparison of the measured and predicted heat fluxes to the back wall of the compartment for the Red Accent Chair is provided in Figure A.68. The point source method accurately predicted the maximum heat flux to the lower elevation heat flux gauge when the chair was in all the positions. FDS overpredicted the maximum heat flux when the chair was in all the positions and underpredicted the heat flux in the decay phase when the chair was in the center position. CFAST underpredicted the heat flux when the chair was in all the positions.

A comparison of the measured and predicted heat fluxes to the right wall of the compartment for the Overstuffed Sofa is provided in Figure A.69. The point source method calculated with the mean HRR provided a reasonable prediction of the mean heat flux when the sofa was in the center and back positions. FDS overpredicted the maximum heat flux and underpredicted the heat flux in the decay phase when the sofa was in all the positions and CFAST accurately predicted the maximum heat flux when the sofa was in the center and corner positions, and underpredicted the heat flux when the chair was in the back position. Although CFAST accurately predicted the maximum heat



(a) Center Position

(b) Back Position



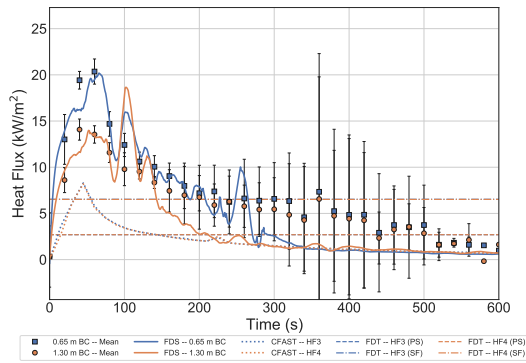
(c) Corner Position

(d) Side Position

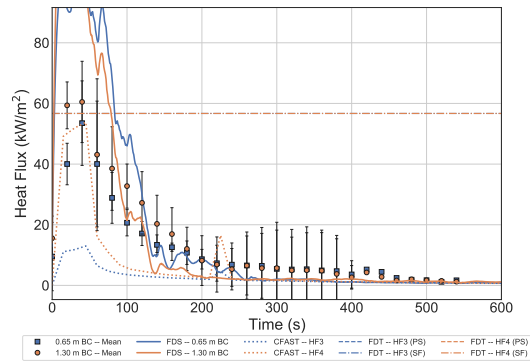
Figure A.65: Comparison of the Heat Flux to the Right Side Wall in the 0.6 m Burner, 500 kW Experiments with Door Closed

flux in some experiments, the qualitative shape of the curve was not predicted, so the duration of the maximum heat flux was not accurately predicted.

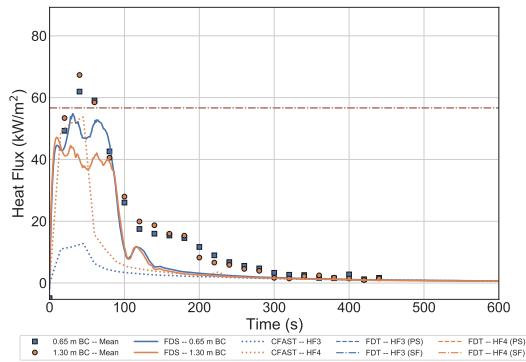
A comparison of the measured and predicted heat fluxes to the back wall of the compartment for the Overstuffed Sofa is provided in Figure A.70. The point source method calculated using the mean HRR provided a good representation of the mean heat flux when the sofa was in all positions. FDS overpredicted the maximum heat flux when the sofa was in the center position, predicted the approximate maximum when the sofa was in the back position, and underpredicted the heat flux when the sofa was in the corner. CFAST approximately represented the maximum heat flux when the sofa was in the center, but the duration of the exposure was not accurately predicted.



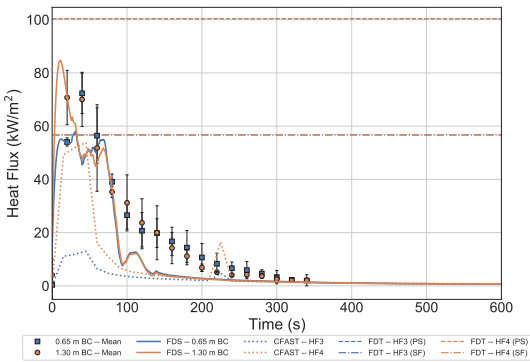
(a) Center Position



(b) Back Position

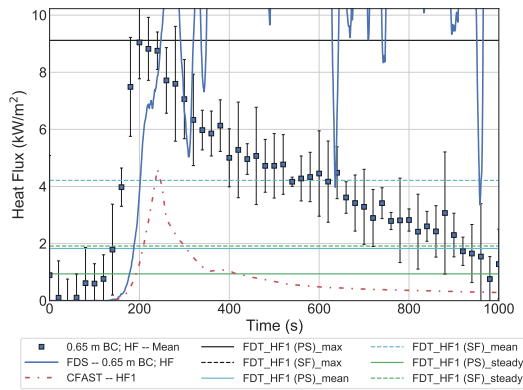


(c) Corner Position

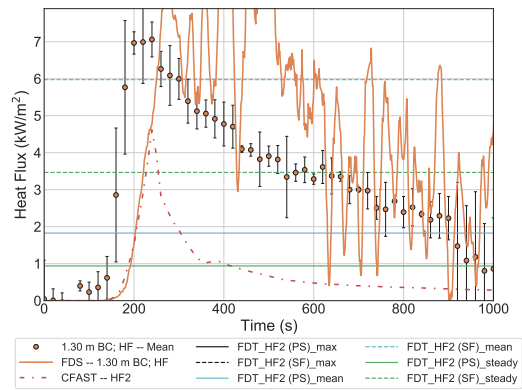


(d) Side Position

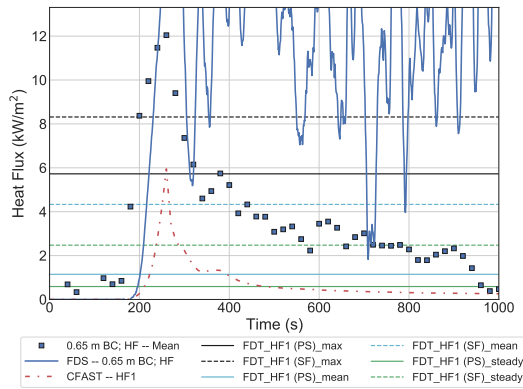
Figure A.66: Comparison of the Heat Flux to the Back Wall in the 0.6 m Burner, 500 kW Experiments with Door Closed



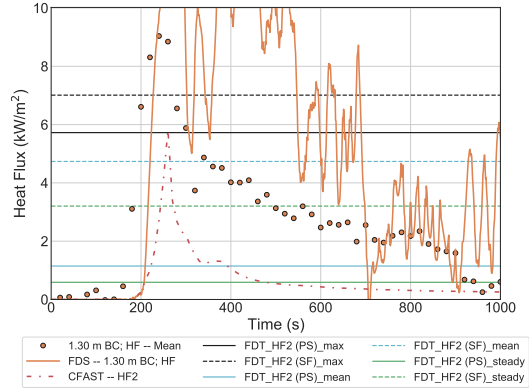
(a) Center Position, Heat Flux Gauge 1



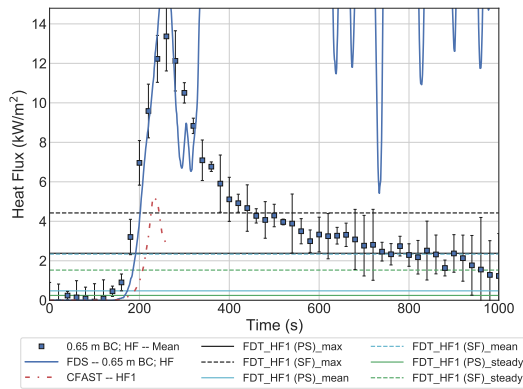
(b) Center Position, Heat Flux Gauge 2



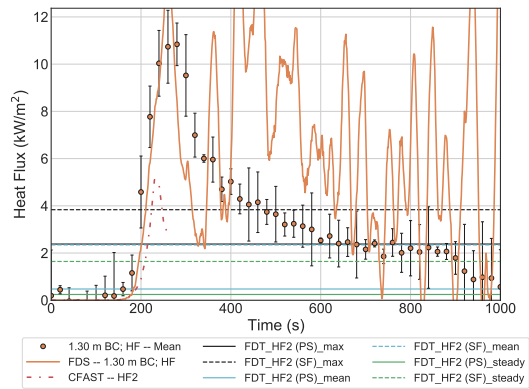
(c) Back Position, Heat Flux Gauge 1



(d) Back Position, Heat Flux Gauge 2

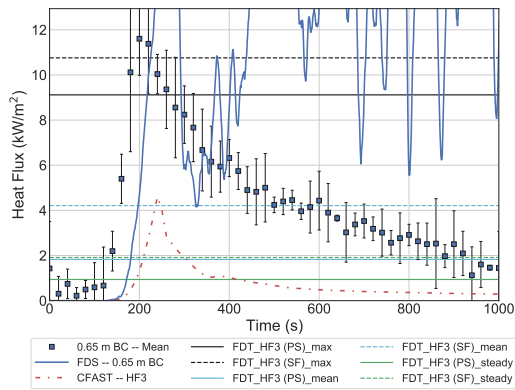


(e) Corner Position, Heat Flux Gauge 1

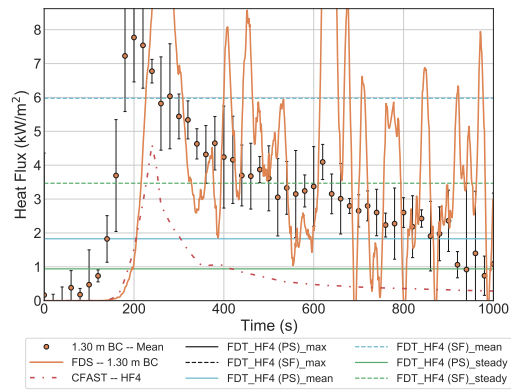


(f) Corner Position, Heat Flux Gauge 2

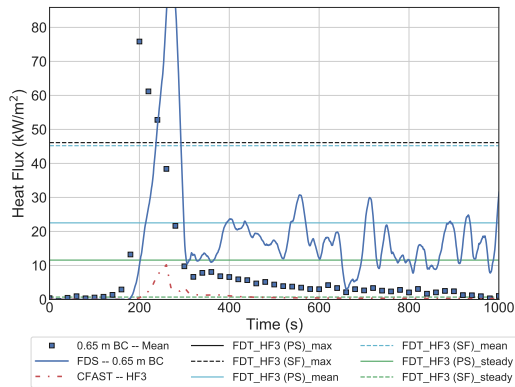
Figure A.67: Comparison of the Heat Flux to the Right Side Wall in the Red Accent Chair Experiments with the Door Closed



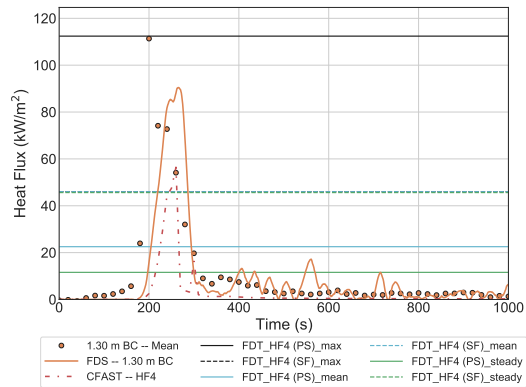
(a) Center Position, Heat Flux Gauge 3



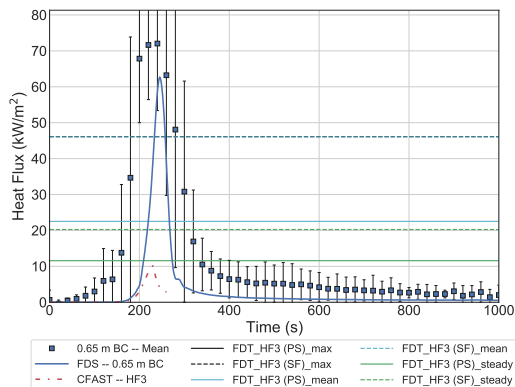
(b) Center Position, Heat Flux Gauge 4



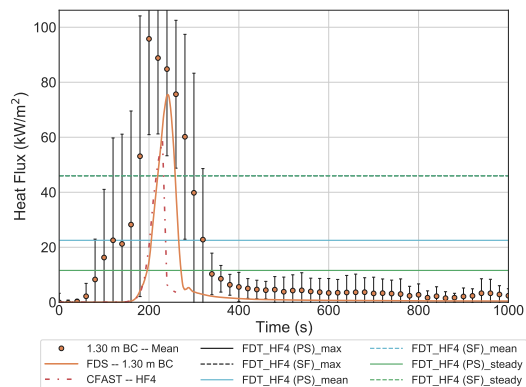
(c) Back Position, Heat Flux Gauge 3



(d) Back Position, Heat Flux Gauge 4

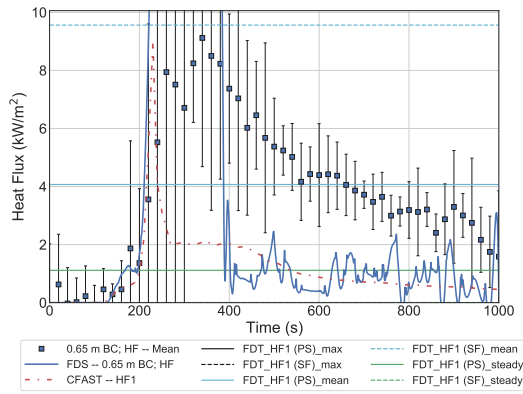


(e) Corner Position, Heat Flux Gauge 3

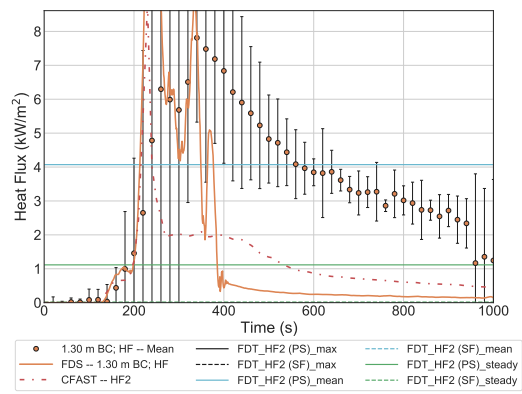


(f) Corner Position, Heat Flux Gauge 4

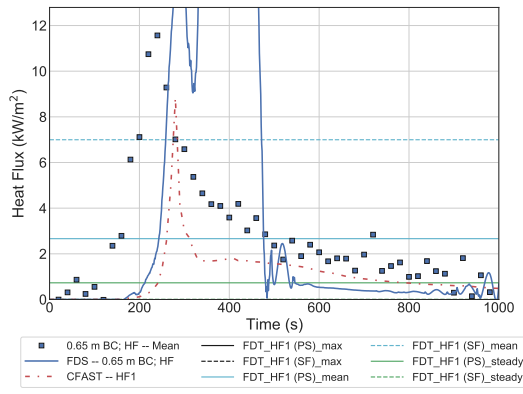
Figure A.68: Comparison of the Heat Flux to the Back Wall in the Red Accent Chair Experiments with the Door Closed



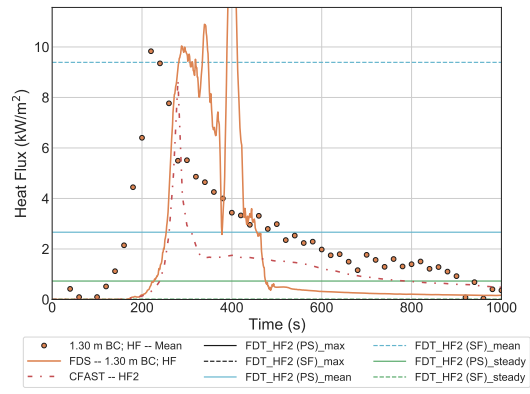
(a) Center Position, Heat Flux Gauge 1



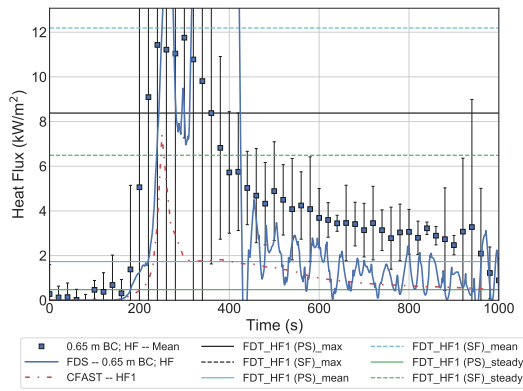
(b) Center Position, Heat Flux Gauge 2



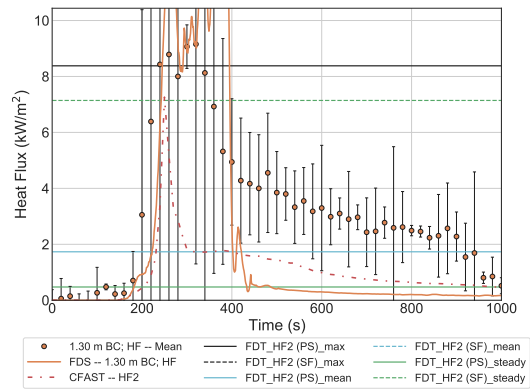
(c) Back Position, Heat Flux Gauge 1



(d) Back Position, Heat Flux Gauge 2

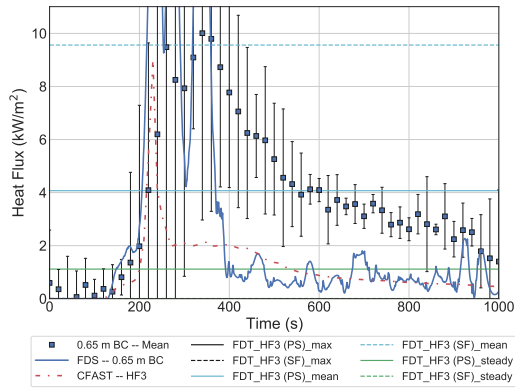


(e) Corner Position, Heat Flux Gauge 1

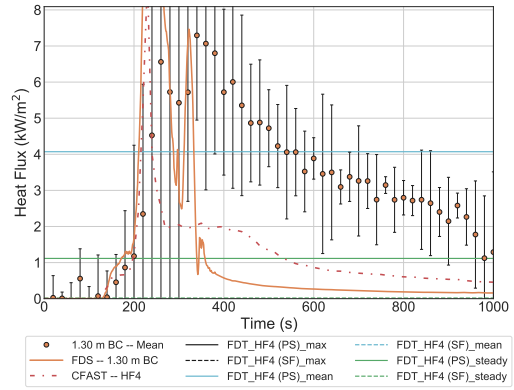


(f) Corner Position, Heat Flux Gauge 2

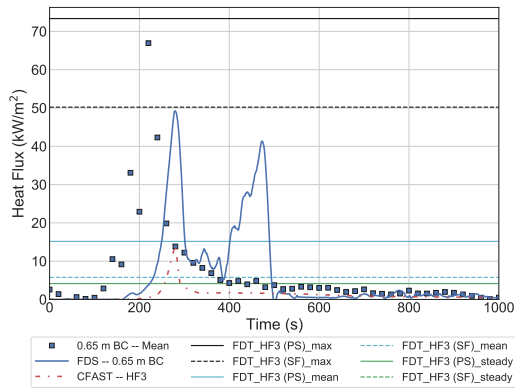
Figure A.69: Comparison of the Heat Flux to the Right Side Wall in the Overstuffed Sofa Experiments with the Door Closed



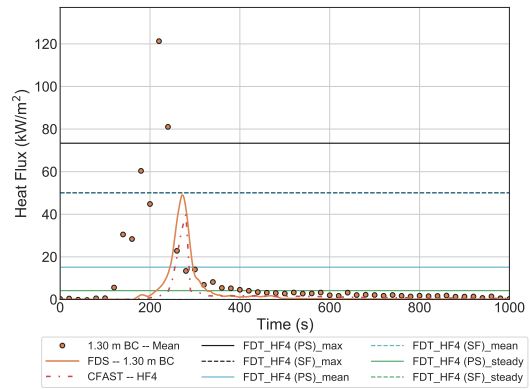
(a) Center Position, Heat Flux Gauge 3



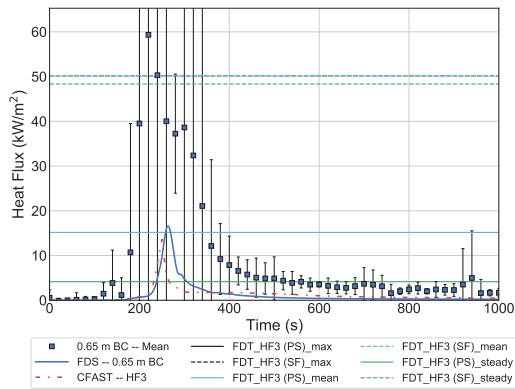
(b) Center Position, Heat Flux Gauge 4



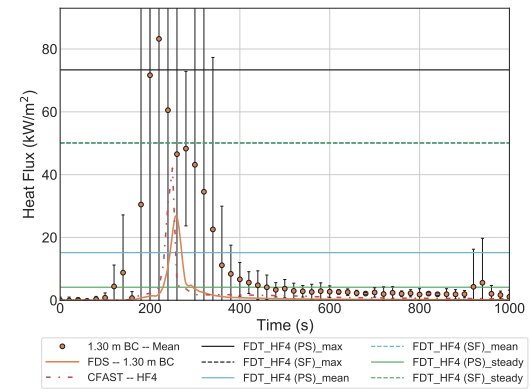
(c) Back Position, Heat Flux Gauge 3



(d) Back Position, Heat Flux Gauge 4



(e) Corner Position, Heat Flux Gauge 3



(f) Corner Position, Heat Flux Gauge 4

Figure A.70: Comparison of the Heat Flux to the Back Wall in the Overstuffed Sofa Experiments with the Door Closed